HUMIDITY SENSORS USING MEMS AND STANDARD CMOS TECHNOLOGIES

A THESIS SUBMITTED TO
THE GRADUATE SCHOOL OF NATURAL AND APPLIED SCIENCES
OF
THE MIDDLE EAST TECHNICAL UNIVERSITY

BY

BURAK OKCAN

IN PARTIAL FULFILLMENT OF THE REQUIREMENTS FOR THE DEGREE OF
MASTER OF SCIENCE
IN
THE DEPARTMENT OF ELECTRICAL AND ELECTRONICS ENGINEERING

AUGUST 2003

Approval of Graduate School of Natural and Applied Sciences.

Prof. Dr. Canan ÖZGEN
Director

I certify that this thesis satisfies all the requirements as a thesis for the degree of Master of Science.

Prof. Dr. Mübeccel DEMİREKLER
Head of Department

This is to certify that we have read this thesis and that in our opinion it is fully adequate, in scope and quality, as a thesis for the degree of Master of Science.

Assoc. Prof. Dr. Tayfun AKIN
Supervisor

Examining Committee Members:

Assoc. Prof. Dr. Cengiz BEŞİKÇİ (Chairman)

Assoc. Prof. Dr. Tayfun AKIN

Assist. Prof. Dr. Özlem AYDIN ÇİVİ

Dr. Deniz SABUNCUOĞLU TEZCAN

Cem KURAL (M.S. in EE, ARÇELİK A.Ş.)

ABSTRACT

HUMIDITY SENSORS USING MEMS AND STANDARD CMOS TECHNOLOGIES

Okcan, Burak

M. Sc., Department of Electrical and Electronics Engineering

Supervisor: Assoc. Prof. Dr. Tayfun Akın

August 2003, 127 pages

This thesis presents the development of humidity sensors using surface micromachining and standard CMOS processes. Two types of humidity sensors are designed and implemented. The first one is a capacitive humidity sensor with a polyimide film as the humidity sensitive dielectric layer. The second sensor is a thermal conductivity based humidity sensor, which measures the amount of humidity using the difference between the thermal conductivity of the air and the water vapor.

The capacitive humidity sensor is fabricated by three mask process, where the humidity sensitive polyimide layer is sandwiched between two metal electrodes. The bottom electrode is designed in a heater resistor shape, which provides humidity measurement at high relative humidity levels where there is the risk of water condensation. Characterization results show that the fabricated sensor tracks the humidity change with a sensitivity of 145fF/%RH, with nonlinearity less than 0.2%.

The hysteresis of the sensor is 2.57% RH. The sensor is hybrid connected to a switched capacitor readout circuit, which dissipates 1.75mW power. The measured sensitivity of the hybrid module is 19.4mV/%RH with nonlinearity less than 0.2%. Operation of the integrated heater is also verified by monitoring the resistance versus temperature and resistance versus power characteristics.

The thermal conductivity based humidity sensor is implemented using thermally isolated p-n junction diodes obtained by standard CMOS and post-CMOS bulk silicon micromachining processes. Thermal isolation is achieved by anisotropic bulk silicon etching using electrochemical etch stop technique in a TMAH solution. One of the suspended diodes is sealed and has a fixed thermal conductance, while the other one is exposed to the ambient and has humidity dependent thermal conductance; therefore, they provide different diode voltages when they are heated with same biasing currents. The difference between the diode voltages are converted into current through a monolithic transconductance amplifier, and this current is integrated by a switched capacitor integrator to obtain an amplified output signal. The measured temperature sensitivity of the diodes is -1.3mV/K within 150ºC to 250ºC range at 100µA bias level. Relative humidity sensitivity of the sensor is 14.3mV/%RH, 26mV/%RH, and 46.9mV/%RH for 20ºC, 30ºC, and 40ºC ambient temperature respectively with a nonlinearity less than 0.3%. The measured hysteresis of the sensor is less than 1% at 20ºC and 30ºC ambient temperature conditions. The sensor operates from a 5V supply and dissipates 1.38mW power.

ÖZ

MEMS VE STANDART CMOS TEKNOLOJİLERİ İLE NEM SENSÖRLERİ

Okcan, Burak
Yüksek Lisans, Elektrik ve Elektronik Mühendisliği Bölümü
Tez Yöneticisi: Doç. Dr. Tayfun Akın

Ağustos 2003, 127 sayfa

Bu tezde MEMS ve standart CMOS süreci kullanılarak geliştirilmiş nem sensörleri anlatılmaktadır. İki çeşit nem sensörü tasarlanmış ve üretilmiştir. Birinci sensör, neme duyarlı dielektrik katmanı polyimide kullanılarak yapılmış kapasitif bir sensördür. Diğer sensör, havanın ve su buharının ısıl iletkenlikleri arasındaki farkı ölçen, ısıl iletkenlik bazlı nem sensörüdür.

Kapasitif sensör, polyimide katmanının iki metal elektrot arasına sıkıştırıldığı üç maskelik bir süreçle üretilmiştir. Alt elektrot, su yoğunlaşması riskinin bulunduğu yüksek nem seviyelerinde ölçüm yapma olanağı sağlayan ısıtıcı direnç şeklinde tasarlanmıştır. Üretilen sensör üzerinde yapılan testler, sensörün nem değişimini 145fF/%RH'lik hassasiyet ve 0.2%'den düşük orantı katsayısı hatası ile algıladığını göstermiştir. Sensör anahtarlamalı kapasitör okuma devresiyle entegre edilmiştir. Hibrid yapının hassasiyeti 19.4mV/%RH, orantı katsayısı hatası 0.2%'den düşük

olarak bulunmuştur. Sensörün histeresisi 2.57% RH'dir. Isıtıcının çalışması da sıcaklığa ve güce bağlı direnç karakteristiğinin ölçümüyle doğrulanmıştır.

Isıl iletkenlik bazlı nem sensörü, standard CMOS ve CMOS sonrası gövde aşındırma işlemleri kullanılarak elde edilen, ısıl olarak yalıtılmış diyotlar kullanılarak elde edilmiştir. Isıl yalıtım, TMAH çözeltisi kullanılarak, yönlü silisyum gövde aşındırması ve elektrokimyasal aşındırma-durdurma yöntemi ile sağlanmıştır. Diyotlardan bir tanesi kapatılarak ısıl iletkenliği sabit tutulmuş, diğer diyot çevreyle temas eder durumda bırakılarak ısıl iletkenliğinin nemle değişmesi sağlanmıştır. Bu nedenle sabit akımla beslendiklerinde farklı çıkış gerilimleri üretmektedirler. Diyotların çıkış gerilimleri arasındaki fark fark-geçiş-ileti yükselticisi ile akıma dönüştürülmüş, akım da anahtarlamalı kapasitör entegratörü ile entegre edilerek yükseltilmiş çıkış sinyali elde edilmiştir. 100µm akım seviyesinde ve 150ºC'den 250ºC'ye olan sıcaklık aralığında, diyotların sıcaklık hassasiyetleri -1.3mV/K olarak ölçülmüştür. Sensörün bağıl nem hassasiyeti 20ºC, 30ºC ve 40ºC sıcaklık şartlarında sırasıyla 14.3mV/%RH, 26mV/%RH ve 46.9mV/%RH olarak ölçülmüştür. Sensörün ölçülen histeresisi 1% RH'den azdır. Sensör 5V ile beslenmektedir ve 1.38mW güç harcamaktadır.

ACKNOWLEDGMENTS

I would like to express my appreciation and thanks to my supervisor Assoc. Prof. Dr. Tayfun AKIN not only for his guidance and support during the development of this thesis, but also for his friendly attitude towards me.

I would like to thank Orhan AKAR for the clean room training sessions, for his great patience, and for his innovative ideas. I would also like to thank Dr. Deniz S. TEZCAN and Yusuf TANRIKULU for their helps in the post processing of the CMOS chips. I am also grateful to Dr. Selim EMİNOĞLU for sharing his circuit design knowledge and experience with me. I would also like to thank METU-MET staff for their help and guidance in the operation and maintenance of the sputtering system. I am also thankful to my office mates Kağan TOPALLI, Mehmet Ünlü, Fırat YAZICIOĞLU, Özge ZORLU, Hüseyin SAĞKOL, Murat TEPEGÖZ, M. Akif ERİŞMİŞ, and Mustafa SANLI for creating a nice working atmosphere.

Finally, I would like to thank my family and all of my friends for their trust and support through all my life.

TABLE OF CONTENTS

LIST OF TABLES

LIST OF FIGURES

CHAPTER 1

INTRODUCTION

Humidity, which is the amount of water vapor in the air, has an important role in the quality of human life. In industry, optimum humidity conditions should be provided on production lines for obtaining high quality products. For example, in textile processing, generation of electrostatic charges during the fabrication may cause the materials to cling. This is prevented by keeping the environment in damp conditions. On the other hand, dry conditions are required in processing silicon wafers in the clean room or assembling electrical products on the assembly line. In agriculture, adequate environmental humidity conditions are needed to grow fruits and vegetables. Similar conditions are needed in the preservation of products such as food, cotton, and tobacco. Thus, the measurement and control of humidity have significant importance in many areas for different purposes.

There have been continuous efforts for the measurement of humidity throughout the development of science and engineering [1]. Several instruments for measuring humidity based on different physical principles were invented in the 17th century. Most important examples of these instruments are the hygroscopic hygrometer, dew-point hygrometer, and psychrometer. These devices have large size and slow response compared to modern instruments. However, their working principles are still in use in the recent instruments.

Today, thin film humidity sensors are widely used due to their small size, low cost, low power consumption, and high performance. Various kinds of thin film humidity sensors are available based on different measurement principles such as resistive, capacitive, hygrometric, gravimetric, and thermal techniques. Thin film humidity sensors still suffer from long term stability and chemical durability problems in harsh environments. Instability at high relative humidity conditions due to water condensation on the sensor surface is another drawback of most of the commercial thin film humidity sensors.

This thesis reports two humidity sensors; one is based on the thin film capacitive technique while the other one is based on the thermal technique. The capacitive humidity sensor is integrated with a heater, which allows humidity measurement at high relative humidity levels by reducing the relative humidity that the sensor sees to a lower level. The fabricated sensor is hybrid connected to a readout circuit for further signal processing of the sensor output. The second sensor uses the difference between the thermal conductivity of air and water vapor. It is fabricated by standard CMOS and post-CMOS processes, which allows the integration of the sensor with the readout circuit monolithically. This sensor already operates at high temperatures, which does not contain any risk of water condensation at high relative humidity conditions.

This chapter presents the humidity concept and an overview of the humidity sensors. Section 1.1 gives the definition of humidity and humidity related formulations. This section also discusses the saturation vapor pressure and relative humidity concepts, which are the fundamental terms used in humidity measurement. Section 1.2 describes different principles of humidity measurement. Section 1.3 reviews the miniaturized humidity sensors and discusses their advantages and disadvantages. Finally, section 1.4 gives the objectives and the organization of the thesis.

1.1 Humidity Definition and Formulations

Humidity is the measure of the water vapor content of the atmosphere. It forms a part of the total atmospheric pressure. The amount of atmospheric moisture is proportional to the partial pressure of the water vapor, which allows a measurement of the absolute humidity in the air. There are various ways of expressing the moisture content of air, such as *absolute humidity, specific humidity, mixing ratio,* and *relative humidity*. *Absolute humidity* is defined as the mass of water vapor per unit volume of dry air [2]:

$$Absolute\ humidity = \frac{mass\ of\ water\ vapor}{volume\ of\ dry\ air} \tag{1.1}$$

Absolute humidity is expressed in g/m^3, which is in fact the measure of the vapor density of water.

Specific humidity and *mixing ratio* are two other ways of expressing the amount of humidity in the air. Specific humidity is the ratio of the weight of water vapor to the unit weight of air containing it [2]:

$$Specific\ humidity = \frac{mass\ of\ water\ vapor}{total\ mass\ of\ air} \tag{1.2}$$

On the other hand, the mixing ratio is the ratio of the mass of water vapor to a unit mass of dry air containing it [2]:

$$Mixing\ ratio = \frac{mass\ of\ water\ vapor}{mass\ of\ dry\ air} \tag{1.3}$$

It is generally impractical to directly measure the quantities that are explained above. There is a relatively simple experimental method of expressing the humidity, which is *relative humidity*.

In order to explain the relative humidity, the saturation vapor pressure concept should be explained. Consider a sample of air confined over water at a given temperature as illustrated in Figure 1.1. The system eventually reaches to equilibrium, where the rate of evaporation is equal to the rate of condensation. In other words, the water vapor pressure becomes constant. The water vapor pressure in this state corresponds to the maximum amount of water vapor that the air can hold, and it is called the *saturation water vapor pressure*.

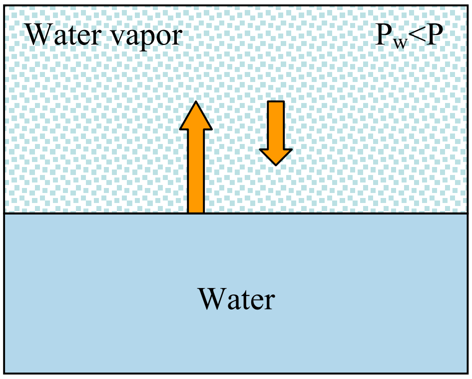

(a)

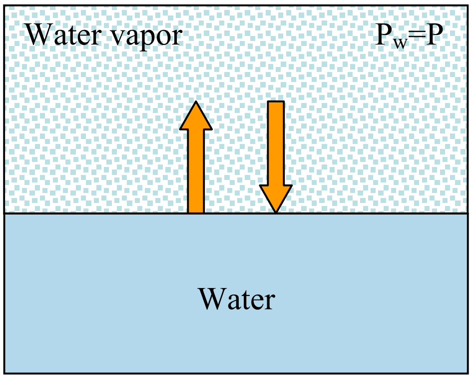

(b)

Figure 1.1: Saturation vapor pressure concept to explain the relative humidity: (a) vapor pressure is less than saturation vapor pressure; (b) system is in equilibrium.

Relative humidity is the ratio of vapor pressure to the saturation water vapor pressure at a given temperature:

$$Relative\ humidity = \frac{water\ vapor\ pressure}{saturation\ water\ vapor\ pressure} \tag{1.4}$$

Relative humidity is generally expressed as a percentage, and it is a temperature dependent parameter. Temperature dependency of the relative humidity comes from the fact that the saturation vapor pressure is a function of temperature. As the temperature increases, saturation vapor pressure increases. Consequently, the relative humidity decreases with increasing temperature if the absolute humidity in the air is kept constant. Figure 1.2 shows the saturation water vapor pressure versus temperature graph [1].

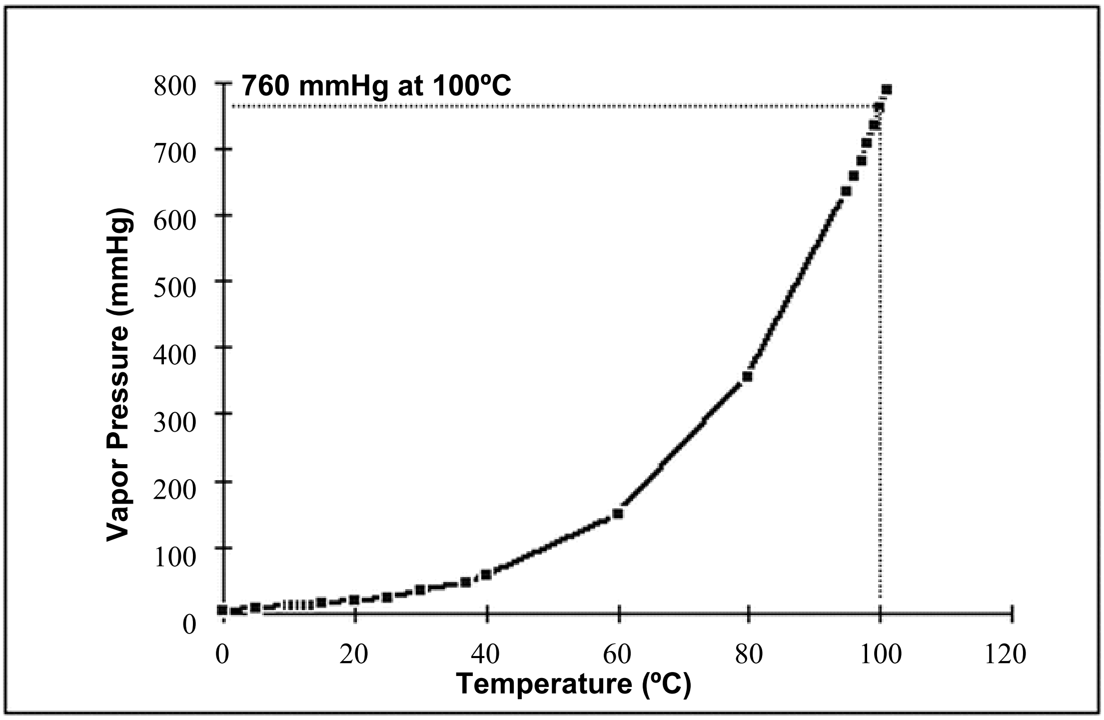

Figure 1.2: Saturation water vapor pressure versus temperature graph [1].

Dew-point temperature is another humidity related parameter, which is defined as the temperature to which the air should be cooled to reach saturation, where the moisture content is constant. In other words, it is the temperature where the relative humidity reaches to 100% due to the decrease in the saturation vapor pressure during cooling down. The dew point temperature gives a measure of the absolute humidity in the air, and it corresponds to the saturation vapor density at that temperature.

1.2 Classical Humidity Measurement Methods

There are various types of classical humidity measuring instruments, using several different measurement methods such as psychrometers, dew-point hygrometers, and hygrometers using hygroscopic materials [2]. All methods have their own advantages and drawbacks, and a proper measurement method can be selected depending on the application. Following subsections briefly explains these methods. Then, Section 1.3 presents humidity sensors based on new micromachining technologies.

1.2.1 The Psychrometer

Psychrometry is one of the oldest methods used in humidity measurements. A psychrometer mainly consists of two thermometers one in ambient air and the other in contact with water as shown in Figure 1.3. The measurement is based on the calculation of the actual vapor pressure using the difference between wet and dry bulb temperatures according to the following empirical formula [3]:

$$P_w = P_s - P_{tot} A(T_d - T_w) \tag{1.5}$$

where T_d is the dry bulb temperature, T_w is the wet bulb temperature, P_s and P_{tot} are the saturation pressure and the pressure of the ambient, respectively, and A is the psychrometer constant which is a function of geometry and air flow.

The *wet bulb temperature* is the temperature reached after cooling due to evaporation from a moist surface. The amount of heat taken by the water for evaporation is equal to the heat loss of air. In addition, the amount of cooling due to the evaporation is a function of the ambient relative humidity. As a result, psychrometers allow the relative humidity estimation based on dry and wet-bulb temperature measurements. The most important advantage of psychrometers is that they do not require calibration. Main drawbacks are the requirement of the regular replacement of distilled water and the requirement of air flow with a high flow rate.

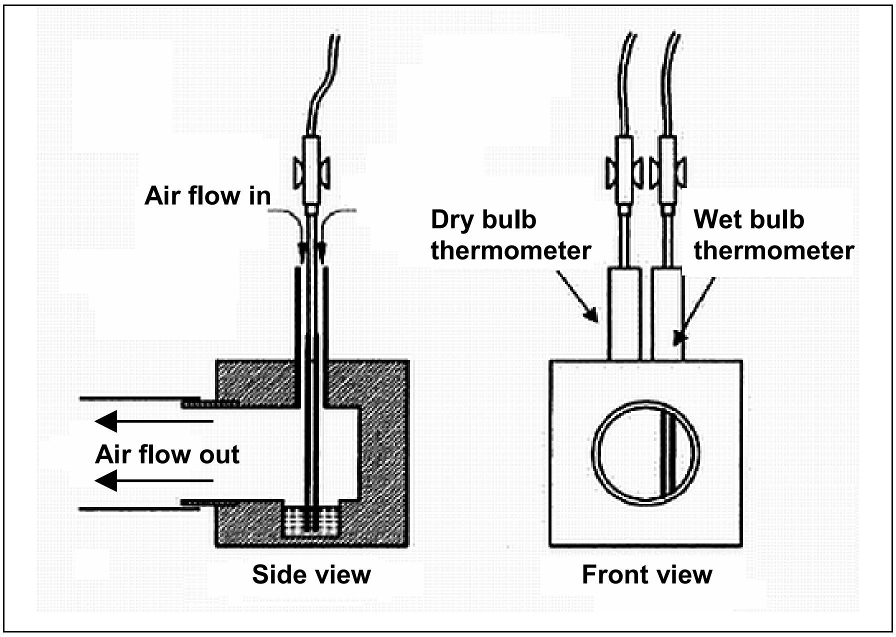

Figure 1.3: The schematic of a psychrometer [4].

1.2.2 The Dew-Point Hygrometer

Water vapor density of the air can be determined by the measurement of the dew-point temperature. The dew-point temperature can be measured by a dew-point hygrometer, which consists of a thermometer, a cooler, and a detector. Dew formation is detected using a light source and a photodetector [1, 2]. Figure 1.4 shows an example of the dew point hygrometer.

In the dew-point hygrometer, a light source is directed on a mirror and the reflected light intensity is measured by a photodetector. The mirror is cooled down using a cooler which is controlled by an electronic circuit. When the mirror temperature reaches the dew point temperature, water condenses on the surface of the mirror, and the light intensity detected by the photodetector changes. The temperature at this instant gives the dew-point temperature.

This measurement method has a wide dynamic range, and it is very accurate. Major disadvantages are the expensive setup, high power consumption, and difficult maintenance of the system, such as the requirement of regular cleaning of the mirror surface.

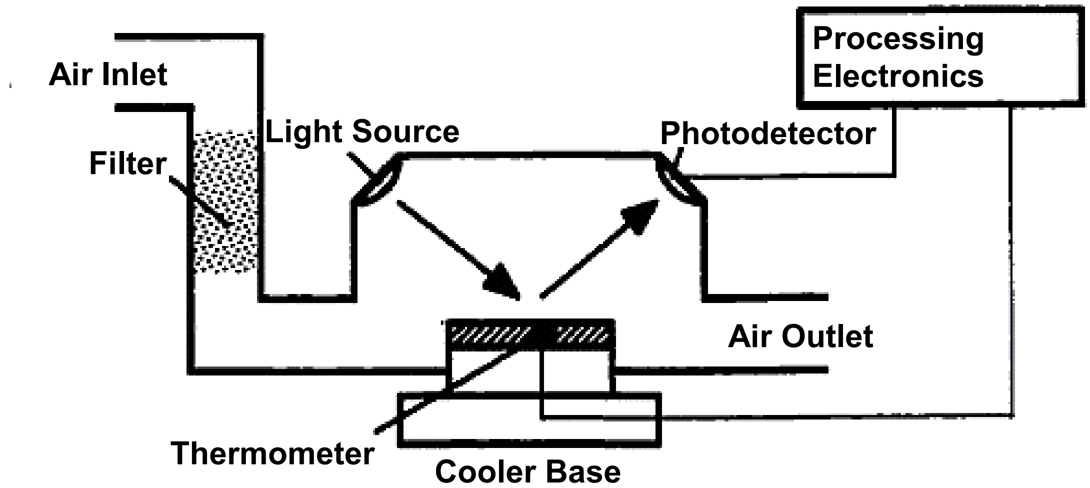

Figure 1.4: The structure of a dew-point hygrometer [1].

1.2.3 Hygrometers Using Hygroscopic Materials

Another fundamental method of humidity measurement is making use of the hygroscopic materials. There is a wide variety of different materials, showing different hygroscopic properties [1]. Hygrometers of this type are divided into two groups as mechanical and electrical types.

In a mechanical hygrometer, the change in the physical dimensions of the hygroscopic material is used. This material can be a human hair, a paper strip, or a polymer fiber. The mechanical hygrometer has a scale to which the hygroscopic material is attached as shown in Figure 1.5. The length of this material changes when exposed to humidity, so the scale of the hygrometer deflects, showing a value depending on the amount of humidity. The mechanical hygrometer has the major advantage that it does not require any power supply. The other advantages include being simple and inexpensive. However, it has nonlinear output characteristics, and shows hysteresis.

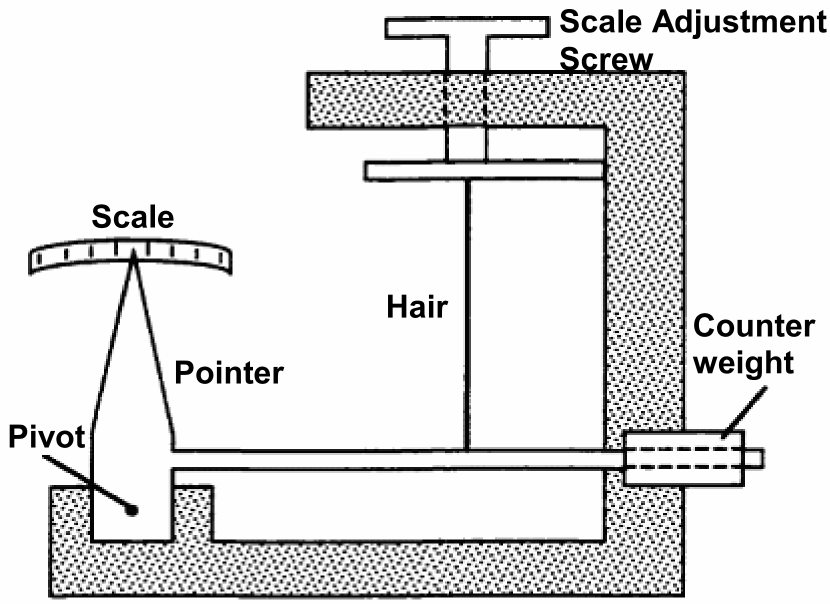

Figure 1.5: A mechanical hygrometer, which uses the human hair as the hygroscopic material [1].

The electrical hygrometer uses a material, which has an electrical parameter sensitive to humidity. Figure 1.6 shows an example of the electrical hygrometer. It is a capacitive hygrometer, which includes a hygroscopic material whose dielectric constant is sensitive to the humidity change. The hygroscopic materials include polymers, ceramics, and electrolytic films. Due to the moisture absorption from the surface, dielectric constants of these materials increase with increasing humidity. Electrical hygrometers are simple and inexpensive, but they have the disadvantage of having hysteresis and sensitivity to contamination.

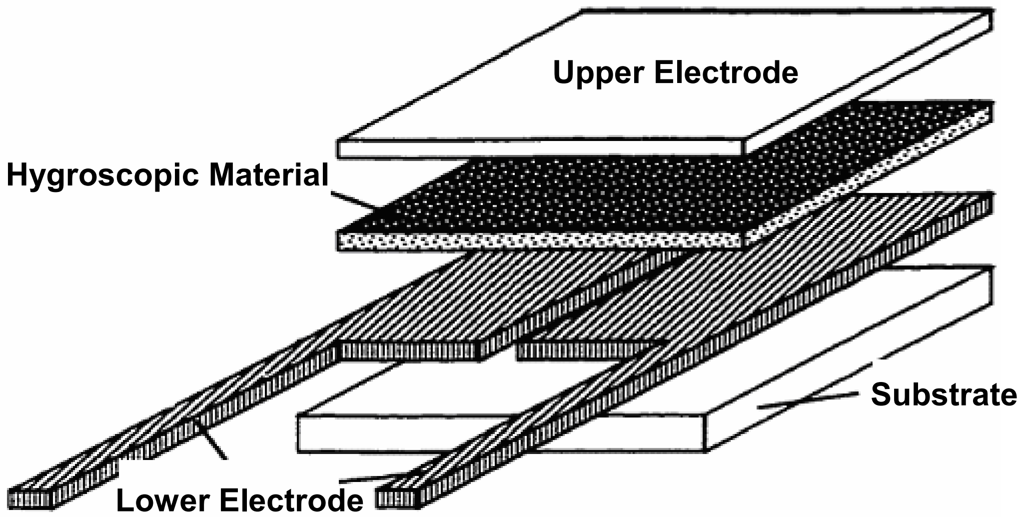

Figure 1.6: The structure of a capacitive hygrometer [1].

1.3 Miniaturized Humidity Sensors

Developments in the micromachining technology have encouraged the development of miniaturized humidity sensors. Miniaturized humidity sensors have the advantage of small size, low cost, low power consumption, and high performance when compared to the classical measurement methods explained in the previous section. Various types of miniaturized humidity sensors have been designed, which use materials having different humidity dependent parameters. Major techniques of measurement methods used in miniaturized humidity sensors can be listed as resistive, capacitive, mechanical, gravimetric, and optical techniques. In addition to these widely used techniques, there are some different techniques based on electromagnetic and thermal humidity sensing methods. Miniaturized humidity sensors have also been used in complex micro systems where they are integrated with other types of transducers and electronic circuitries. Following subsections shortly describe the humidity sensors based on micromachining techniques.

1.3.1 Resistive Humidity Sensors

Resistive humidity sensors are transducers that convert the humidity change into resistance change. Ceramics, polymers and electrolytes are the main groups of materials that have been used and reported for resistive humidity measurement. These materials have humidity induced resistance characteristics, which allow the humidity measurement by the measurement of resistance.

Various kinds of ceramics have been investigated as humidity sensitive materials, such as TiO_2, $LiZnVO_4$, $MnWO_4$, C_2O, and Al_2O_3 [5-10]. In general, ceramics have good chemical stability, high mechanical strength, and resistance to high temperature. However, they have nonlinear humidity-resistance characteristics and are not compatible with standard IC fabrication technologies.

Polymer based humidity sensors are another type of resistive humidity sensors that are present in the literature. Some researchers have examined the impedance changes of PVA (polyvinyl alcohol), TA (phthalocyaninosilicon), and Nafion with relative humidity [11]. It has been reported that the humidity response and the stability of the polymer films are dependent on different chemical properties such as hydrophilicity, molecular, and ionic forms [11, 12]. Polymers also have nonlinear humidity-resistance characteristics.

An example of the electrolyte based humidity sensors is the LiCl dew point hygrometer fabricated with a composite of porous polymer and the salt [13]. The humidity measurement is achieved by using the conductivity change of the LiCl-polymer composition. The film is formed on an alumina substrate over interdigitated platinum electrodes. The device is integrated with a heater and a temperature sensor, which are connected to a control circuit to keep the vapor pressure of the saturated LiCl solution equal to the vapor pressure of the atmosphere. The humidity measurement is achieved by the measurement of the dew point temperature. Figure 1.7 presents a prototype of the dew point hygrometer.

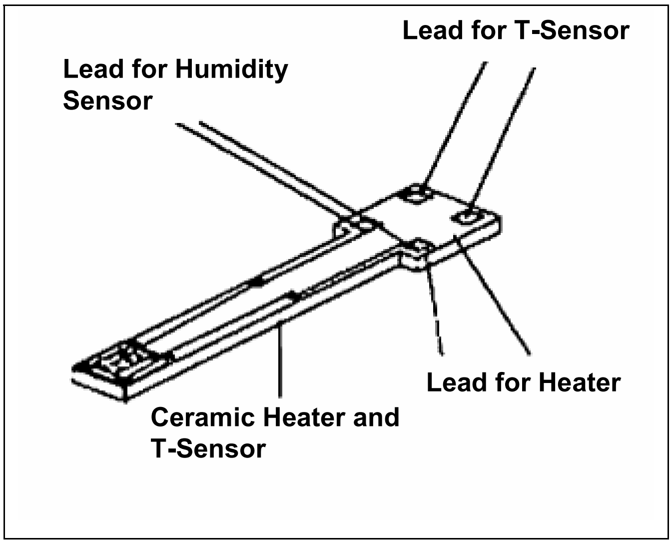

Figure 1.7: A prototype of the dew point hygrometer [13].

The major advantage of this sensor is that it is suitable for batch fabrication. However, it requires regular maintenance of the LiCl solution to guarantee the stable operation of the device, which is an important disadvantage.

1.3.2 Hygrometric Humidity Sensors

One of the very well known mechanical transduction techniques is the usage of piezoresistivity. Piezoresistivity is simply defined as the resistance change of a material with respect to a change in mechanical stress. In order to use this property in humidity sensor applications, a humidity dependent mechanical stress should be obtained. Humidity sensitivity of mechanical properties of polyimide films has been investigated [14]. It has been reported that humidity-induced extension of polyimide films is quiet linear in a wide range of humidity. However, the material behavior strongly depends on the conditions of the polyimide fabrication process. Using the humidity-induced swelling property of polyimide thin films, piezoresistive humidity sensors have been developed [15].

Another example of micro mechanical humidity transduction method is an application of hygroscopic humidity sensing described in Section 1.2.3 into micro technology. A mechanical-optoelectronic sensor unit has been developed using the contraction-expansion property of black hair versus humidity [16]. Hair is attached to a window, which determines the light intensity emitted from a LED to a photodiode. This way, photocurrent of the photodiode changes with humidity. It has been stated that the sensor response is less dependent on temperature because the temperature expansion coefficient of hair is very small.

1.3.3 Gravimetric Humidity Sensors

Gravimetric humidity sensors are developed on the fact that the mass of a hygroscopic material changes by humidity absorption. In this measurement method, a resonator structure is fabricated with a hygroscopic material deposited on it. Assuming that the absorbed water vapor behaves like a rigid mass, the change in frequency is approximated with the equation of Sauerbrey [4]:

$$\Delta f = -2\frac{1}{A}\frac{f_o^2}{\sqrt{\mu\rho}}\Delta m \tag{1.6}$$

where A is the surface area, f_0 is the nominal frequency, μ is the shear modulus, ρ is the density and Δm is the change of mass caused by absorption.

Humidity absorptive properties of fullerene films have been investigated by means of their effect on the resonance frequency of quartz resonators [17]. Test results have shown that the resonance frequency of the resonators increase with the increasing relative humidity of the environment. Resonators provide very high sensitivity and low response time, but the frequency change with respect to relative humidity demonstrates exponential characteristics.

Another example of gravimetric humidity sensors is the Quartz Crystal Microbalance (QCM) used as a humidity sensor [18]. Figure 1.8 shows the schematic diagram of the QCM humidity sensor. In this method, water condensation is produced by a Peltier element integrated with the QCM. A change of mass on the crystal surface results in a decrease in the resonance frequency. Humidity measurement is achieved by the measurement of the delay time between the beginning of the Peltier supply and the beginning of the water condensation on the quartz. The most important feature of this sensor is its relatively low response time. Major disadvantages are the nonlinear characteristics and high temperature dependence.

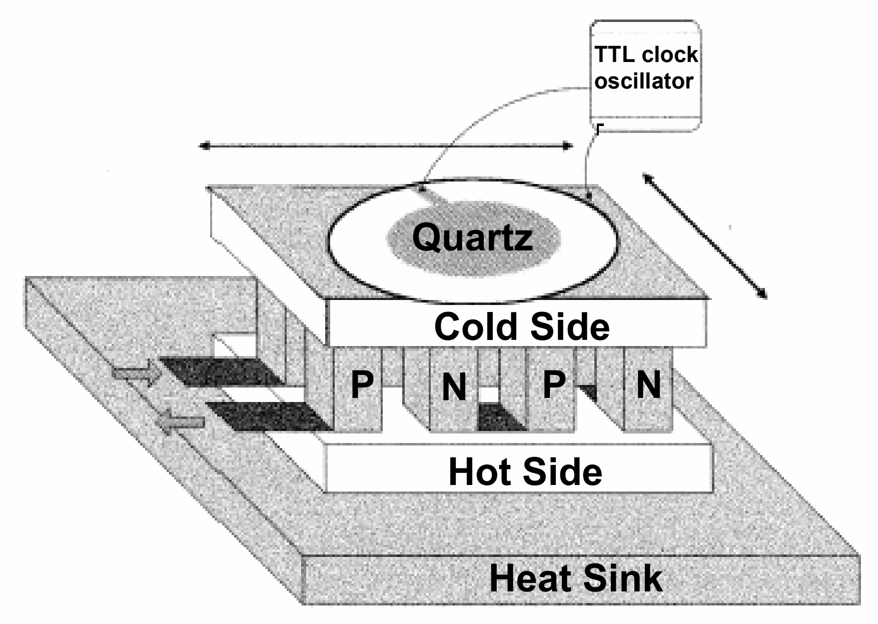

Figure 1.8: The schematic diagram of the QCM humidity sensor [18].

There are other types of gravimetric humidity sensors such as the Surface Acoustic Wave devices, where the phase velocity of surface waves change with the absorption of water vapor [19, 20]. These devices also have nonlinear output characteristics and require complicated systems for signal processing of sensor outputs.

1.3.4 Optical Humidity Sensors

Optical methods have also been developed for humidity sensing applications. The optical humidity measurements are based on the humidity dependence of the amplitude, the polarization, and the frequency of an optical signal. Humidity dependence of these parameters arises from the humidity induced dielectric constant change of the medium where the signal propagation takes place.

An example of this type of humidity sensors is the optical fiber humidity sensor fabricated using a hydrophilic gel (agarose) deposited on the thinner zone of a biconically tapered single mode optical fiber [21]. The sensing mechanism relies on the refractive index change of the agarose gel with respect to the relative humidity. A variation of 6.5dB of the transmitted optical power has been obtained within the 30% to 80% relative humidity range. The sensor material shows a good reproducibility and low hysteresis.

There are similar sensor structures present in the literature, which use the refractive index change of the optical medium as a function of the absorbed water vapor [22, 23]. These devices also show good reproducibility and low hysteresis characteristics. However, they have quite nonlinear humidity response.

1.3.5 Thermal Humidity Sensors

Thermal humidity sensors have been developed by making use of the difference in the thermal conductivity of air and that of water vapor. An absolute humidity sensor has been demonstrated using a single micro air bridge heater [24]. The micro heater sensing region is heated up to a low temperature level at which the thermal conductivity of the air and the water vapor is almost the same. Then, same region is heated up to a temperature level where thermal conductivity difference between the air and water vapor becomes significant. Heating is achieved by applying double pulse currents. The resistance of the micro heater changes due to the temperature coefficient of resistance (TCR) property. As a result, the difference of the voltages in two cycles becomes a function of the absolute humidity in the air. Figure 1.9 shows an SEM picture of the micro bridge heater humidity sensor.

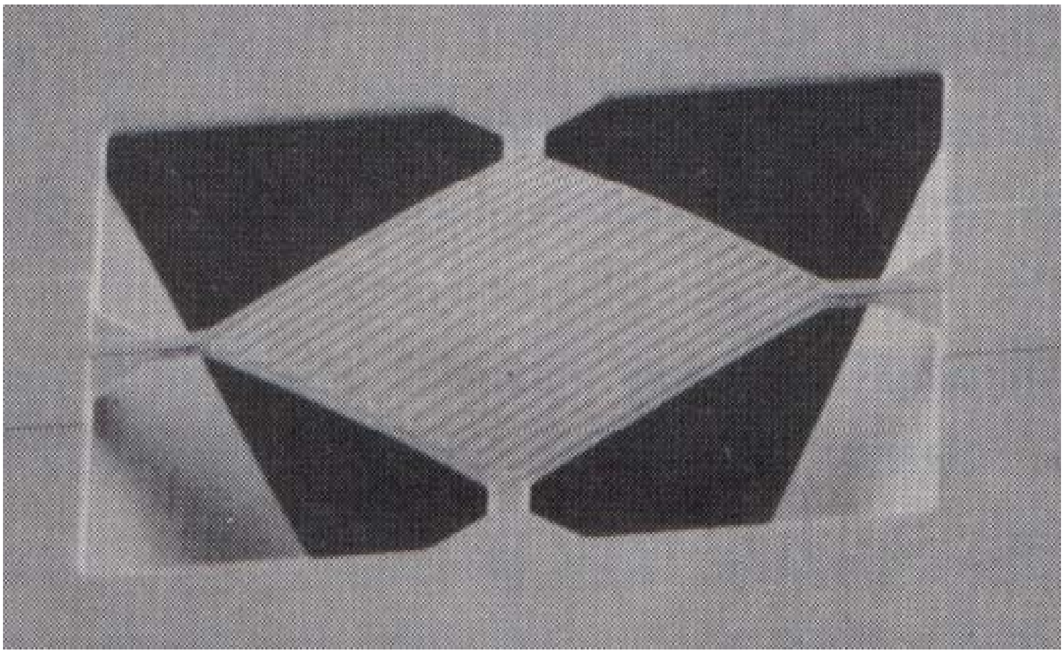

Figure 1.9: An SEM picture of the micro bridge heater humidity sensor [24].

A similar approach has been used in the robust humidity sensor, which has been developed using meander shaped resistors fabricated on thermally isolated membranes [25]. Figure 1.10 demonstrates the device structure. In this sensor, resistors are heated up to a temperature around 250ºC using self heating effect by applying constant voltage. One of the resistors is passivated from the humid environment by proper packaging. The other resistor is exposed to the environment, whose resistance changes with respect to the change in relative humidity due to the thermal conductivity difference. Test results have shown that the sensors have fairly linear response and almost zero hysteresis. However, the power dissipation of the sensor is very high compared to the other methods.

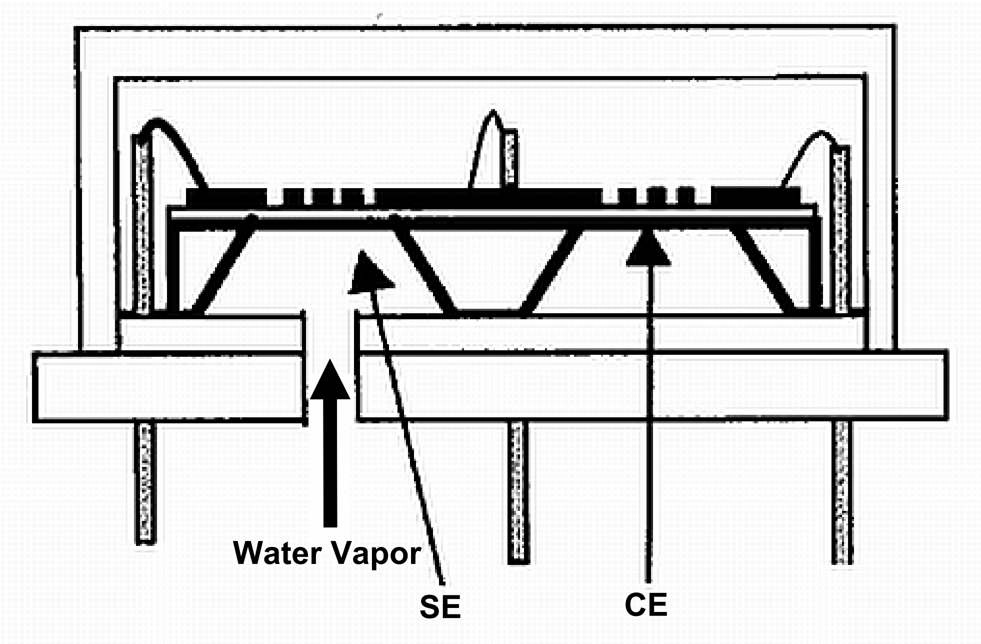

Figure 1.10: The cross sectional view of the thermal conductivity based humidity sensor structure [25].

1.3.6 Capacitive Humidity Sensors

Capacitive humidity sensors are based on dielectric constant changes of thin films during moisture absorption. There are several different types of materials used as humidity sensitive dielectric layers. Most widely used ones are polymers, ceramics, and porous silicon.

A compact, robust humidity sensor has been presented using WO_3 as the humidity sensitive ceramic [26]. The sensor has a sapphire base with a pair of interdigitated Pt film electrodes and a Pt film heater on both sides of sapphire. The WO_3 layer has been thermally evaporated on interdigitated electrodes. Test results have shown that the sensor capacitance has very high sensitivity to the humidity, due to the high humidity sensitivity of the dielectric constant of the ceramic film. A major disadvantage of the sensor is that the humidity response is highly nonlinear.

Another example of the ceramic humidity sensors is the thick-film humidity sensor based on a metal oxide, $MnWO_4$ [27]. Figure 1.11 shows a cross sectional view of the sensor structure. The sensor has a sandwich structure formed by depositing the $MnWO_4$ between Pt electrodes. The sensor has been fabricated on an alumina substrate and a refresh heater has been printed on the back side of the substrate. This sensor also has high sensitivity to humidity with nonlinear characteristics. Another important disadvantage of ceramic sensors is their high sensitivity to contaminants such as dust and smoke. However, this problem can be solved by burning out the contaminants by heating the sensor to temperatures around 400ºC.

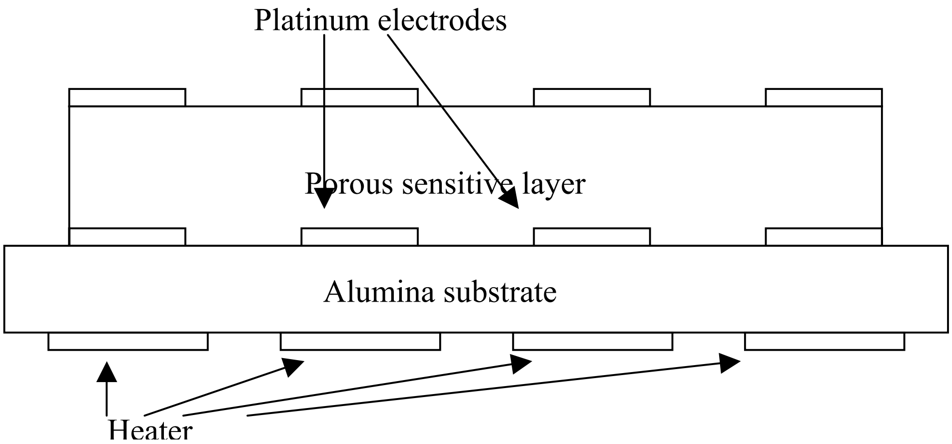

Figure 1.11: The cross sectional view of the capacitive humidity sensor with ceramic humidity sensitive layer [27].

Porous silicon is another widely used humidity sensitive dielectric, which is formed by anodic or galvanic etching of silicon in hydrofluoric acid [28]. A capacitive porous silicon humidity sensor with integrated refresh resistor has been presented [29]. The device consists of a capacitor with porous silicon dielectric, a refresh resistor and thermo-resistors. Figure 1.12 shows an SEM picture of the sensor. According to the test results, it has been found out that the humidity response of the sensor depends on the porous silicon formation conditions. An advantage of porous silicon humidity sensors is their stability at elevated temperatures. The major disadvantage is their nonlinear humidity response.

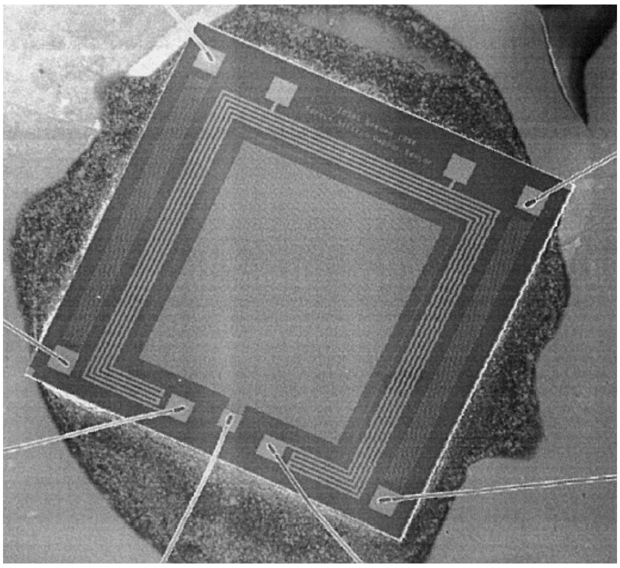

Figure 1.12: An SEM picture of the porous silicon capacitive humidity sensor [29].

Similar results have been obtained using oxidized porous silicon as the humidity sensitive dielectric layer [30]. In this work, the sensor has been attached to a thermo electric cooler (TEC). Measurement principle is to detect the increase of the capacitance during water condensation induced by cooling. An advantage of using TEC is that it can also be heated to refresh the sensor. This sensor also has shown nonlinear humidity response.

Capacitive humidity sensors based on polymer films have also been presented [31-37]. An example is the silicon dew-point detector using polyimide as the humidity sensitive polymer [33]. Figure 1.13 shows the top view of the sensor structure. The sensor has been formed by depositing polyimide on interdigitated electrodes. Two heaters and a thermometer have been integrated to the sensor area using metal resistors. An important feature of this device is that the sensor is formed on a silicon membrane of 50μm thickness, in order to improve the thermodynamic properties of the device.

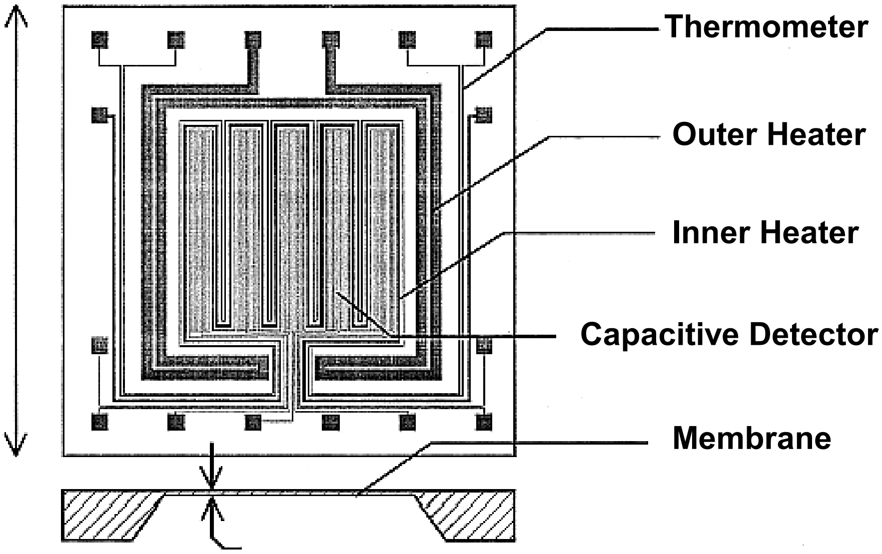

Figure 1.13: The top view of the capacitive dew point detector [33].

Another polyimide based humidity sensor has been developed for monitoring internal humidity level in anodically bonded hermetic micropackages [37]. The polyimide film has been sandwiched between two metal electrodes to sense moisture. The fabricated sensors have shown a linear response within the relative humidity range from 20% to 70%. Above 70% relative humidity, nonlinearity of the dielectric constant change of polyimide increases. Influence of the polyimide thickness on the sensitivity of the sensor has also been investigated. Test results have demonstrated that the sensitivity of the sensors increase with decreasing polyimide thickness.

In applications where high relative humidity values are measured, there is the risk of water condensation on the sensor surface. A method to measure high relative humidity levels has been proposed by integrating the sensor with a polysilicon heater [34]. Figure 1.14 shows the sensor structure. The polysilicon heater has been fabricated on top of a Si_3N_4 layer underneath the sensor. In addition, the response time of the sensor has been improved by allowing the moisture to diffuse into polyimide film circumferentially. This sensor also has linear humidity response. It has been verified that the heater can be used to estimate the high relative humidity values with an error of 2% relative humidity.

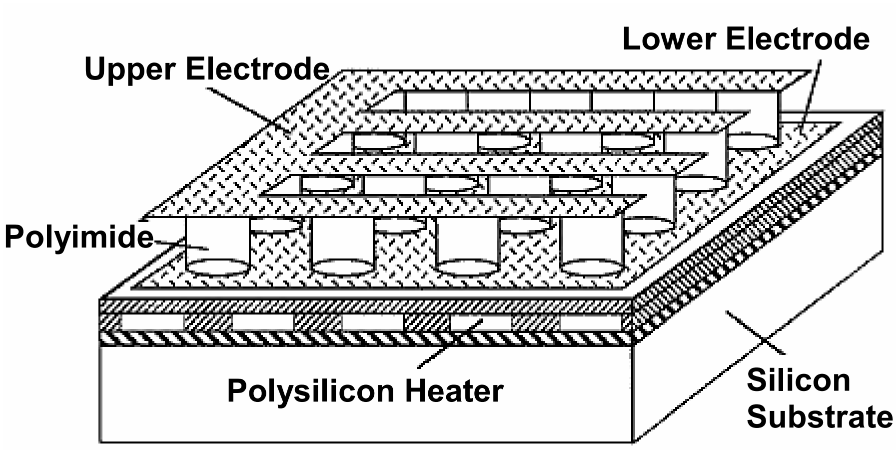

Figure 1.14: The capacitive humidity sensor with cylindrical polyimide columns integrated with polysilicon heater [34].

A major advantage of the polyimide films is their compatibility with standard CMOS fabrication. This property has been used to obtain capacitive humidity sensors using CMOS fabrication [36]. Humidity sensing property has been achieved by deposition of the polyimide film on the chip after the standard CMOS fabrication. Figure 1.15 shows a picture of the fabricated humidity sensor chip.

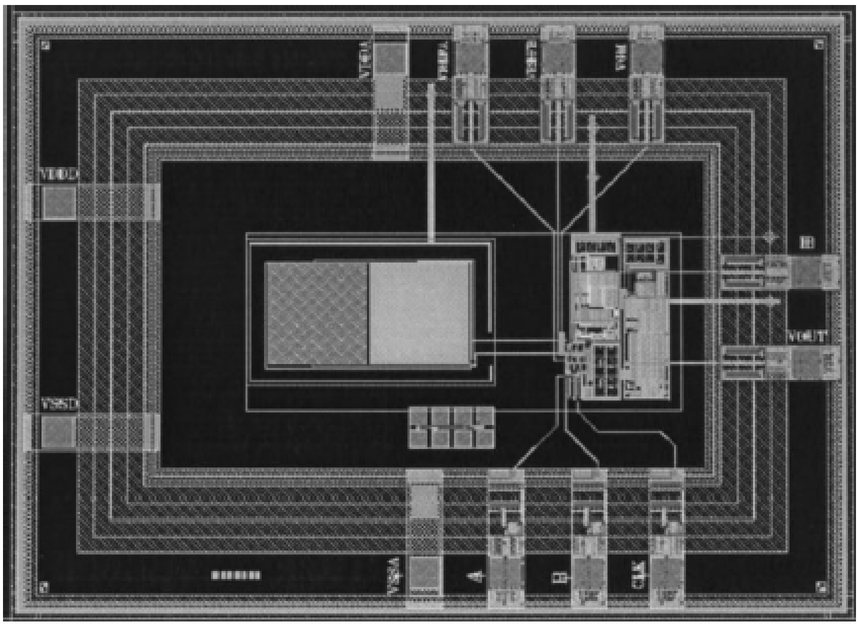

Figure 1.15: The capacitive humidity sensor fabricated in a standard CMOS process [36].

Capacitive humidity sensors based on polyimide thin films have the advantage of high sensitivity, linear response, and low power dissipation. In addition, polyimide films are compatible with standard CMOS fabrication, which allows the monolithic integration of the sensors with the readout circuitry. The major disadvantage of the polyimide thin films is their long term stability and chemical durability problems in harsh environments [38].

1.4 Research Objectives and Thesis Organization

In this thesis work, it was aimed to develop humidity sensors using surface micromachining and standard CMOS processes. Two different humidity sensors were designed; one of them is based on capacitive technique, while the other one is based on thermal properties of water vapor. Specific objectives of the thesis work can be summarized as follows:

1. Development of a polyimide based capacitive humidity sensor with an integrated heater, which is capable of providing humidity measurement at high relative humidity conditions.

2. Development of a CMOS readout circuit for capacitive humidity sensors. Integration of the fabricated humidity sensors with the readout circuit.

3. Characterization of the capacitive humidity sensors at different ambient temperature conditions. Performing hysteresis and response time measurements.

4. Development of a thermal conductivity based humidity sensor using standard CMOS fabrication and post-CMOS processing. Integrating the sensor with the readout circuit monolithically using standard CMOS fabrication.

5. Measurement of the humidity response and the hysteresis characteristics of the thermal humidity sensor at different temperatures.

The research started with a literature search on the humidity sensors that have been developed using various different measurement techniques. After the decision on the method to be focused on in this study, masks of the sensor layers were designed. Fabrication of the capacitive sensors was processed in the clean room facilities of METU. Readout circuit for the capacitive humidity sensor was designed and fabricated in AMS 0.8μm CMOS process. Thermal conductivity based humidity sensor was designed and fabricated in AMS 0.6μm CMOS process. Characterization tests of the sensors were performed in testing laboratories of METU. Rest of the thesis is organized as follows:

Chapter 2 describes the design of the capacitive humidity sensor and the integrated heater. This chapter discusses the important geometrical parameters that affect the sensor performance. The theory of self heating is also explained and the thermal simulations of the integrated heater are presented. Finally, mask layouts of the sensors are given.

Chapter 3 presents the CMOS readout circuit developed for capacitive humidity sensors. This chapter includes a summary of the capacitive readout techniques that have been presented in the literature. Design of the analog and digital blocks of the readout circuit are explained, and the chip layout is given.

Chapter 4 presents the characterization results of the capacitive humidity sensors. Humidity response of the capacitive sensors is demonstrated with the hysteresis test results and the response time measurements. Characterization results of the integrated heater are also presented, and the effect of heating on the sensor response is investigated. This chapter also presents the characterization results of the hybrid humidity sensor module, which is obtained by connecting the capacitive sensor with the readout circuit.

Chapter 5 describes the design of a thermal conductivity based humidity sensor developed in a standard CMOS process. This chapter discusses the effect of structural parameters on the sensor performance and presents the layout of the sensor. In addition, design of the readout circuit is explained, and the post processing of the chip is discussed. This chapter also includes the characterization results of the thermal conductivity based humidity sensor.

Finally, Chapter 6 presents the conclusions of the thesis and gives suggestions for future studies.

CHAPTER 2

A CAPACITIVE HUMIDITY SENSOR WITH AN INTEGRATED HEATER

This chapter presents the design and implementation of a capacitive type humidity sensor with an integrated heater. Section 2.1 discusses polyimide films and their important characteristics for humidity sensing applications. These characteristics include some figures of merit such as sensitivity, long term stability, chemical durability and also processing methods in microfabrication. Sections 2.2 and 2.3 describe the capacitive sensor and integrated heater structures, respectively. These sections also include some theoretical calculations and simulation results regarding the performances of the sensor and the heater. Following sections present the fabrication and test results of both the sensor and the heater. Finally, test results are discussed, and further improvements are proposed.

2.1 Polyimide as a Humidity Sensitive Material

Polyimide films are developed for electronic industries to be used as interlayer dielectrics, passivation layers, and stress buffers. They also have applications in the field of integrated circuit fabrication as inter-metal dielectrics, sacrificial layers, and surface planarizers [38].

There are several reasons that make polyimide films have applications in microelectronics industry. The polyimide is chemically inert in its cured form, and thermally stable material up to temperatures around 450 °C. In addition, it is a perfect planarizer used to planarize irregular surfaces. It also has a low relative permittivity and high breakdown voltage, which makes it desirable for high speed applications. However, it has some important disadvantages for the integrated circuit fabrication. Most important disadvantage is its high humidity sensitivity, which results in humidity dependency of the output response of circuits. Although this property is unwanted in microelectronic circuits, it makes polyimide films very attractive for humidity sensing applications. Being thermally stable and fully compatible with silicon processing technology, polyimide is the most widely used humidity sensitive dielectric in capacitive humidity sensors.

Humidity responses of polyimide films have been investigated in many works [31-35]. Experiments show that the dielectric constant of polyimide films change from about 3 to 4 as the relative humidity changes from 0%RH to 100%RH. Moreover, the dielectric constant change with respect to the humidity change is almost linear especially within the 20%RH to 70%RH range. Polyimide deposition can be performed at the end of a CMOS fabrication process, and therefore humidity sensors, which are monolithically integrated with the readout circuit, can be obtained [36]. Major drawbacks of polyimide films can be stated as long term stability and chemical durability problems [38]. In harsh environments, humidity responses of polyimide films may drift in time. In addition, the presence of water for a long time may cause the failure of the device.

Polyimide films can be divided into two groups according to the method that they are processed in microfabrication. Photosensitive polyimide films are processed like photoresists. They are masked, exposed to UV light, and patterned by their own developers. Non-photosensitive polyimide films are patterned by dry or wet etching like a regular layer in microelectronics, so an additional photolithography step is required in the fabrication. On the other hand, using photosensitive polyimide films considerably reduces the number of processing steps and makes the process easier. Furthermore, since they are directly masked and developed, the resulting pattern has better defined features.

2.2 Sensor Design

In this study, a capacitive humidity sensor with a sandwich structure was designed. The sensor is simply a capacitor with two metal electrodes and a polyimide layer as the humidity sensitive dielectric. Figure 2.1 shows a symbolic view of the sensor structure.

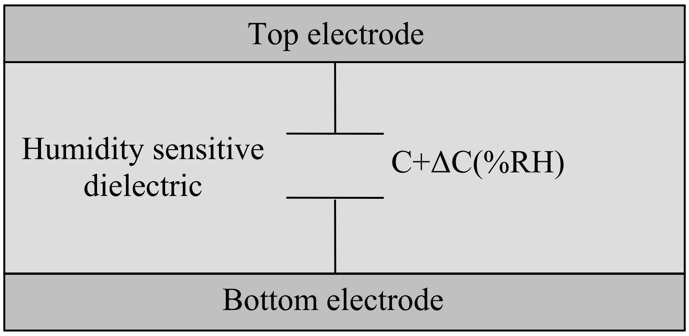

Figure 2.1: A symbolic view of the sensor structure. It is a variable capacitor with two metal electrodes and a dielectric layer.

The capacitance of the capacitor changes with respect to %RH due to the humidity sensitive dielectric constant of the polyimide layer. The capacitance of the capacitor is expressed as:

$$C = \varepsilon \times \frac{A}{d} \tag{2.1}$$

where ε is the permittivity of the dielectric, A is the area of the capacitor, and d is the dielectric layer thickness. The permittivity of the dielectric can be written as:

$$\varepsilon = \varepsilon_i + \alpha \times RH \tag{2.2}$$

where ε_i is the initial permittivity of the dielectric, RH is the relative humidity, and α is the humidity sensitivity of the permittivity, which is a constant assuming that the humidity sensitivity is linear. If Equation 2.2 is inserted into Equation 2.1, the capacitance is written as:

$$C = \varepsilon_i \times \frac{A}{d} + RH \times \alpha \times \frac{A}{d} \tag{2.3}$$

In the sandwich structure, the area of the capacitor is equal to the area of the metal electrodes. In microfabrication, there is no limitation on the surface area of a deposited metal, so very high capacitance values can be achieved using the sandwich structure. This is the major advantage of the sandwich shaped capacitors over the interdigitated electrode capacitors where the capacitor area is dependent on the electrode thickness, which is limited by the process. High capacitance values make it easier to convert the capacitance change into voltage change using electronic circuits, since the effect of parasitic capacitances becomes less important.

The most important parameter of a capacitive humidity sensor is its sensitivity. In capacitive humidity sensors, the sensitivity of a device is generally expressed in capacitance per %RH form. From Equation 2.3, sensitivity of the sensor is found as:

$$S = \alpha \times \frac{A}{d} \tag{2.4}$$

The sensitivity is directly related with the humidity sensitivity of the polyimide film and the geometry of the sensor. It should be noted that the sensitivity increases with increasing initial sensor capacitance. The sensitivity of a sensor can also be increased by increasing the amount of moisture absorbed by the polyimide layer [37]. In order to increase the amount of absorbed moisture, the top electrode of the sensor is designed in a meshed structure. This way, a wider access path is provided for the moisture into the polyimide film, so the sensitivity of the sensor is improved. Figure 2.2(a) shows the structure of the top electrode.

Another important parameter of humidity sensors is the response time. The response time is directly proportional to the contact area of the polyimide layer with the humid environment [34]. It is important to realize that the polyimide under the openings of the top electrode does not affect the capacitance much. This means that if the polyimide layer which lies underneath the metal parts of the top electrode has a wide contact surface with the moisture, the response time is improved. This is achieved by patterning the polyimide layer with the same meshed structure of the top electrode. This fact is explained in Figure 2.2(a) and 2.2(b) showing the top and the side views of both the top electrode and the polyimide layer.

It is observed from Figure 2.2 that the polyimide layer has an extension from the sides. This extension not only increases the absorption surface area but also provides a safety margin for precision errors in the process. If the two layers are tried to be exactly matched, there may be short circuit problems between the two metal electrodes due to lithography errors during the fabrication.

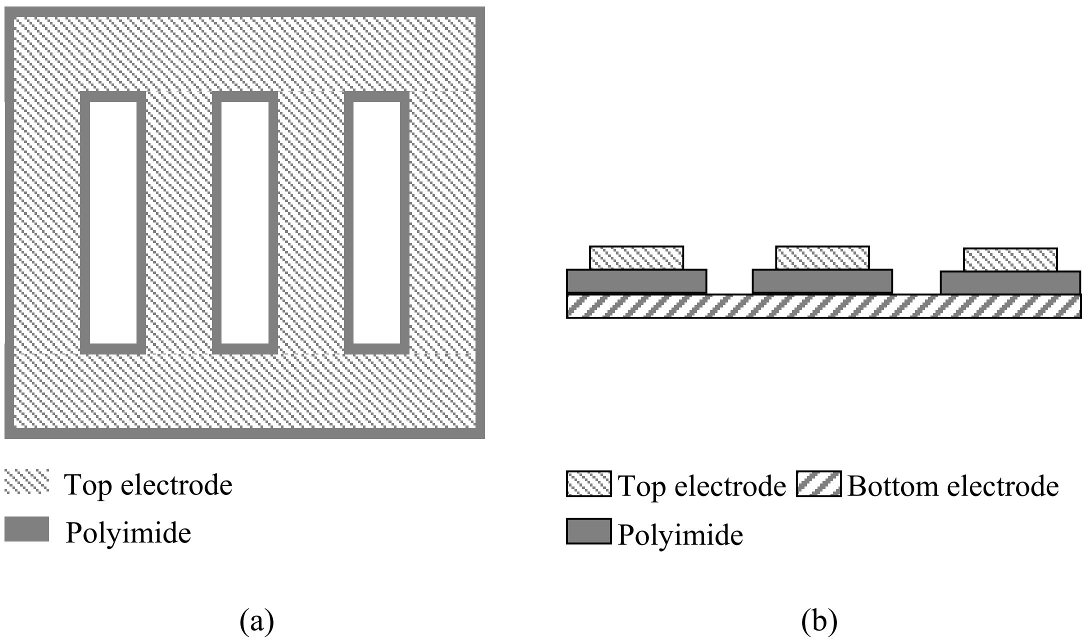

Figure 2.2: (a) Top views of both the top electrode and the polyimide layer, (b) cross section of the structure.

Another important issue to be discussed is the polyimide thickness. From the sensitivity expression derived above, it is observed that the sensitivity is inversely proportional to the thickness of the polyimide film. In order to increase the sensitivity of the sensor, the polyimide film thickness should be reduced. It is obvious that the thickness of the polyimide film can not be reduced below a certain value due to the limitations coming from the process. As a result, it can be stated that the sensitivity of the sensor is limited by the process.

In this work, two different capacitive sensor structures were designed. The difference of two types is the thicknesses of the metal parts of the top electrodes and the opening widths for moisture diffusion. One mask is required for the fabrication of one layer, so three masks were designed for each sensor. Figures 2.3, 2.4, and 2.5 show the mask layouts drawn in the CADENCE software. Table 2.1 summarizes the layout dimensions and expected capacitance values. It should be noted that the bottom electrode has exactly the same shape with the top electrode in the mask layout, which reduces the parasitic capacitance.

Table 2.1: Design parameters of the two humidity sensors mask layouts. Pad frame and dicing lines are not included in the total area calculation. Expected capacitance values are calculated for 0.5 μm polyimide thickness.

	Layout 1	Layout 2
Total Area (mm^2)	1	1
Effective Area (mm^2)	0.525	0.55
Metal Line Width (μm)	25	50
Opening Width (μm)	25	50
Expected Capacitance (pF)	30.665	32.126

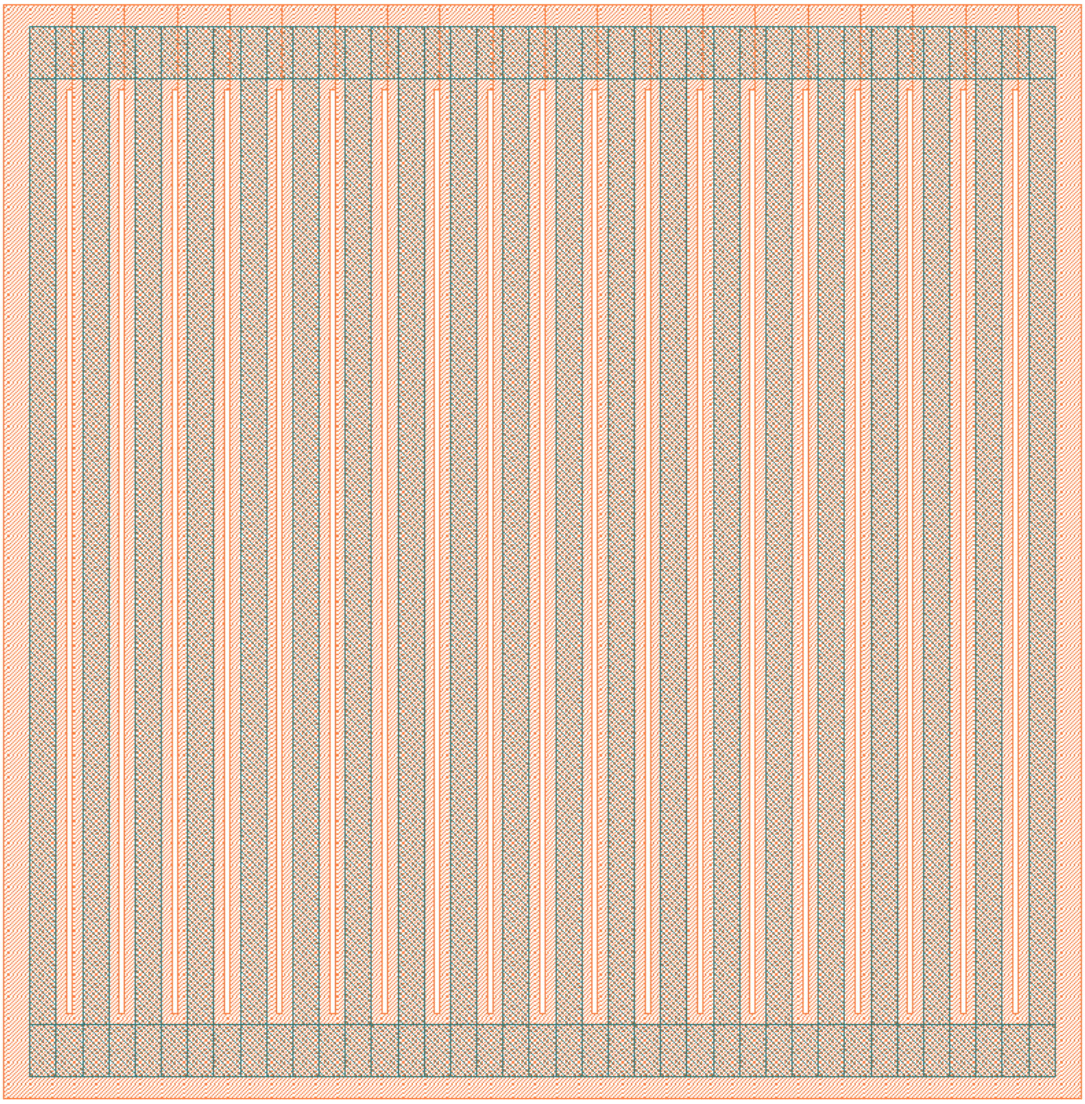

Figure 2.3: The layout of the capacitive humidity sensor with 25µm metal line width. Total layout dimensions are 1mm x 1mm.

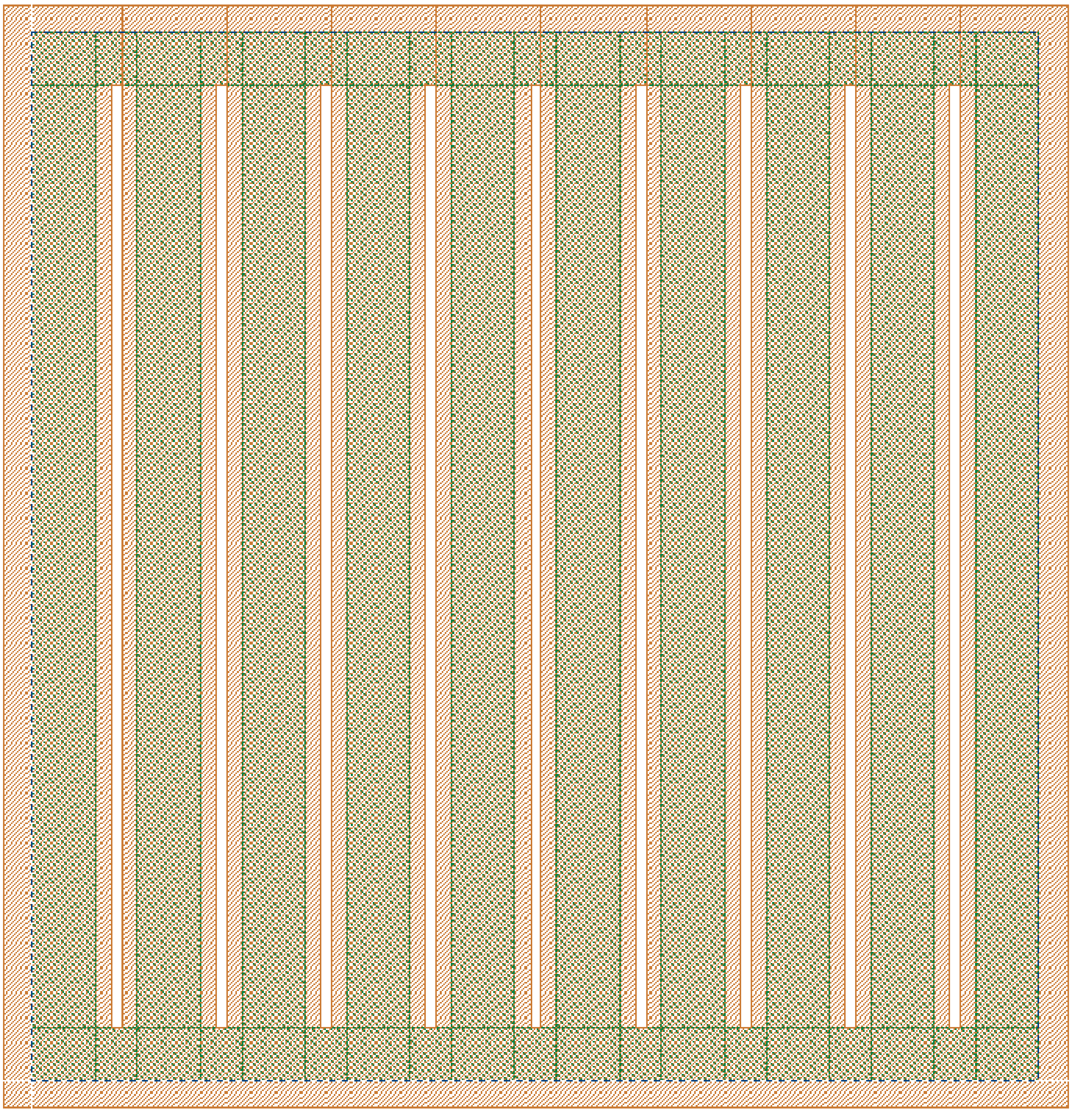

Figure 2.4: The layout of the capacitive humidity sensor with 50µm metal line width. Total layout dimensions are 1mm x 1mm.

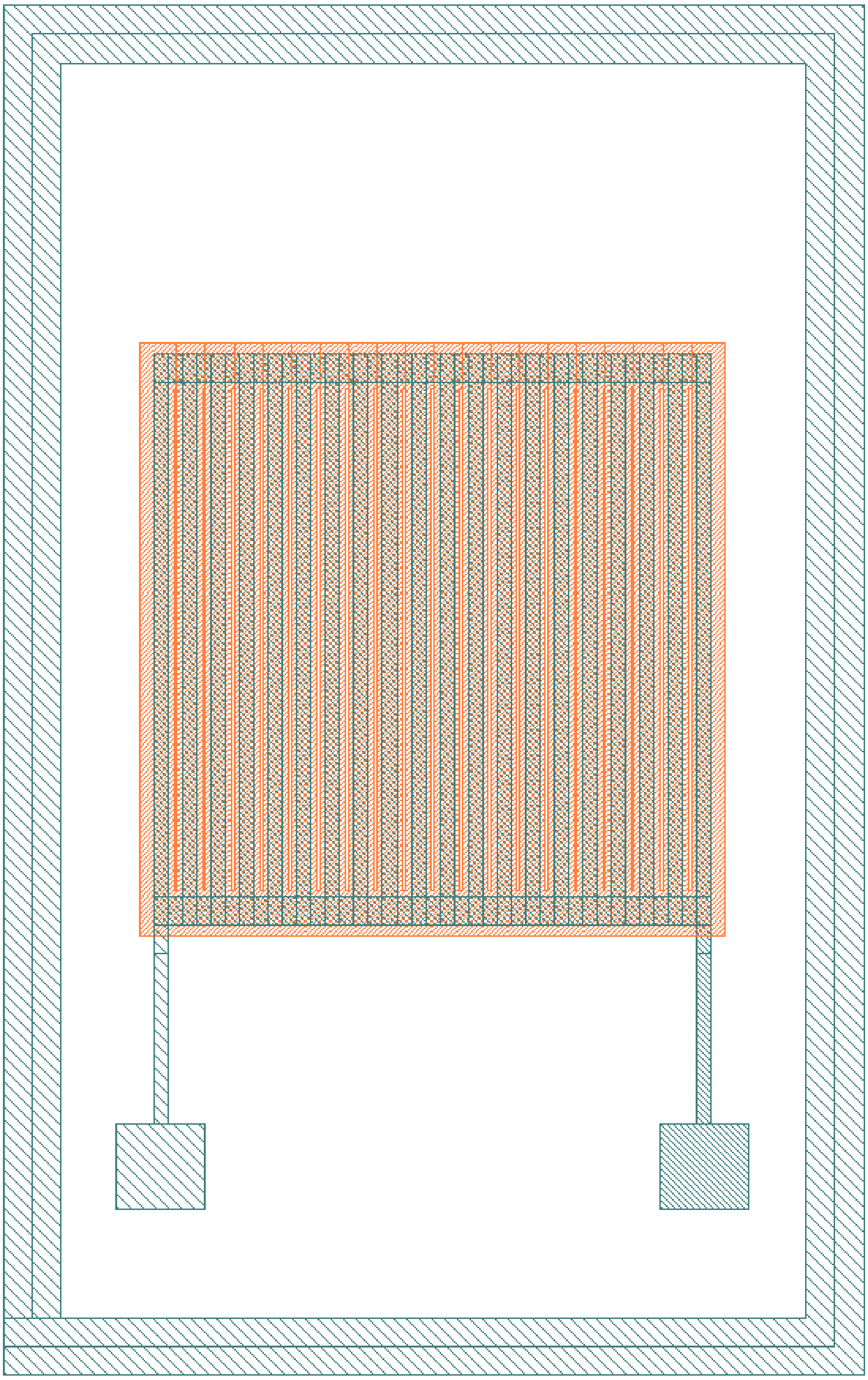

Figure 2.5: The layout of the capacitive humidity sensor with 25µm metal width including the pads and dicing lines. Total layout dimensions are 2400 µm x 1500 µm.

2.3 Integrated Heater Design

In some humidity sensing applications, implementation of a heater with a humidity sensor is necessary as discussed in Chapter 1. In general, the heater is implemented around or underneath the sensor with a resistor structure or a discrete heating element is attached to the sensor. These methods require extra fabrication steps or complex packaging, which increase the cost of the device.

The capacitive humidity sensor developed in this study is integrated with a heater using a different approach than the reported ones in literature. Bottom electrodes of the humidity sensors are designed in a meander resistor shape as demonstrated in Figure 2.6. This shape provides a high thermal resistance, which allows the material to heat up to higher temperatures by lower power dissipation.

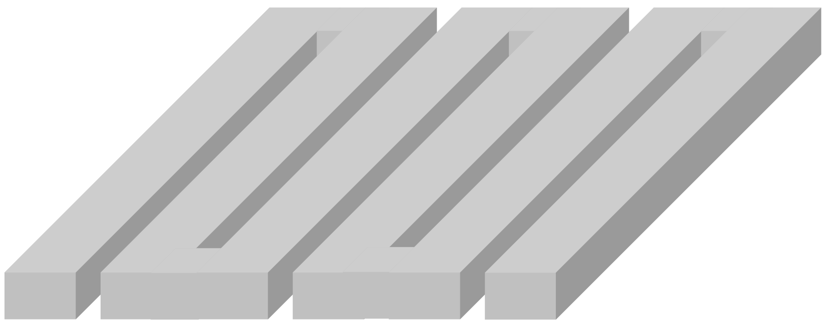

Figure 2.6: Three dimensional view of the bottom electrode designed in heater resistor shape.

Heater resistors are biased with a constant voltage or current source, and the heating is achieved by dc power dissipation on the resistor. Self heating of a resistor driven with a voltage source can be represented with a lumped element thermal circuit, which is shown in Figure 2.7 [39]. The circuit contains a dependent current source that supplies the heating power, a thermal capacitor that stands for the heat capacity, and a resistor representing the thermal resistance. If the circuit is solved for the steady state conditions, the relation between dissipated power and temperature change is found as:

$$P = G_{th} \times \Delta T \tag{2.5}$$

where P is the dissipated power, ΔT is the temperature difference, and G_{th} is the thermal conductance of the material [39]. The thermal conductance is given as:

$$G_{th} = \sigma \times \frac{A}{l} \tag{2.6}$$

where l and A are the length and cross sectional area of the resistor respectively, and σ is the thermal conductivity, which is a specific value for the material that forms the resistor. It is obvious that the thermal conductance of the resistor decreases with the decreasing cross sectional area or the increasing length. It can be concluded from Equation 2.5 that if the resistor has a lower thermal conductance, it can be heated with less power.

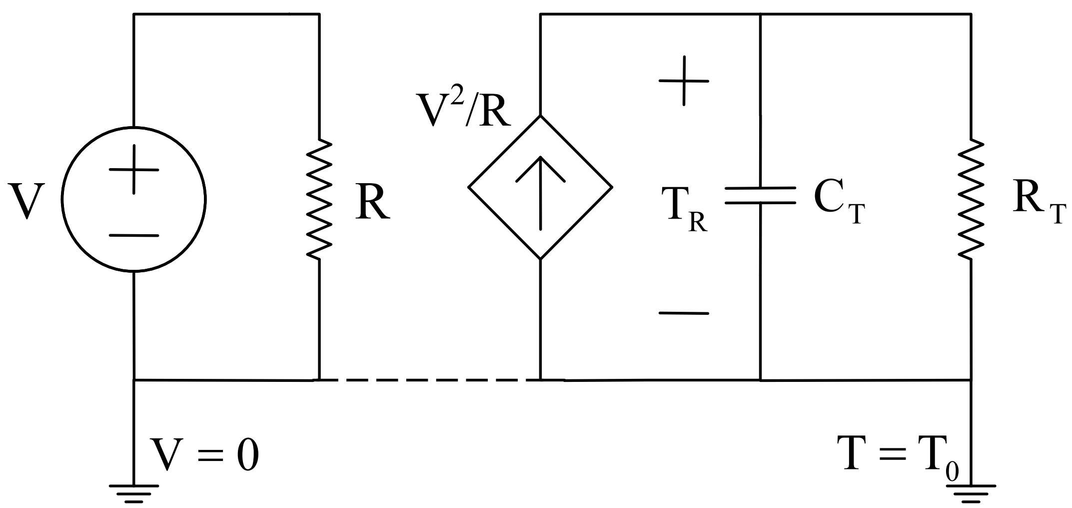

Figure 2.7: The schematic of the lumped element thermal circuit representing the self heating of the heater electrode.

Two different mask layouts were designed for the heater electrodes of the two sensor structures demonstrated in the previous section. It should be noted that the masks for the polyimide layer and the top electrode are exactly same as the previously demonstrated layouts. Only the mask for the heater electrode was modified according to the heater resistor shape. Figures 2.8 and 2.9 show the mask layouts for the heater electrodes and the layout including the pad frame and dicing lines respectively. Table 2.2 summarizes the expected resistance and the thermal conductance values of the two heater structures assuming that the heaters are 0.5μm thick aluminum.

Table 2.2: Expected resistance and the thermal conductance values of the heater electrodes. The resistivity and the thermal conductivity of aluminum were taken as 2.665×10^{-8} Ω.m and 237 W/m.K respectively.

	Layout 1	Layout2
Resistance (Ω)	43	11
Thermal Conductance (W/K)	1.46×10^{-7}	5.72×10^{-7}

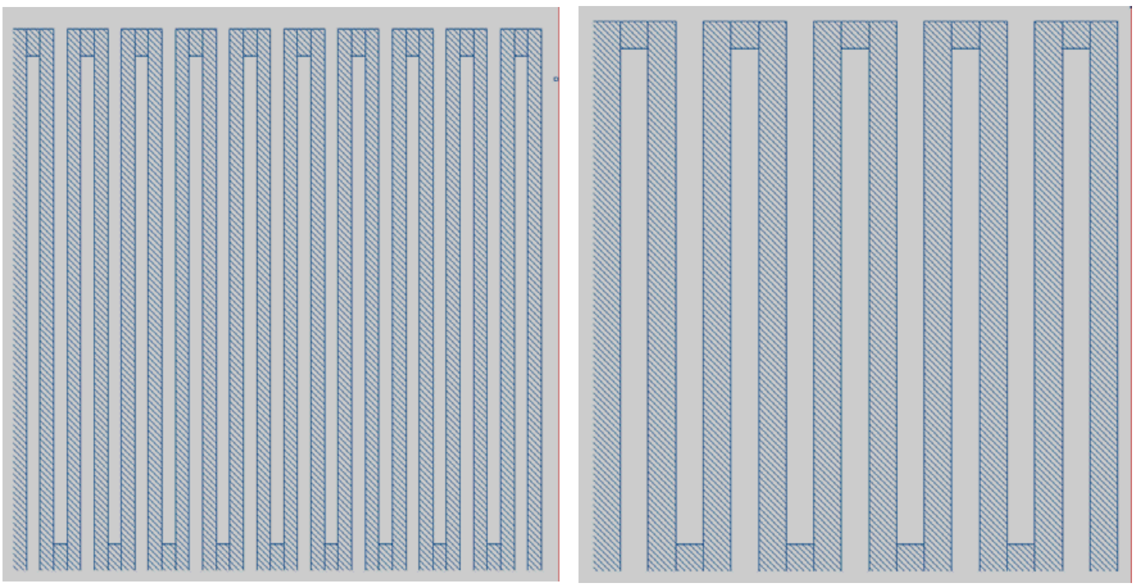

(a) (b)

Figure 2.8: The layout of the heater with (a) 25μm, (b) 50μm metal width.

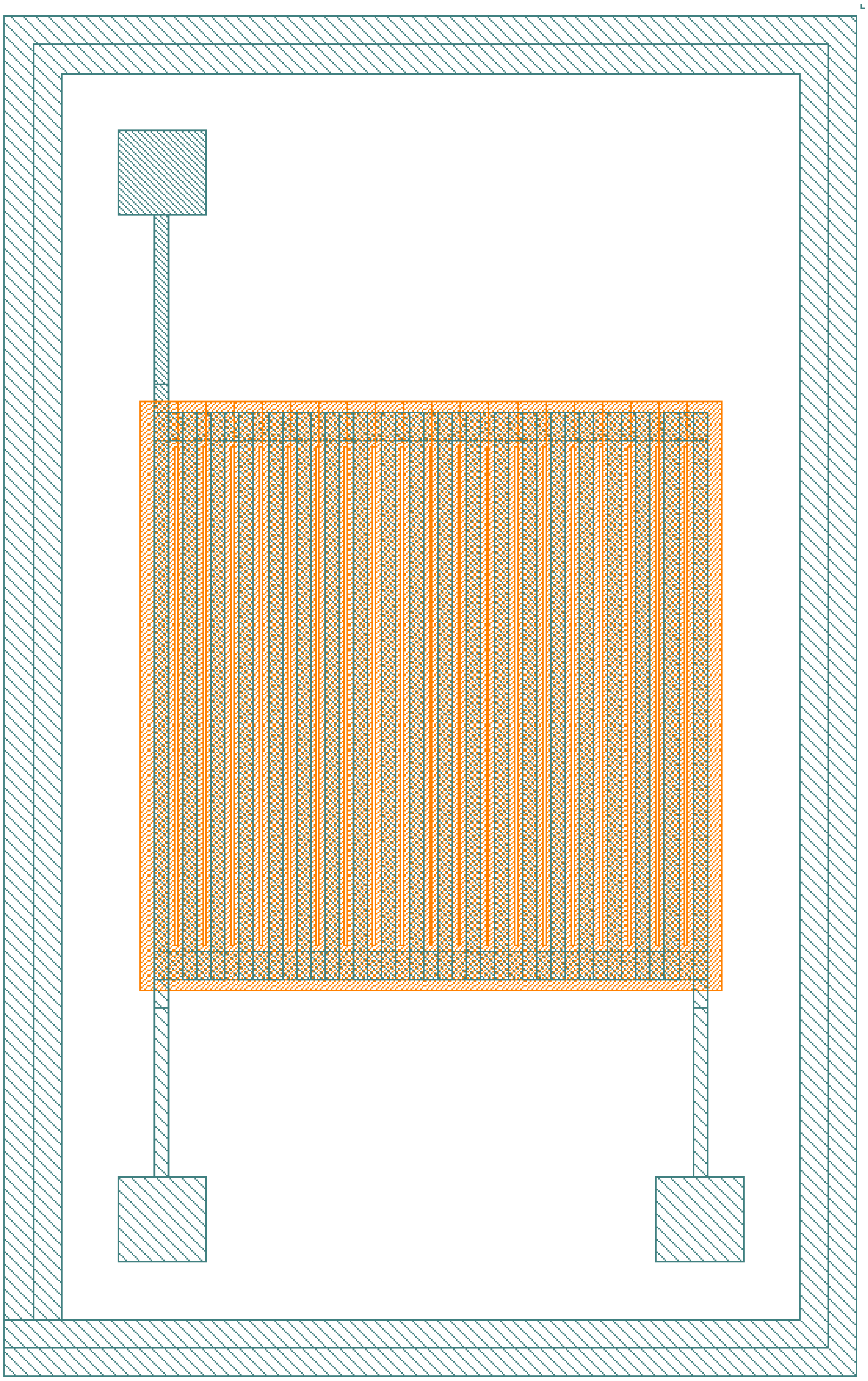

Figure 2.9: The layout of the capacitive humidity sensor with heater electrode including the pad frame and dicing lines. Layout dimensions are 2400 x 1500 µm.

In the capacitive humidity sensor application, the capacitor is built on a silicon base. It is well known that the silicon has a high thermal conductivity, which increases the thermal conductance of the overall structure. Consequently, fabricating the sensor on a silicon wafer prevents the resistor from heating up to the desired temperature levels. In order to reduce this effect, the sensor is fabricated on silicon dioxide, which has a low thermal conductivity. This way, the sensor is thermally isolated from the substrate. Fabricating the sensor on the silicon dioxide has the disadvantage that a parasitic capacitance is formed between the sensor and the substrate. Figure 2.10 shows the cross section of the final structure. It should be mentioned that another way to decrease the thermal conductance is to fabricate the sensor on a glass substrate, which does not introduce any parasitic capacitance.

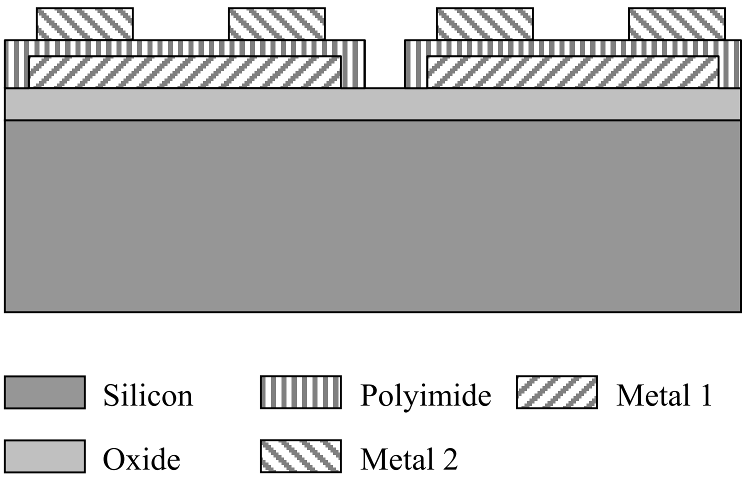

Figure 2.10: The cross sectional view of the capacitive humidity sensor with the heater electrode.

It should be noted that the temperature that the resistor reaches at a given dc power dissipation can not be directly calculated from Equation 2.5. There are other sources of heat transfer such as convection and radiation, which affects the final temperature of the resistor [39]. In addition, the surfaces that the resistor touches generate thermal conduction paths, which may reduce the final temperature of the device. In the final temperature calculations, these effects can be taken into account by the help of computer simulations.

2.3.1 Thermal Simulations

The self heating of the heater electrodes are simulated using the MemETherm tool of the ConventorWare software. This tool solves the conservation of the electrical charge and the thermal energy to compute the steady state potential and temperature fields. For the self heating problem, boundary conditions are specified as voltages applied to the two pads of the heater electrode.

Table 2.3 summarizes the information required for the thermal simulation. In the simulation, 100mW dc power is applied to the heater electrode. Simulation results show that the temperature of the sensor increases up to 483K, which shows that the heater idea works. Overall thermal conductance of the structure is calculated as 2.07×10^{-4} W/K. Figure 2.11 shows the CoventorWare windows that demonstrate the simulation results.

Table 2.3: Thickness, thermal conductivity, and electrical resistivity values of the capacitive humidity sensor layers used in the thermal simulation.

Layer	Material	Thickness (μm)	Thermal Conductivity (W/m.K)	Electrical Resistivity (Ω.m)
Base	Silicon	350	148	2300
Dielectric 1	SiO_2	1	1.3	10^{15}
Metal 1	Aluminum	0.5	237	2.665×10^{-8}
Dielectric 2	Polyimide	0.5	0.14	10^{15}
Metal 2	Cr/Au	0.2	205	7.625×10^{-8}

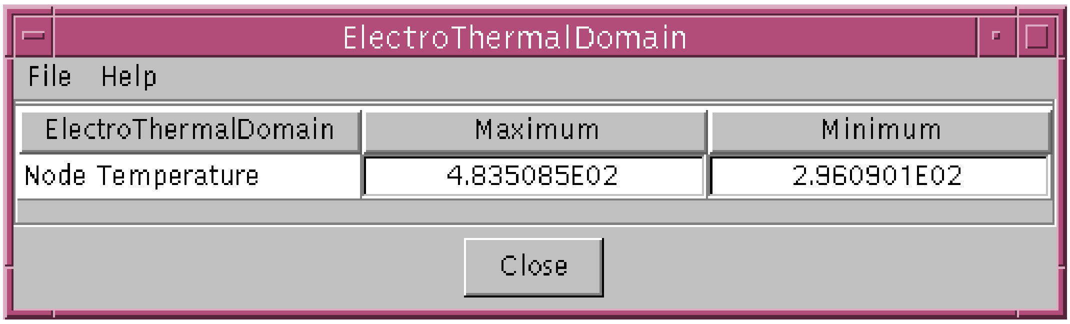

(a)

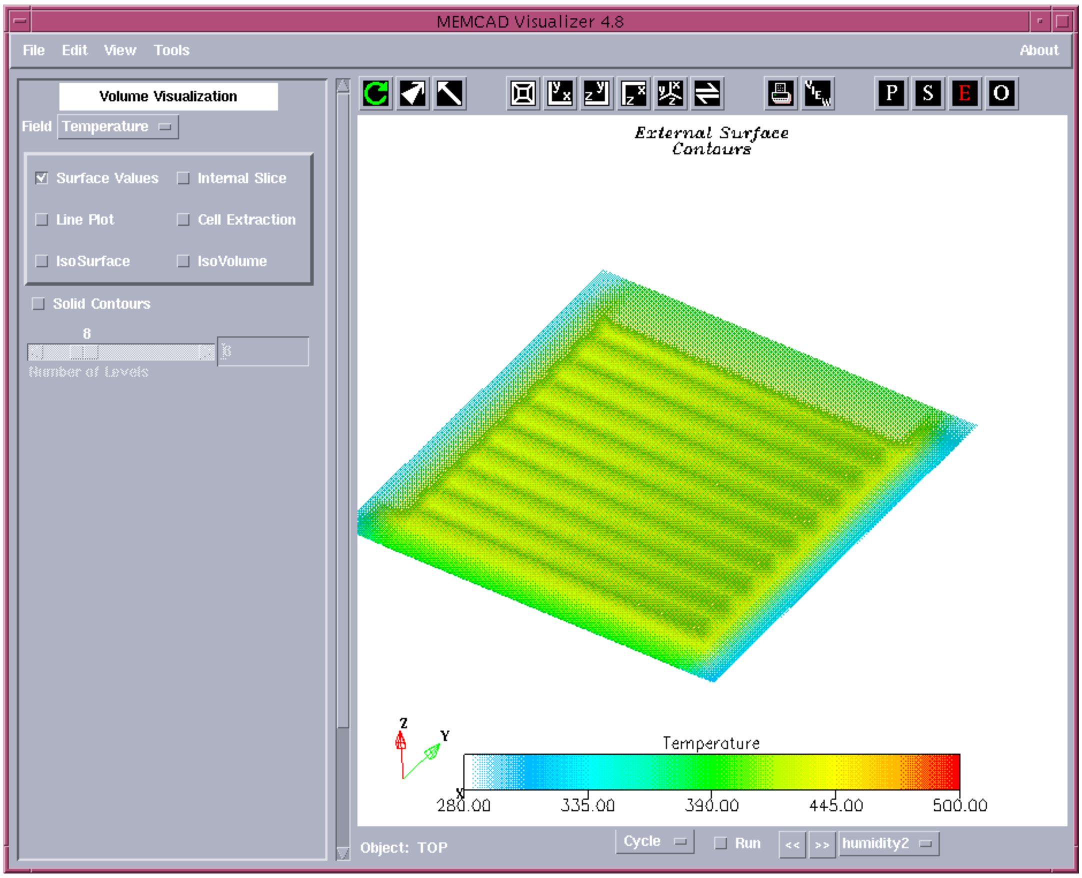

(b)

Figure 2.11: CoventorWare windows that demonstrate the simulation results: (a) maximum and minimum node temperature values, and (b) temperature distribution of the sensor. Since the silicon base is very thick compared to the other layers, it is not shown. Maximum temperature of the sensor reaches to 483 K at 100mW dc power dissipation

2.4 Device Fabrication

Fabrication of the capacitive humidity sensors has three main steps. These are two metallization and one polyimide deposition steps, which require lithography and patterning operations.

The first metallization is performed by the sputter deposition technique. In the sputter deposition, a target material which is to be deposited is bombarded by argon ions. This is achieved by keeping the target material at a negative potential and creating positively charged argon ions by the help of an electric field. The target material is sputtered away by momentum transfer, and ejected surface atoms are deposited on the substrate placed on the anode.

In the fabrication of the bottom electrode, Al is sputtered on SiO_2 coated three inch wafers at 2kW power for 20 minutes using a magnetron sputtering system, which results in 0.5μm aluminum thickness. Patterning of the bottom electrode is performed using wet etching technique, using a mixture of acetic acid, nitric acid, phosphoric acid, and de-ionized water.

The second layer of the capacitive humidity sensor is the humidity sensitive dielectric layer. A negative photo definable polyimide (PI2723) was used as the dielectric layer. Photo definable polyimide films can be directly patterned by photolithography as explained in Section 2.1. Table 2.4 gives the polyimide process flow in detail.

The most critical step of the polyimide process flow is the spin coating step, which determines the polyimide film thickness, so the sensitivity of the sensor. In this step, the spin speed can be varied for different wafers so that humidity sensors with different initial capacitance values can be obtained. Figure 2.12 gives the spin speed versus film thickness curve for the polyimide PI2723.

Table 2.4: Process flow for polyimide coating and patterning.

Step #	Process Details	
1	Dehydration Bake	30ºC 30 min. in convection oven
2	Spin Coating	4500 rpm. 35 sec.
3	Soft Bake	4 min. 75ºC on hot plate
4	UV Exposure	200 mJ/cm^2
5	Development	45 sec. in DE6180 developer
6	Overlap	7 sec. in Developer/Rinser
7	Rinse	45 sec. in RI9180 rinser
8	Cure	30 min. 400ºC in convection oven

It should be mentioned that the curing step also reduces the film thickness. The curing temperature given in Table 2.4 is a standard value given in the process documentation of the polyimide PI2723. However, a different curing approach is present for capacitive humidity sensor applications in order to reduce the film thickness further [37]. Polyimide was cured on a hot plate, ramping up the temperature from 100ºC to 300ºC with 100ºC increments and 30 minute cure at each temperature. This way, it is possible to reduce the film thickness to the one fourth of the values given in Figure 2.12.

The last step of the fabrication is the formation of the top electrode by lift-off technique. In the lift-off technique, photoresist is coated and patterned in such a way that the regions that the metal will remain are removed. The metal is then deposited and patterned by lifting off the photoresist. This method is preferred in the formation of the top electrode because it does not require any etching process. In an etching process, there is the risk of damaging the pad connections of the bottom electrode, which are unprotected.

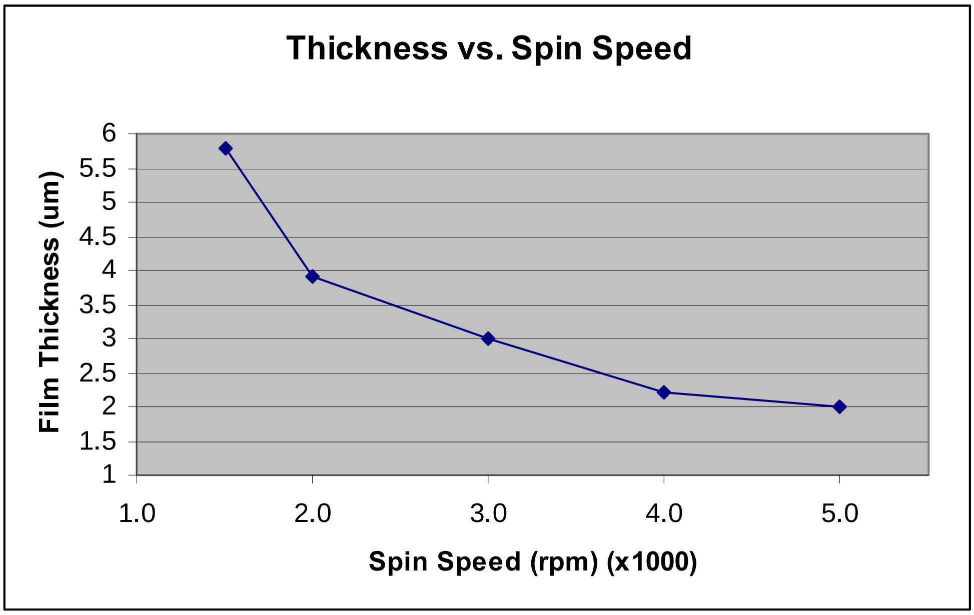

Figure 2.12: Thickness versus spin speed graph for the polyimide film used as the dielectric layer.

The top metal layer is patterned using lift-off process. A Cr/Au layer (200Å/1800Å) is deposited on top of photoresist PR2823 by evaporation. Evaporation was preferred in the deposition because evaporated films have poor step coverage so that the photoresist under the metal layer can easily be removed using the lift-off process. In addition, PR2823 is a relatively thick photoresist, which also makes the removing process easier.

Another important point about the final metallization step is the adhesion of the metal layer to the polyimide. Polyimide films generally have very smooth surfaces such that metal films can not adhere easily. This may cause the peeling of the metal completely from the surface during the lift-off. In order to prevent this problem, wafers are kept in oxygen plasma for one minute before the metal deposition. This way, the surface of the polyimide film becomes rough such that the metal can stick on it easily. Details of the fabrication process flow of the capacitive humidity sensor are given in the Appendix.

2.5 Conclusion

This chapter presents the design and fabrication of a capacitive humidity sensor with an integrated heater. The integrated heater is implemented by fabricating the bottom electrode of the capacitive humidity sensor in a heater resistor shape. Two types of capacitive humidity sensors are developed. Their difference is the opening widths for moisture diffusion and dimensions of the heater electrodes. Expected capacitances of the humidity sensors are around 30pF for 0.5μm polyimide film thickness. The fabrication of the sensors is completed in three mask process. Next chapter presents the design of a switched capacitor readout circuit for capacitive humidity sensors, and Chapter 4 presents the fabrication and test results of the capacitive humidity sensors and the readout circuit.

CHAPTER 3

THE CAPACITIVE READOUT CIRCUIT

This chapter presents the design and implementation of a switched capacitor CMOS readout circuit for capacitive humidity sensors. Section 2.1 summarizes the capacitive readout techniques present in the literature, including the RC oscillator, switched capacitor integrator, and capacitance to current converter circuit structures. Section 2.2 describes the readout circuit structure designed in this study and its operating principle. This section also includes the design of the building blocks of the circuit. Finally, Section 2.3 briefly explains the floor planning of mixed signal circuits and demonstrates the layout of the chip.

3.1 Capacitive Readout Techniques

Capacitive sensors require readout circuits that convert the capacitance change into voltage change for further signal processing of the sensor outputs. There are various techniques of capacitance reading reported in literature. Among these techniques, the most important ones are the RC oscillator and the switched capacitor integrator circuits. Based on these fundamental techniques, different circuit structures and output signal processing methods have been developed and presented [40-44]. Following subsections explain some of these readout techniques.

3.1.1 RC Oscillator

RC oscillators are the oldest circuits used for reading capacitance change. In this method, the sensor capacitor is charged and discharged through a resistive path in order to create an oscillating output [43]. The frequency of the output is measured, which is proportional to the sensor capacitance.

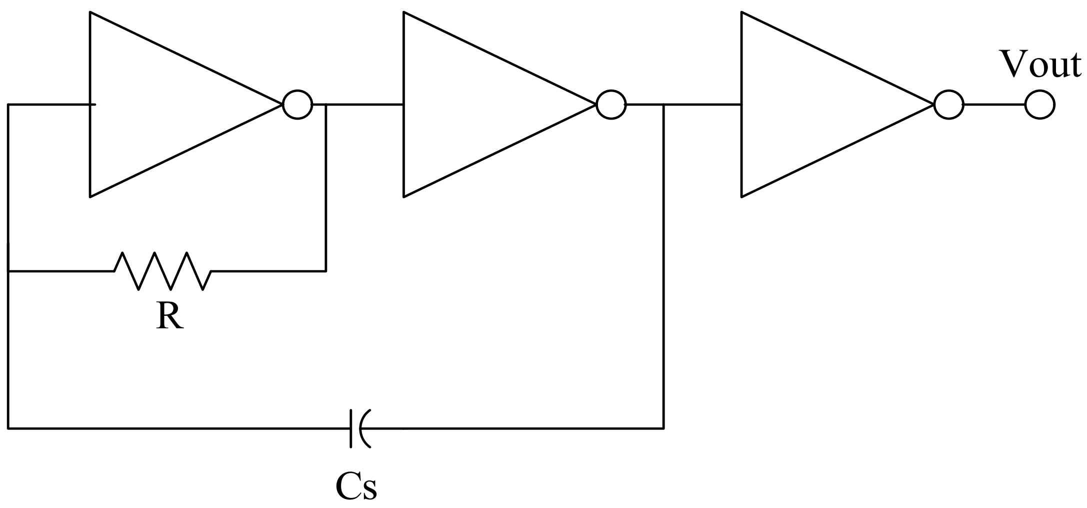

Figure 3.1: RC oscillator circuit structure.

Figure 3.1 demonstrates an example of the RC oscillator circuit structure. In this circuit, oscillating signal is generated using CMOS inverters. When the output is at high state, the capacitor is charged through the resistor until the input of the first inverter reaches to the high state. At this moment, the output switches to low state and the capacitor starts discharging through the resistor. The period of the output signal is given by:

$$T_{osc} = RC_s \ln\left[\frac{(2V_s - V_{sw})(V_s + V_{sw})}{(V_s - V_{sw})V_{sw}}\right] \tag{3.1}$$

where V_s is the supply voltage and V_{sw} is the switching voltage of the CMOS inverters. From the equation, it is clear that the period of the output signal is directly proportional to the sensor capacitance.

RC oscillators are simple circuits and provide linear outputs. The major disadvantage of this type of circuits is their high sensitivity to parasitic capacitances. In addition, they are sensitive to temperature changes, which is an important drawback for sensor applications.

3.1.2 Capacitance to Current Converter

Another type of capacitive readout method present in the literature is the capacitance to current conversion technique [44]. In this method, the charging or the discharging current of a sensor capacitance is measured.

Figure 3.2 shows the circuit schematic of such a system. In this circuit, the sensor capacitor is charged and discharged through a buffer with zero quiescent current. The operation of the circuit is as follows. When the input is switched to the V_{ref} level, the negative input terminal of the comparator also rises to V_{ref} instantaneously. Output of the comparator saturates at V_{ss} and turns on the M2 transistor. Then the sensor capacitor charges until the negative input voltage of the comparator approaches to zero. This makes the comparator go out of saturation, and M2 is driven into cut-off. After this point, both transistors at the output buffer remain at cut-off until the next discharging phase. If the input is switched with a frequency of F_s, the supply current is given by;

$$I_s = F_s V_{ref} C_s \tag{3.2}$$

The output current gives the absolute value of the sensor capacitor with a scale factor, assuming that the comparator has high gain and fast response.

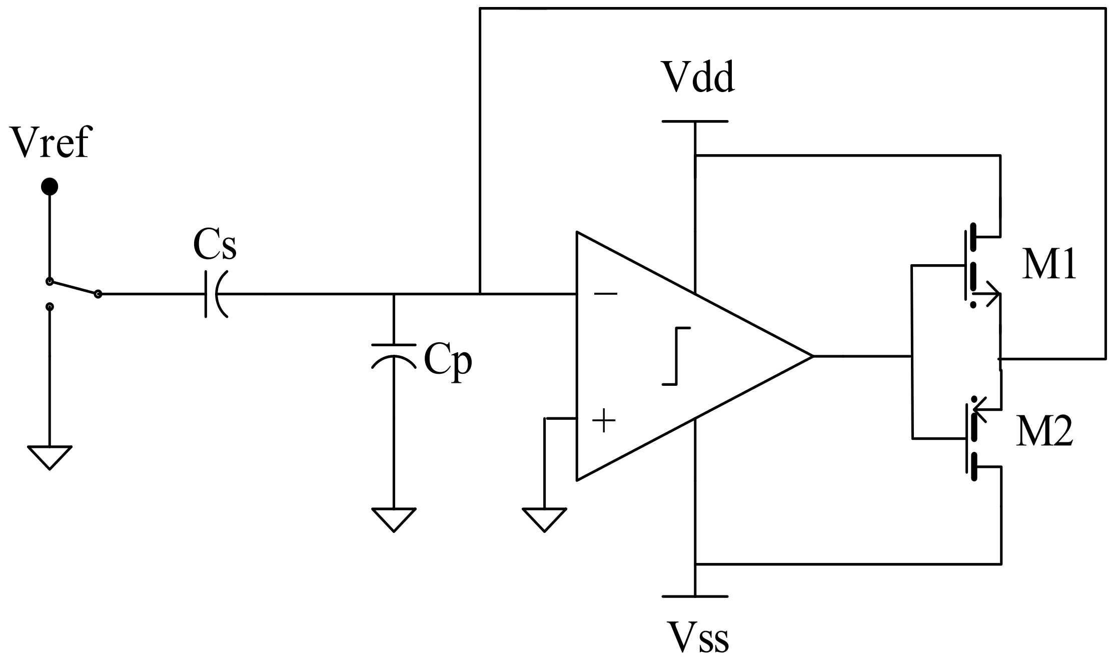

Figure 3.2: The circuit schematic of the capacitance to current converter.

The most important advantage of this circuit is that the supply current value does not depend on the amplifier offset and parasitic capacitances. However, the circuit does not provide a comparison of the sensor capacitance with a reference. This causes a limitation on the gain and the output dynamic range of the circuit, which is an important disadvantage for sensor applications.

3.1.3 Switched Capacitor Charge Integrator

Switched capacitor charge integrators are the most frequently used capacitance measurement circuits. The measurement idea is to connect the sensor capacitor to the input branch of a switched capacitor amplifier and obtain a voltage output proportional to the sensor capacitance.

Figure 3.3 demonstrates an example of the switched capacitor charge integrator [36]. The switched capacitor branch from C_s to C_{f1} forms a non-inverting amplifier circuit, where C_r to C_{f1} forms an inverting amplifier circuit. The dc transfer function of the circuit is:

$$V_{out} = V_{refA}\left(\frac{C_s}{C_{f1}}\right) - V_{refB}\left(\frac{C_r}{C_{f1}}\right) \tag{3.3}$$

where C_s stands for the sensor capacitor and C_r stands for the reference capacitor. V_{refA} and V_{refB} can be used to compensate for the offset voltage which may arise due to the mismatch between the sensor and the reference capacitors. The C_{f2} capacitor performs a low-pass function in order to avoid the rapid variation of the output voltage. OP2 is an output buffer, which is used to drive an off-chip load.

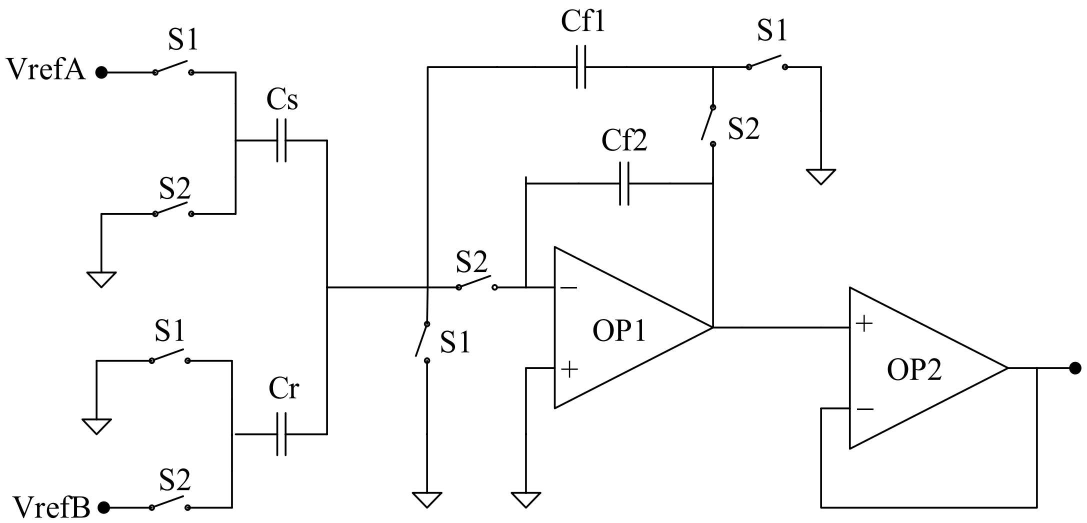

Figure 3.3: The circuit schematic of the switched capacitor charge integrator.

Switched capacitor charge integrators are the most convenient circuits for capacitive sensor readout applications, since they directly provide voltage outputs. The output voltage is proportional to the difference of the sensor capacitance and the reference capacitance, which is an important feature of these types of circuits. In addition, it is possible to compensate for the effect of any parasitic capacitance or amplifier offset on the output by using proper switching configurations.

3.2 Capacitive Readout Circuit Designed in This Study

In this work, a switched capacitor readout circuit is designed for capacitive humidity sensors using a 0.8µm CMOS process. The circuit is composed of a switched capacitor integrator and a digital section. The sensor and the reference capacitors are connected to the input stage of the integrator, which generates an output proportional to the difference of the two capacitances. The digital section is used to generate the switching signals of the integrator.

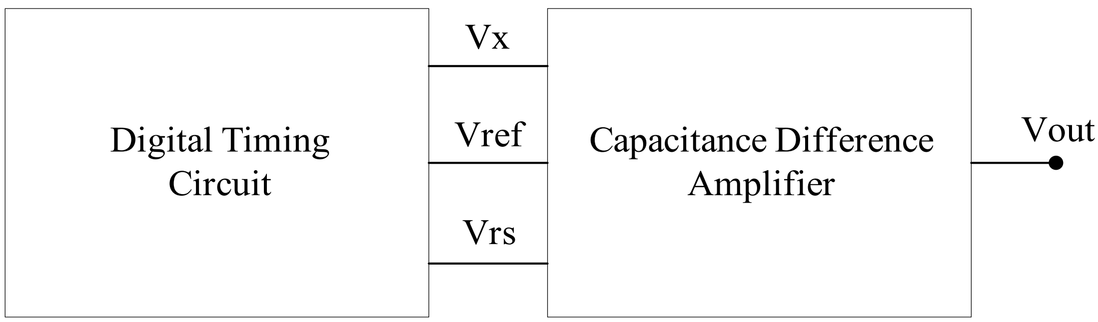

Figure 3.4: The block diagram of the readout circuit developed in this study.

Figure 3.4 shows the general block diagram of the readout circuit. As observed from the figure, three signals are generated by the digital section. V_r and V_x are two complementary clock pulses, which are used to drive the input stage of the integrator. The sensor and the reference capacitors are charged and discharged by complementary clock pulses instead of charging and discharging through switches. This charging method avoids the risk of some parasitic effects, which may occur due to switches such as charge injection and clock feed-through.

V_{rs} signal is generated in order to drive the reset switch of the integrator. This switch periodically resets the output of the integrator to the virtual ground level. The circuit is designed in 0.8 μm CMOS process, which works in the 0-5 Volts supply voltage range. The virtual ground of the circuit is set to 2.5V dc level, in order to achieve maximum output voltage swing.

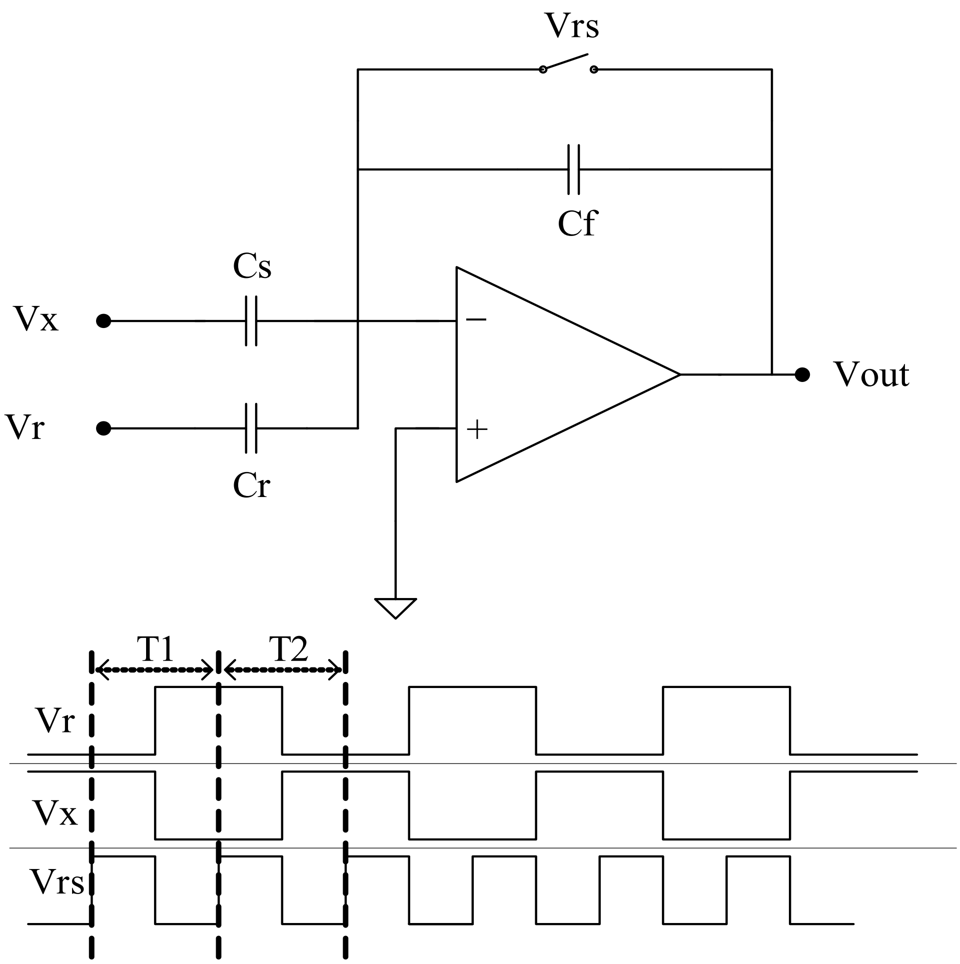

Figure 3.5: Switched capacitor charge integrator and the digital timing signals generated by the digital section.

Figure 3.5 shows the circuit schematic of the integrator and the signals generated by the digital section. C_s and C_r stand for the sensor and the reference capacitors respectively. The feedback capacitor C_f performs a low-pass function and determines the gain of the integrator. A detailed analysis of the circuit can be done as follows. In the T1 cycle, when V_x is high and V_r is low, the sensor capacitor C_s is charged by the V_{ref} signal. The reference and the feedback capacitors are discharged, so the total amount of charge stored in the circuit is:

$$Q_1 = (V_{ref} - V_{in-})C_s \tag{3.4}$$

where V_{in-} stands for the negative input terminal of the operational amplifier. When V_r rises to the V_{ref} level, the reference capacitor C_r is charged, and the sensor capacitor C_s is discharged through the feedback capacitor C_f. Total amount of charge stored in the circuit is:

$$Q_2 = (V_{ref} - V_{in-})C_r + (V_{in-} - V_{out})C_f \tag{3.5}$$

From the charge balance equation, Q_1 should be equal to Q_2. Assuming that the operational amplifier has a gain of A_0, following equations can be derived:

$$V_{out} = -A_0 V_{in-} \tag{3.6}$$

$$\left(V_{ref} + \frac{V_{out}}{A_0} \right)(C_s - C_r) = -V_{out}\left(\frac{1}{A_0} + 1 \right) C_f \tag{3.7}$$

If Equation 3.7 is solved for V_{out}, output function is found as:

$$V_{out} = \frac{-A_0 V_{ref}(C_s - C_r)}{(A_0 + 1)C_f + C_s - C_r} \tag{3.8}$$

Assuming that the gain A_0 is large enough such that $(A_0 + 1)C_f >> C_s - C_r$, the output expression reduces to:

$$V_{out} = -\frac{(C_s - C_r)}{C_f} V_{ref} \tag{3.9}$$

For the T2 cycle, same derivation can be performed, which results in a sign change of Equation 3.9. In conclusion, the output of the circuit oscillates around the 2.5V virtual ground level amplifying the difference between the reference and the sensor capacitances with a gain of V_{ref} / C_f.

This derivation is performed assuming that the operational amplifier has no dc offset voltage. However in practice, offset voltages of the operational amplifiers significantly affect the output voltage level. A simple way of removing this effect is to store the offset voltage on the feedback capacitor and subtract it from the output by using proper switching configuration. Figure 3.6 shows the circuit schematic with switching configuration for offset cancellation.

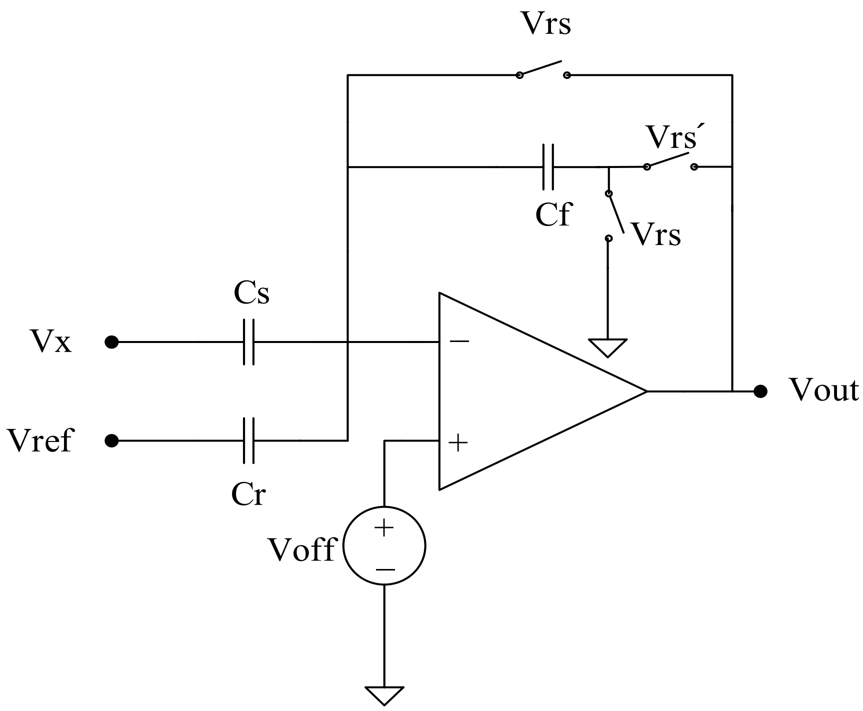

Figure 3.6: The circuit schematic of the switched capacitor integrator with offset cancellation.

The offset voltage can be modeled with a voltage source connected to one of the input terminals of the amplifier [45]. In the reset cycle, the offset voltage of the operational amplifier is stored on the feedback capacitor C_f. When the reset signal drops to the low level, stored charge on the capacitor is subtracted from the output node.

3.2.1 Digital Section

The digital section generates the timing signals and the signals driving the input stage of the switched capacitor integrator. As explained above, all of the digital signals are square waves with amplitude of 5V peak to peak and 2.5V dc offset. In order to generate these signals, a 2-bit ripple counter is used. Output signals of the ripple counter are connected to a combinational logic circuitry. Figure 3.7 shows the block diagram of the digital section.

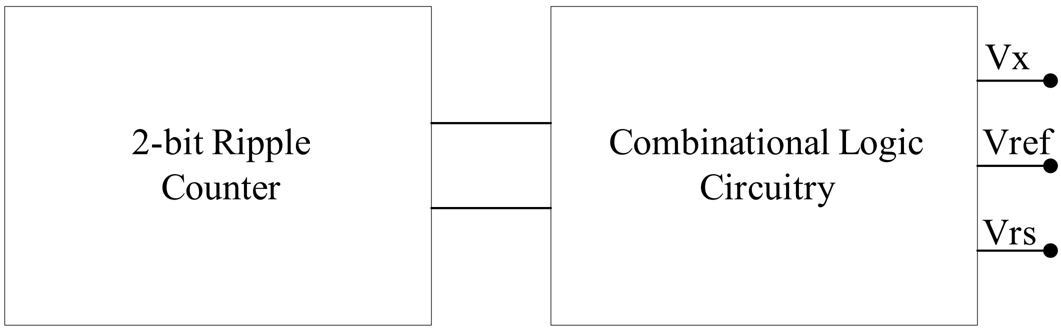

Figure 3.7: The block diagram of the digital timing circuit.

Input signals of the integrator should be the complement of each other with approximately zero delay. A phase shift between these signals can cause unwanted voltage rises at the integrator output, which disturbs the operation of the readout circuit. In order to generate exactly complementary clock pulses, dummy gates were used in the combinational logic circuitry. These dummy gates equalize the propagation delay time of the two circuit branches generating the signals.

3.2.2 Operational Amplifier

The amplifier used in the integrator part is a single stage operational transconductance amplifier (OTA). OTAs do not contain output stages, so they can not drive large resistive or capacitive loads. However, they can be used in the interior stages of the switched capacitor integrators [45]. The most important advantage of OTAs is that they have a simple structure and provide high gain in a single stage. Furthermore, they have stable frequency-phase characteristics without phase compensation.

Figure 3.8 shows the circuit schematic of the operational transconductance amplifier designed in this study. The OTA has a folded cascode structure composed of a differential amplifier with two cascode current sources as the load. This loading configuration provides a high gain in single stage. The operation of the circuit is as follows. Assume that voltages of $v_d/2$ and $-v_d/2$ are applied on the gates of M1 and M2 transistors, respectively. Drain currents of these transistors are amplified by $\Delta I = \pm gm_{1,2}\upsilon_d / 2$, where $gm_{1,2}$ is the tranconductance of M1 and M2 transistors. Drain currents of M6 and M7 transistors increase by the same amount, since the drain currents of M4 and M5 are constant. This current change is mirrored by the M12, M13, M14, M15 current mirror, generating an increase at the output voltage, which can be expressed as:

$$\Delta\upsilon_o = -gm_{1,2} r_o \upsilon_d \tag{3.10}$$

where r_o is the output resistance of the OTA. The output resistance is given by:

$$r_o = \frac{gm_{15} r_{ds15} r_{ds13} gm_6 r_{ds6} r_{ds5}}{gm_{15} r_{ds15} r_{ds13} + gm_6 r_{ds6} r_{ds5}} \tag{3.11}$$

If the Equations 3.10 and 3.11 are combined and arranged properly, the differential mode gain of the OTA is found as:

$$A_d = -gm_{1,2} \frac{gm_{15} r_{ds15} r_{ds13} gm_6 r_{ds6} r_{ds5}}{gm_{15} r_{ds15} r_{ds13} + gm_6 r_{ds6} r_{ds5}} \tag{3.12}$$

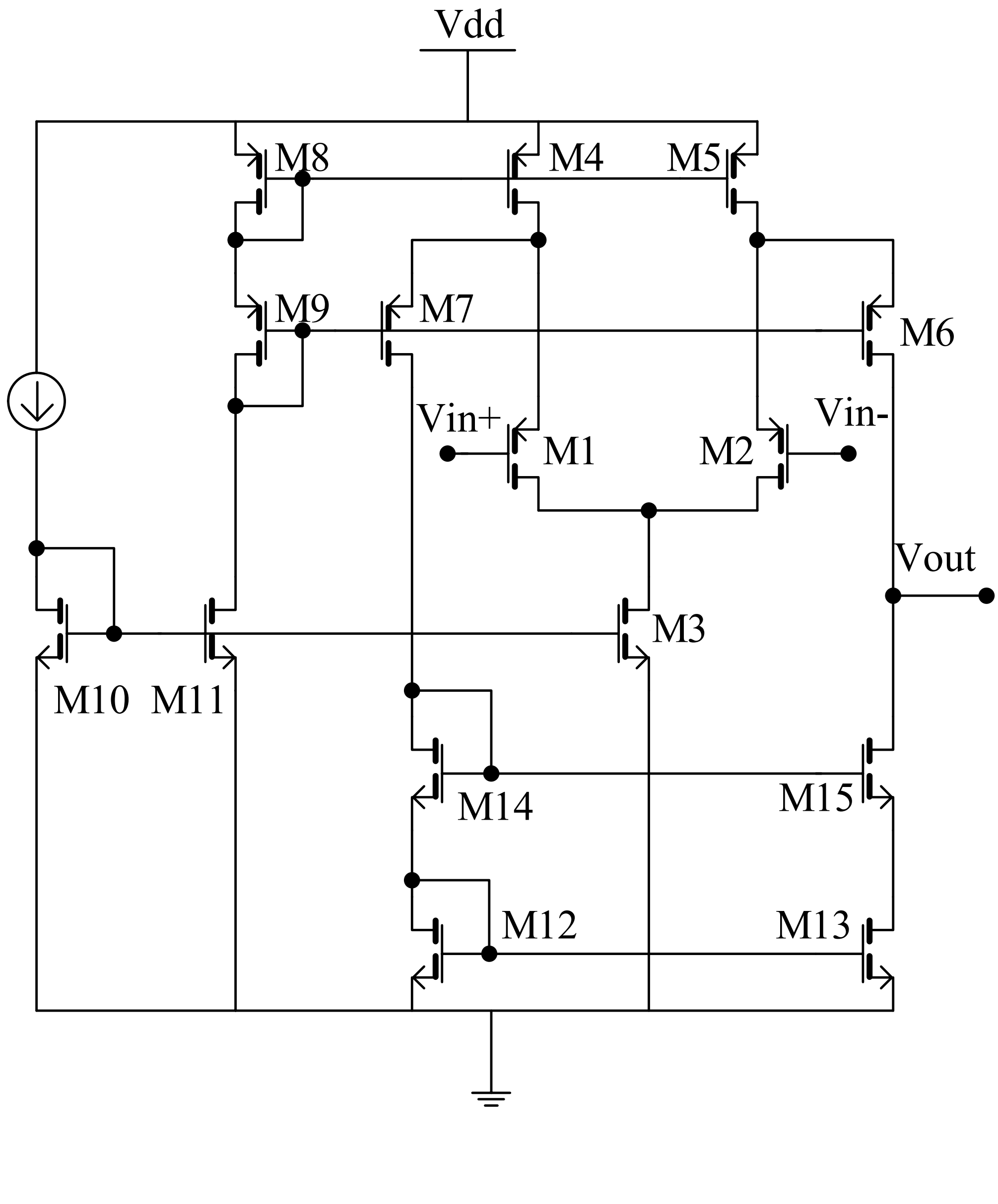

Figure 3.8: The circuit schematic of the folded cascode operational transconductance amplifier.

Transistors M3, M8, M9, M10, and M11 are bias transistors, which determine the dc operating points of the transistors of the differential amplifier stage. The M10 transistor is used as a current source, which determines the output bias current of the amplifier. In order to be able to adjust the differential gain of the amplifier, the gate terminal of this transistor was connected to an input pin. Table 3.1 shows the channel lengths and widths of the transistors.

Table 3.1: Channel widths and lengths of the transistors used in the OTA.

Transistor	Channel Width (μm)	Channel Length (μm)
M1-M2	50	0,8
M3-M10-M11	20	1,6
M4-M5	30	3
M6-M7	10	1
M8-M9	20	2
M12-M13	30	1,2
M14-M15	30	1,2

Another important feature of operational transconductance amplifiers is the stable frequency-phase characteristics. As observed from Figure 3.8, the amplifier has only one high impedance node, which is the output node. This node introduces a single low frequency pole into the frequency phase characteristics. Thus, the amplifier does not require frequency compensation for a stable phase response [45]. The frequency-phase characteristic of the OTA was simulated using the Analog Simulation tool of the CADANCE software. Figure 3.9 demonstrates the graphics showing the simulation results. The dc gain of the OTA is 82.61 dB, with a gain-bandwidth product of 3.42 MHz. The phase margin is 59.97°, which leads to stable frequency response. Table 3.2 shows the simulated figures of merit of the OTA.

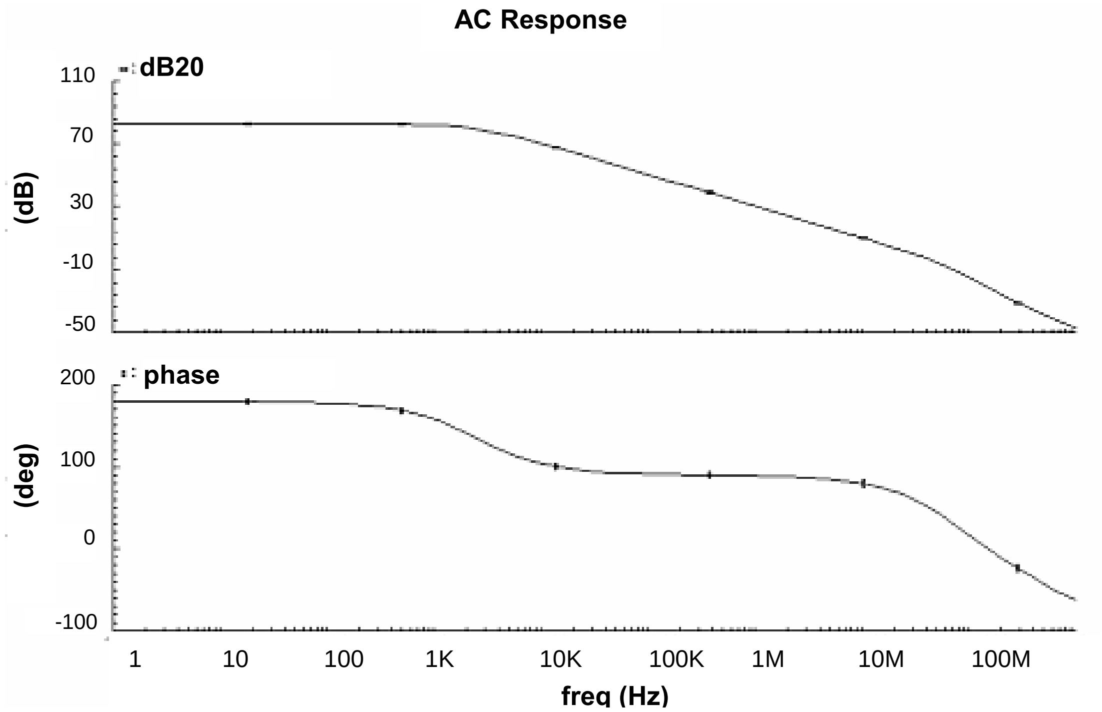

Figure 3.9: Simulated gain and phase characteristics of the operational transconductance amplifier.

The layout of the OTA was designed in AMS 0.8µm CMOS process. The most important point in the layout design of the OTA is the matching of the transistors with the same W/L ratio. Any mismatch between the dimensions of the input stage transistors not only introduce dc offset at the output, but also decrease the CMRR of the OTA significantly [45].

The layout design of the OTA was performed using the stacked layout technique [46]. Figure 3.10 shows the layout of the OTA. Layouts of the transistors are divided into parts such that all transistors of the same channel type are inserted into a fixed diffusion line. This method allows the merging of the common source and drain terminals of the transistors. As a result, the source to bulk and the drain to bulk capacitances are significantly reduced. Furthermore, layouts of the input transistors are drawn interdigitated in order to guarantee the matching between the transistor dimensions.

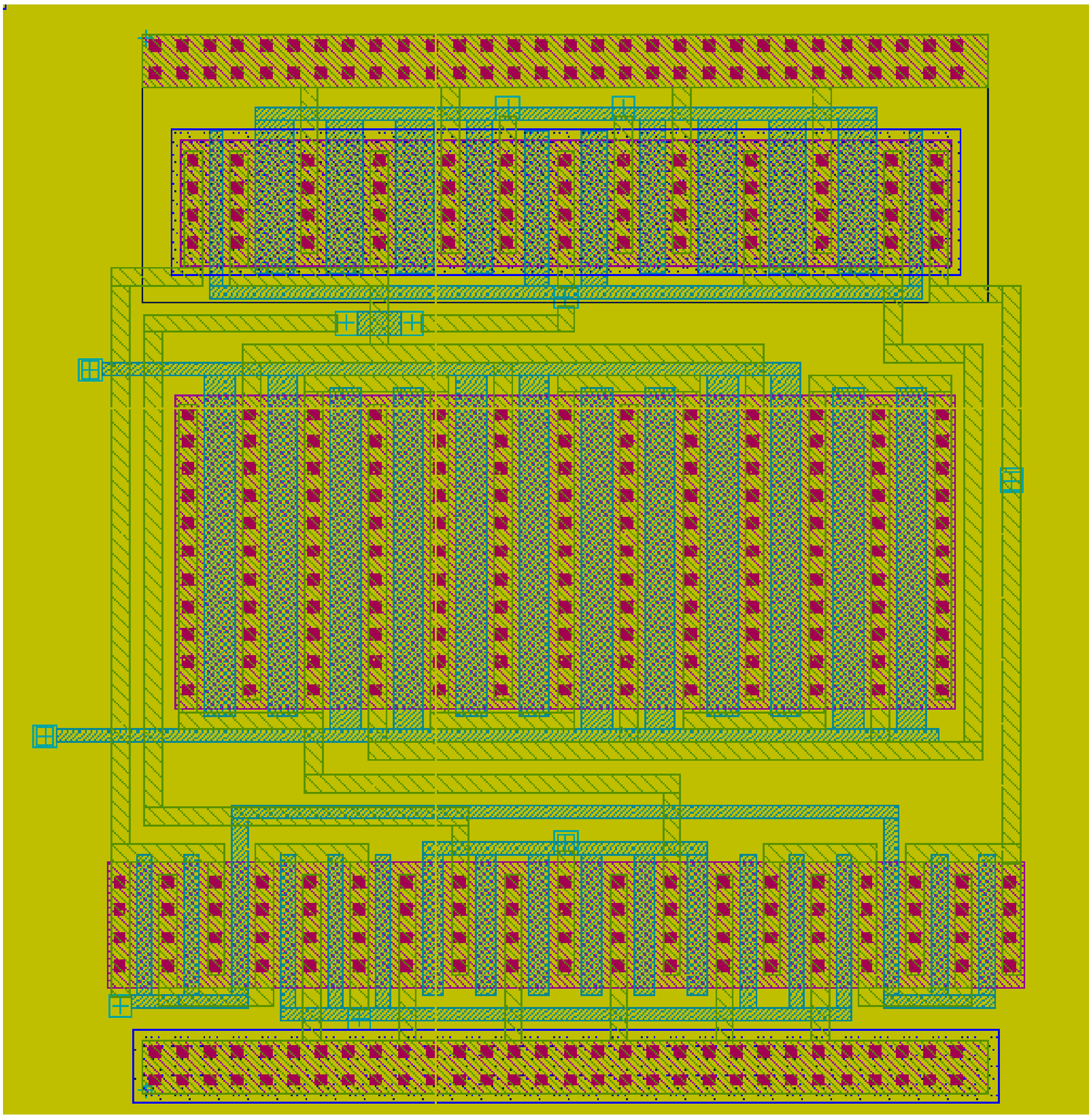

Figure 3.10: The layout of the operational transconductance amplifier designed in 0.8μm CMOS process. Transistors arrangement is done according to the stacked layout technique. Total layout dimensions are 75μm x 90μm.

Table 3.2: Simulated figures of merit for the operational transconductance amplifier.

Parameter	Value
DC gain	82.61 dB
Gain-bandwidth product	3.42 MHz
Phase margin	59.97°
CMMR	132.91dB
3-dB bandwidth	41.12 kHz

3.2.3 Floor Plan and Layout

The switched capacitor integrator is a mixed signal circuit composed of analog and digital blocks. In mixed signal circuits, there is a wide variety of noise sources affecting the output signal [46]. Therefore, floor planning of mixed signal circuit layouts are extremely important in the performance of the fabricated circuit.

The most important type of digital noise coupling is the capacitive coupling [46]. Capacitive coupling occurs between the analog and digital signal busses especially when they are routed close to each other. In order to prevent this type of coupling, analog and digital blocks were placed far away from each other. Capacitors and switches were placed between the analog and the digital sections.

Further protection against the digital noise coupling is achieved by guard rings surrounding the main blocks of the circuit. It is possible to implement guard rings in two ways. One is the n-well contact, which is biased to the positive supply voltage level. This type of guard ring provides a surface barrier for the noisy currents. The other way is to place substrate contacts around the block to be protected. Substrate contacts are connected to the ground of the circuit in order to provide a low impedance path for noisy currents. The digital section was protected by a double guard ring composed of both the n-well contact and the substrate contact.

Figure 3.11 shows the layout of the switched capacitor readout circuit including the pad connections.

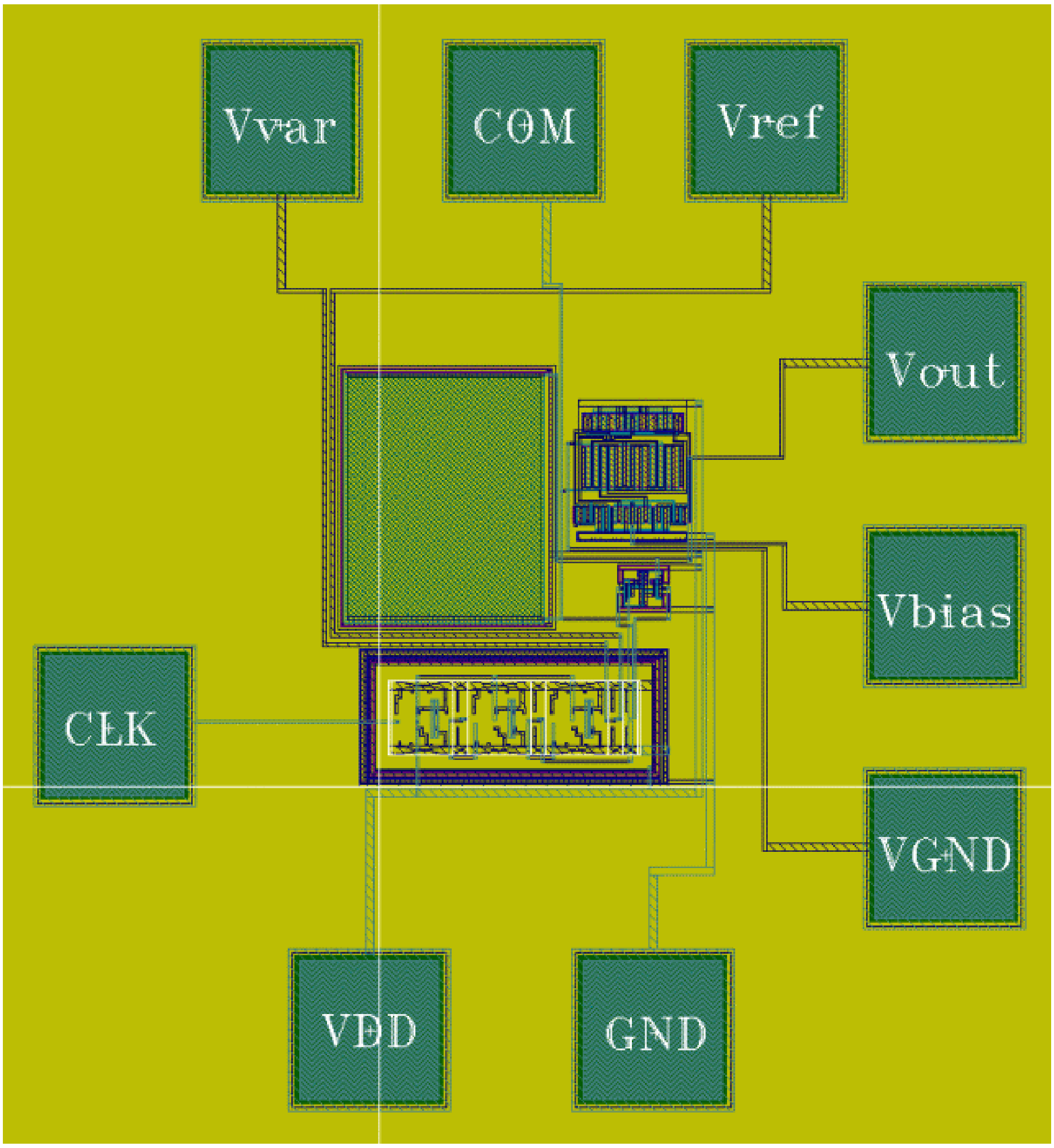

Figure 3.11: The layout of the switched capacitor readout circuit designed in a 0.8μm CMOS process. Total layout dimensions are 640μm x 675μm.

3.3 Conclusion

This chapter presents the design of a switched capacitor readout circuit for capacitive humidity sensors. The circuit is composed of a switched capacitor integrator and a digital timing circuit used for the generation of the signals driving the integrator. The layout of the circuit was designed in the AMS 0.8μm CMOS process. Next chapter presents the fabrication and test results of the capacitive humidity sensors and the hybrid humidity sensor module.

CHAPTER 4

FABRICATION AND TEST RESULTS

This chapter presents the fabrication and test results of the capacitive humidity sensor and the switched capacitor readout circuit. Section 4.1 demonstrates the fabricated capacitive humidity sensors and results of some initial measurements. Section 4.2 gives the characterization results of the capacitive humidity sensors. This section presents the humidity response, hysteresis characteristics, temperature dependency of the humidity response, and the response time measurements. Section 4.3 explains the tests performed on the integrated heater. This section presents the effect of heating on the sensor response. Section 4.4 presents the hybrid humidity sensor module, which is obtained by wire bonding the humidity sensor directly to the readout circuit. This section also gives the test results on the hybrid humidity sensor module.

4.1 Fabrication Results

Capacitive humidity sensors are fabricated by three mask process as explained in Section 2.4. Figure 4.1 shows the SEM pictures of the fabricated capacitive humidity sensors with the heater electrodes.

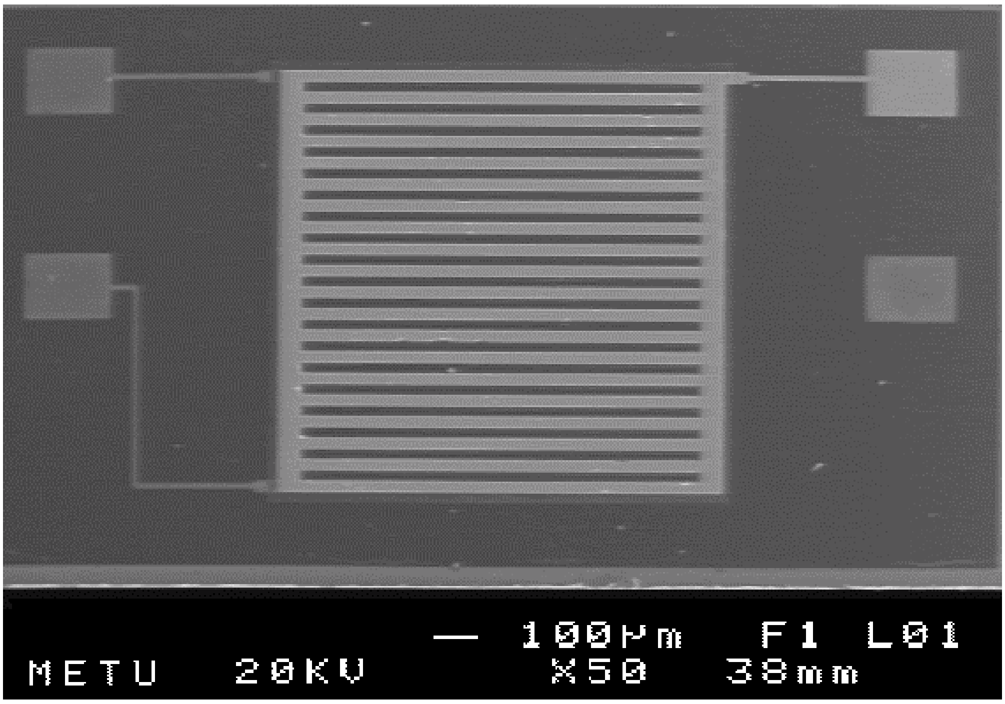

(a)

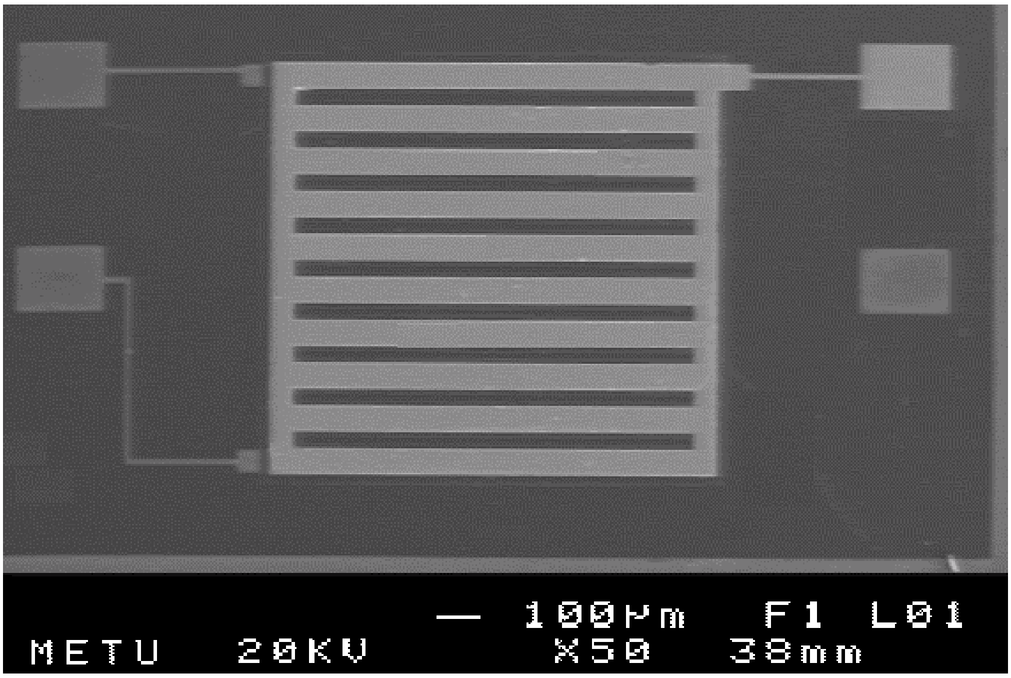

(b)

Figure 4.1: SEM pictures of the fabricated capacitive humidity sensors with heater electrodes with (a) 25µm metal line width, (b) 50µm metal line width.

In order to demonstrate the three layers of the capacitive humidity sensor, a three dimensional zoomed photograph is taken by SEM. Figure 4.2 demonstrates the photograph showing the top electrode, the polyimide layer and the heater electrode of the capacitive humidity sensor.

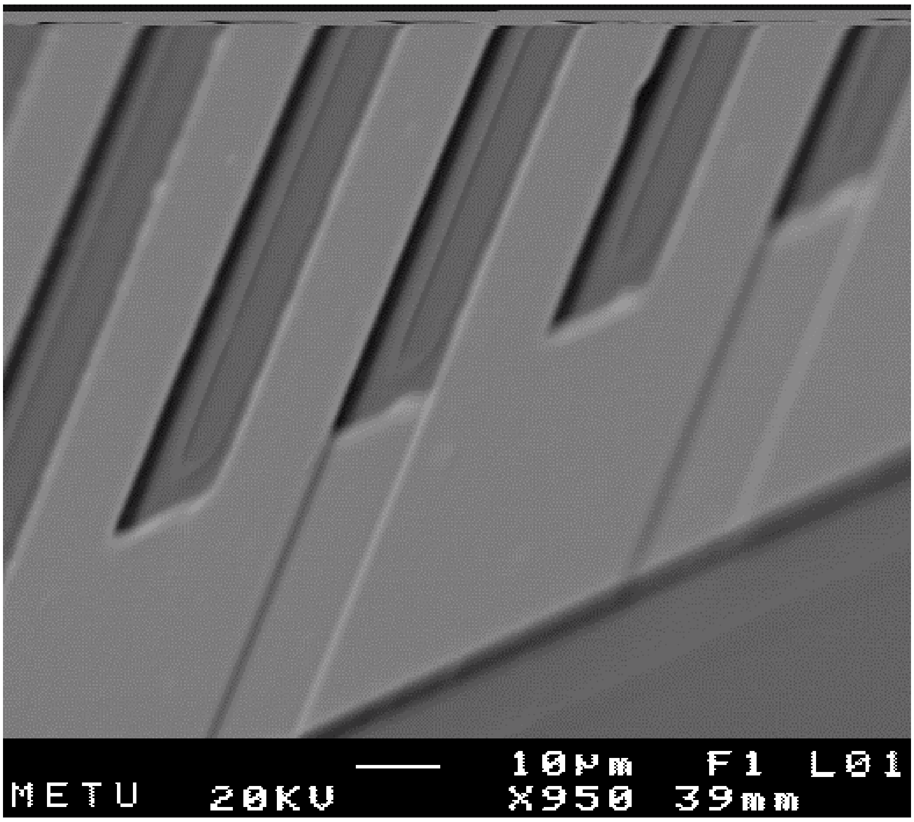

Figure 4.2: A zoomed view of the capacitive humidity sensor with the heater electrode.

The first test performed on the sensor is the initial capacitance measurement. This measurement is done under a probe station by directly contacting the pads of the humidity sensor and monitoring the capacitance by an impedance analyzer. It can be observed from Figure 4.3 that the initial capacitance of the humidity sensor with narrow metal lines is 31.1239pF, where the capacitance of the one with wide metal lines is 32.6267pF. These results are similar to the calculated capacitance values demonstrated in Chapter 2.

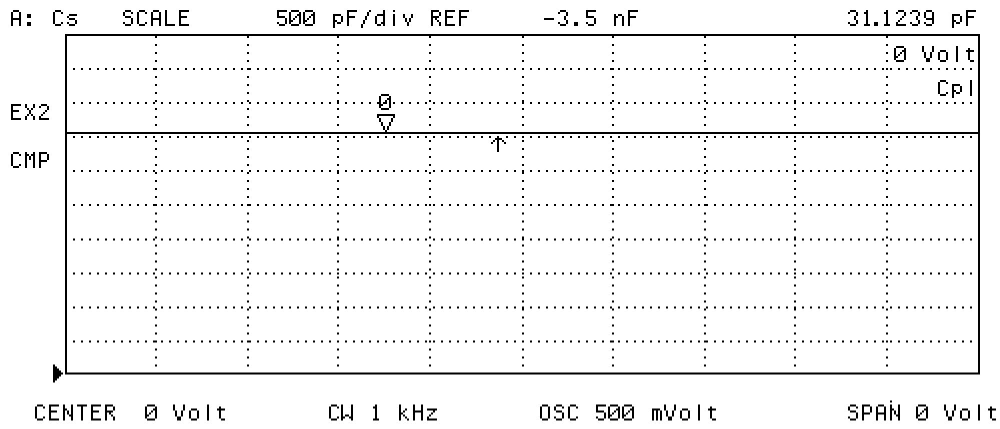

(a)

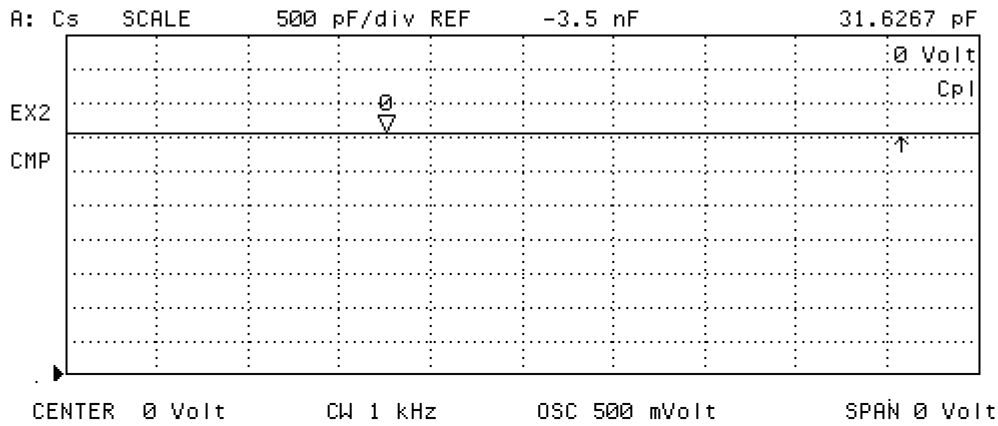

(b)

Figure 4.3: Initial capacitance measurements of the two capacitive humidity sensors with (a) 25µm opening width, (b) 50µm opening width. Measurement frequency is 1 kHz.

4.2 Characterization Results

Characterization of the humidity sensor was performed in an environmental chamber. The humidity range of the chamber is from 20% to 90% relative humidity within the temperature range from 20ºC to 70ºC. For the characterization, humidity sensors were wire bonded on a three pin alumina substrate to be able to make wire connections to the measurement instruments. All of the capacitance measurements were performed by the Agilent 4294A impedance analyzer. Figure 4.4 shows a picture of the capacitive humidity sensor wire bonded on an alumina substrate. Sections 4.2.1, 4.2.2, and 4.2.3 explain the test results of a capacitive humidity sensor with 25μm opening width. Section 4.2.4 summarizes these results as well as the test results of the sensor with 50μm opening width.

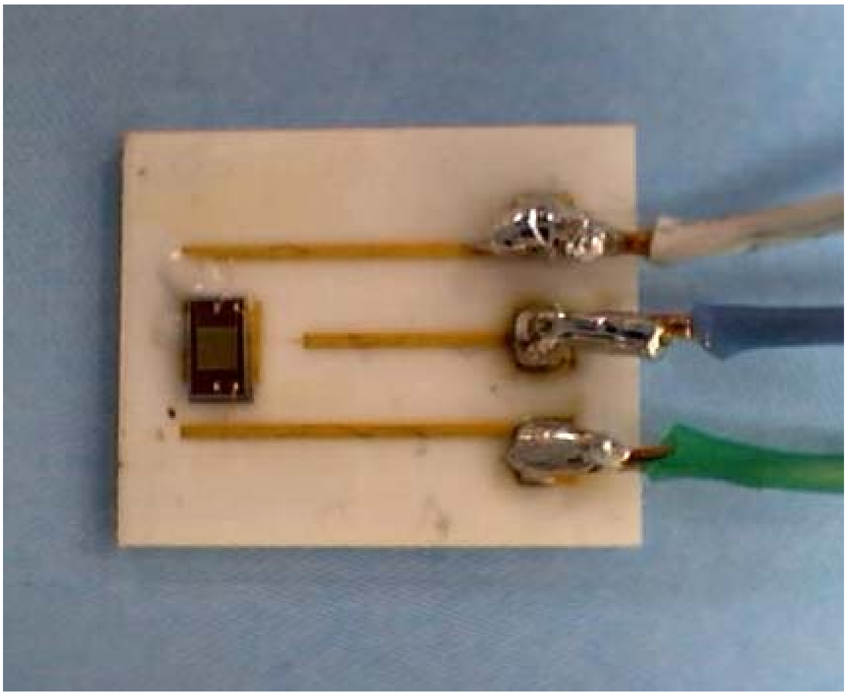

Figure 4.4: The capacitive humidity sensor wire bonded on a three pad alumina substrate.

4.2.1 The Humidity Response

The relative humidity inside the chamber was varied from 20%RH to 70%RH and the capacitance of the sensor was monitored. The measurement was performed in every 10% increase of the relative humidity. Figure 4.5 demonstrates the characterization results performed at 20ºC ambient temperature.

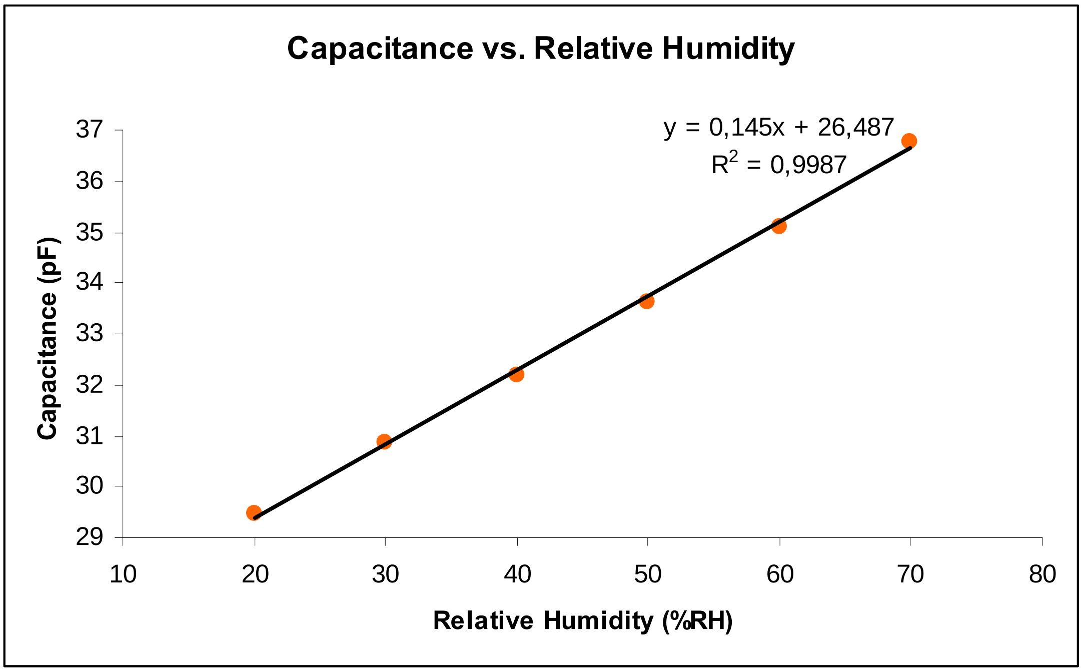

Figure 4.5: Capacitance versus relative humidity characteristics of the capacitive humidity sensor performed at 20ºC ambient temperature. Sensitivity of the sensor is 145fF/%RH, with a nonlinearity of 0.13%.

As observed from Figure 4.5, the humidity response of the capacitive humidity sensor is 145fF/%RH and it is almost linear. This is an expected result since it is well known that the dielectric constant change of polyimide film is linear within the relative humidity range from 20% to 70%. However in some applications, the response of the humidity sensor at high humidity levels is also important as discussed in Chapter 1. In order to characterize the extended range of operation, same measurement is performed from 20%RH to 90%RH. Figure 4.6 shows the measurement results. It can be stated from Figure 4.6 that the nonlinearity increases at relative humidity levels above 70%. This increase arises from the instability of polyimide films at high humidity levels. Due to this instability, dielectric constants of polyimide films increase more rapidly resulting in an increase in the nonlinearity.

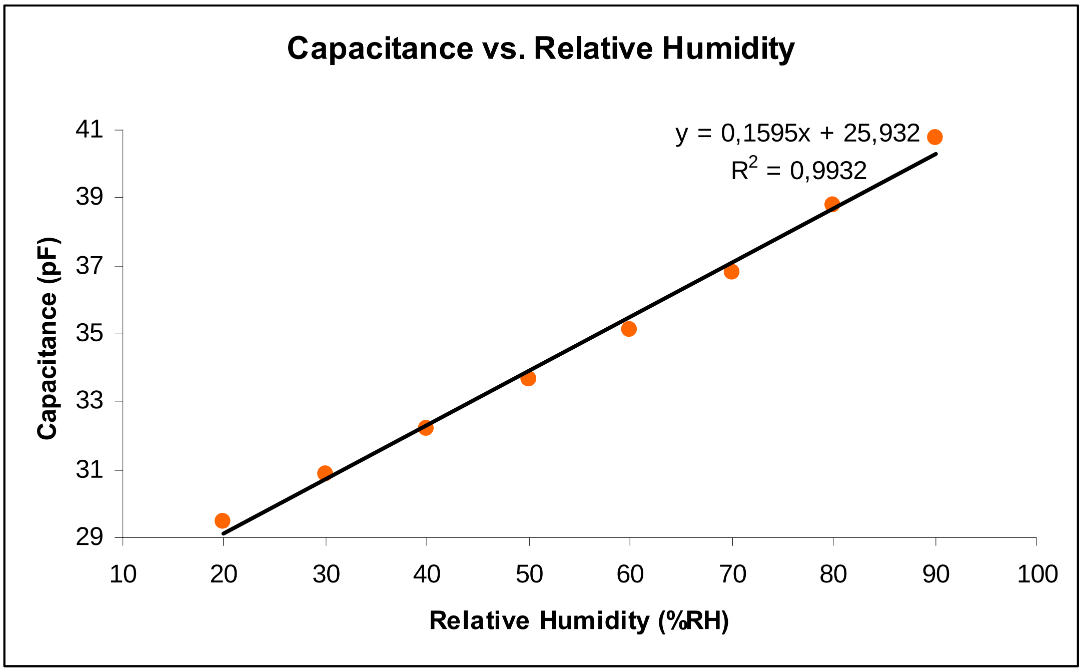

Figure 4.6: The humidity response of the capacitive humidity sensor in the extended range of operation at 20ºC ambient temperature. Nonlinearity increases above 70% relative humidity.

The effect of the ambient temperature on the sensor output was also investigated. Characterization of the humidity sensors were performed at different ambient temperature levels within the same relative humidity range. Capacitance versus relative humidity curves were obtained for temperatures of 20ºC, 30ºC, 40ºC, and 50ºC. Figure 4.7 shows the capacitance versus relative humidity curves for different ambient temperatures.

As the ambient temperature increases, the capacitance of the sensor increases for the same relative humidity level. This increase comes from the fact that the amount of moisture in the air is higher at higher temperatures for the same relative humidity level. Consequently, the polyimide film absorbs more moisture at higher ambient temperature levels and at constant relative humidity conditions, resulting in a shift in the capacitance versus relative humidity curve. Another important result that can be derived from Figure 4.7 is that the sensitivity of the sensor is almost the same for all temperature levels.

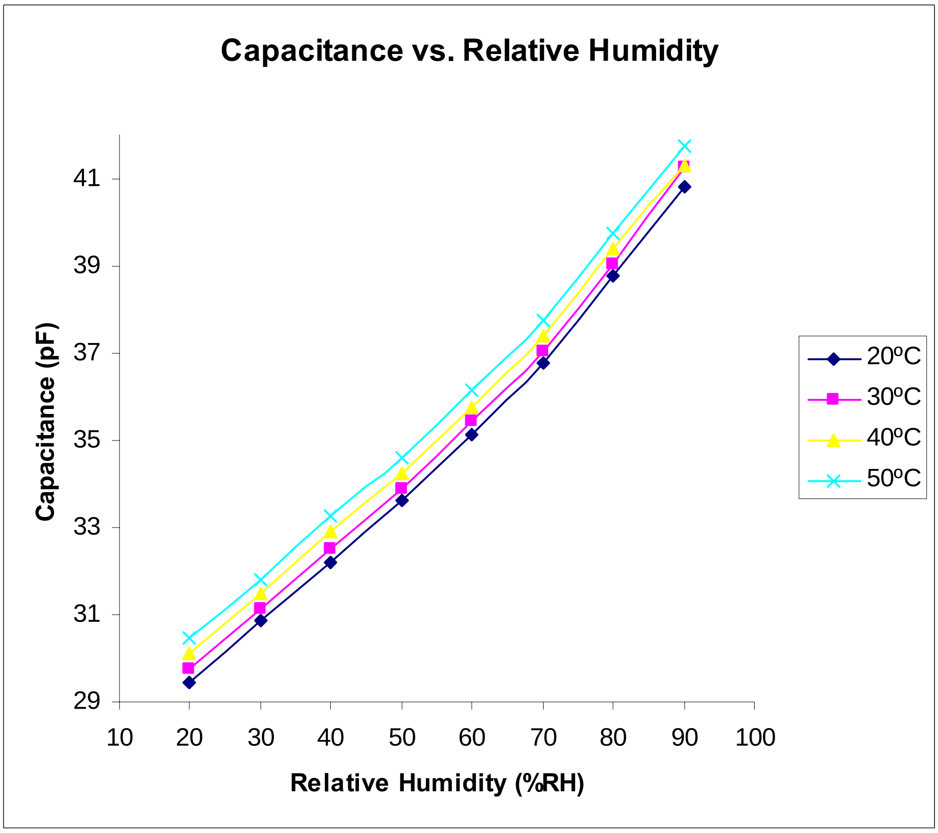

Figure 4.7: The humidity response of the capacitive humidity sensor at different ambient temperature levels.

4.2.2 Hysteresis Characteristics

Another important figure of merit for humidity sensors is the hysteresis characteristics. In order to figure out the hysteresis characteristics, the relative humidity was increased from 20% to 90%, and then decreased back to 20% and the response of the sensor was monitored in both cycles. The measurement was performed at 20ºC ambient temperature after waiting for approximately 30 minutes at every measurement point. Figure 4.8 shows the hysteresis test results.

The hysteresis of the sensor is measured as 2.57% RH. This value is found by taking the difference of the capacitance values corresponding to the same relative humidity levels and then converting them into %RH form using the sensitivity expression. In the ramp down cycle, the capacitance of the sensor is higher than the one at the same relative humidity level of the ramp up cycle. In other words, when the relative humidity is increased and then decreased back to its initial value, the capacitance of the sensor does not drop back to its initial value. This means that the absorbed moisture does not diffuse out of the polyimide film in a short time when the relative humidity is decreased. This property may cause problems in applications where rapid changes in relative humidity are to be monitored. In order to solve this problem, the polyimide film should be refreshed and cleaned from residual moisture by the help of a heater.

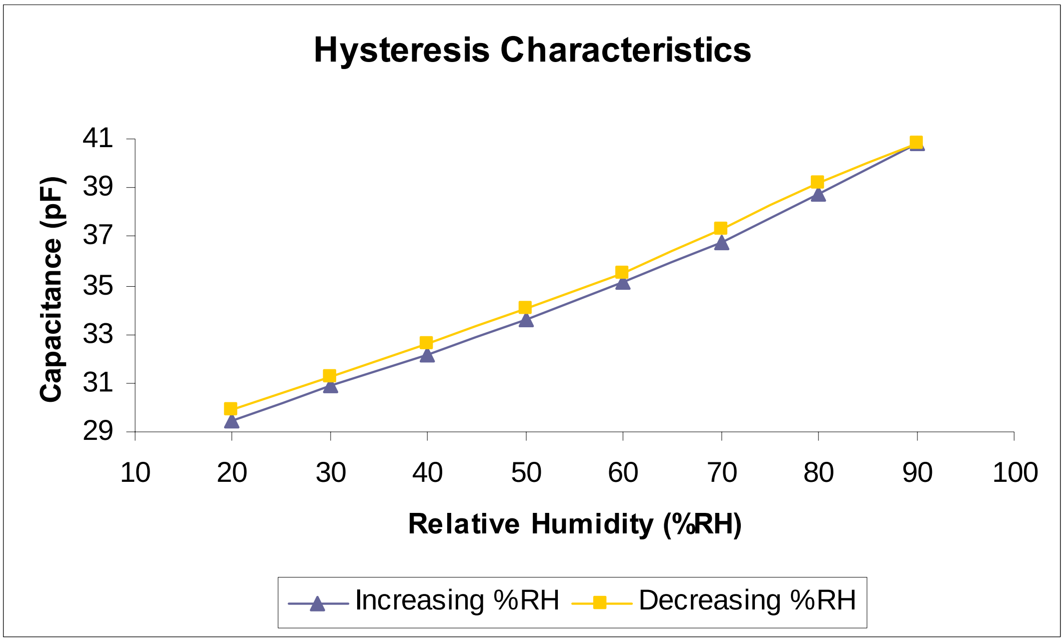

Figure 4.8: Hysteresis test results of the capacitive humidity sensor. Calculated hysteresis is 2.57% RH at 20ºC ambient temperature.

4.2.3 Response Time Measurements

The response time of the humidity sensor can be measured by changing the relative humidity of the environment rapidly and measuring the time it takes for the sensor output to change. However, the expected response time of the capacitive humidity sensors is on the order of several hundred milliseconds and such a fast humidity change can not be generated by the environmental chamber.

One way of measuring the response time is to submit the sensors to breathe and monitor the capacitance in time [47]. Breathing on the sensors generates an instantaneous humidity change and the rise time of the capacitance can be measured. Figure 4.9 shows the results of the response time measurement using this method. Response time was found as 1.654 seconds.

It should be mentioned that the response time measured by this method is the absorption time of the polyimide. In other words, it gives a measure of the rise time of the sensor output when the humidity of the environment increases. Similar measurement method can be performed to calculate the desorption time of the polyimide. This time, the sensor was submitted to breath and the time it takes for the sensor output to drop to its initial value was measured. Due to the hysteresis, the final value was selected 0.4pF above the initial value according to the hysteresis curve given in Figure 4.8. The desorption time of the sensor is found as 12.1 seconds. Figure 4.10 demonstrates the desorption time measurement results.

4.2.4 Characterization Summary

Humidity sensitivities of the two humidity sensors types are almost equal. This is an expected result since the base capacitances of the two sensors are equal, and the humidity sensitivity is directly proportional to the base capacitance as explained in Chapter 2. Absorption time of the humidity sensor with wide electrodes is smaller since the opening width of this sensor is larger. Large opening width provides a wider path for the moisture to diffuse into the film, so the diffusion occurs more quickly. Similar results can be observed for the desorption time due to the same reason.

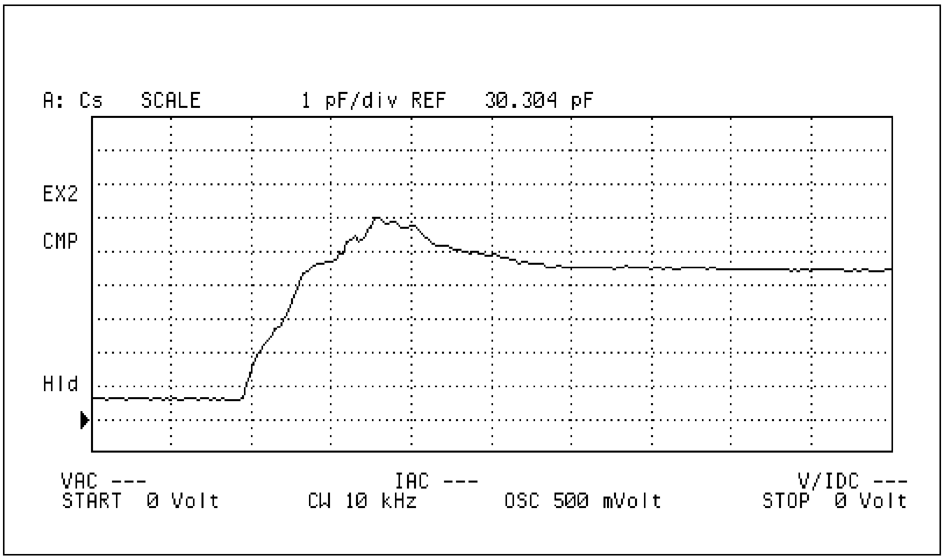

(a)

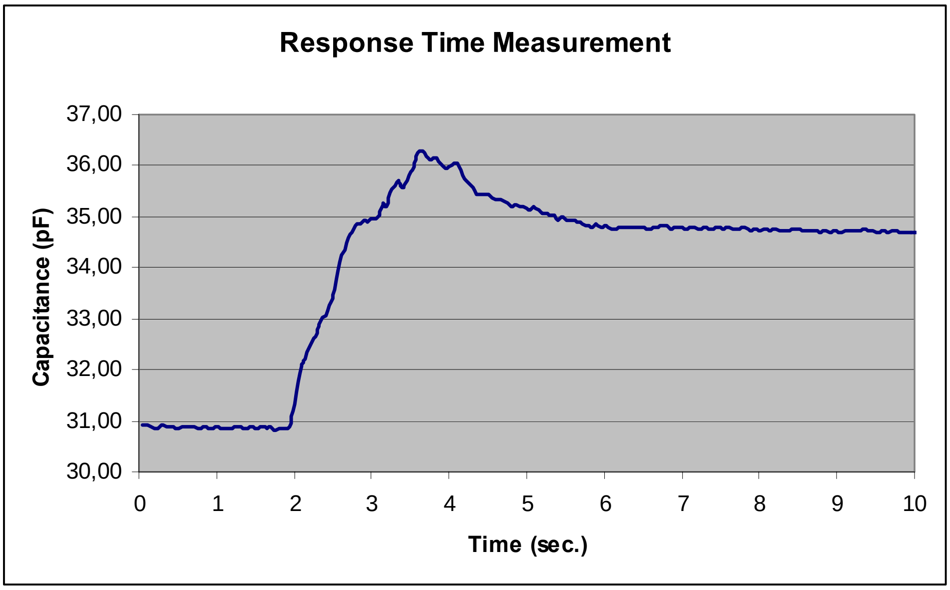

(b)

Figure 4.9: (a) The capacitance change monitored by the impedance analyzer during the response time measurement; (b) impedance analyzer data converted to excel graph.

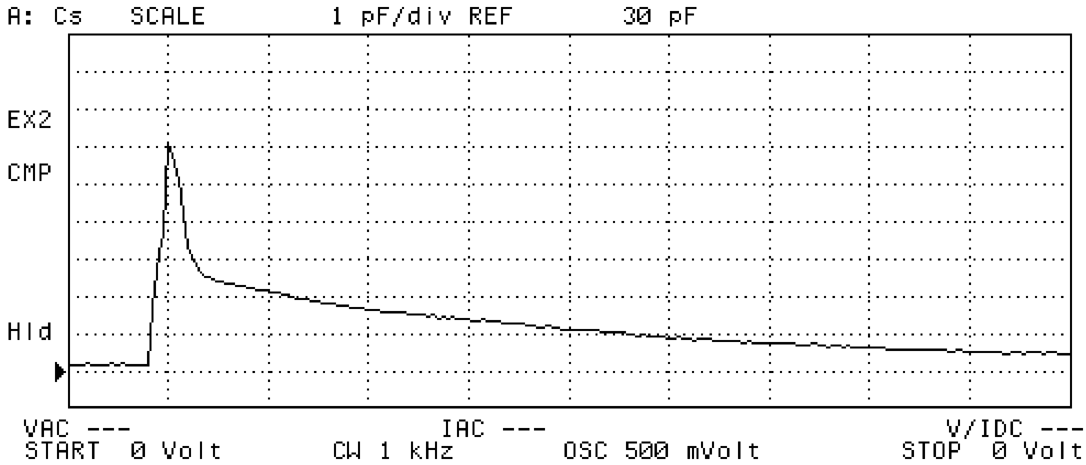

(a)

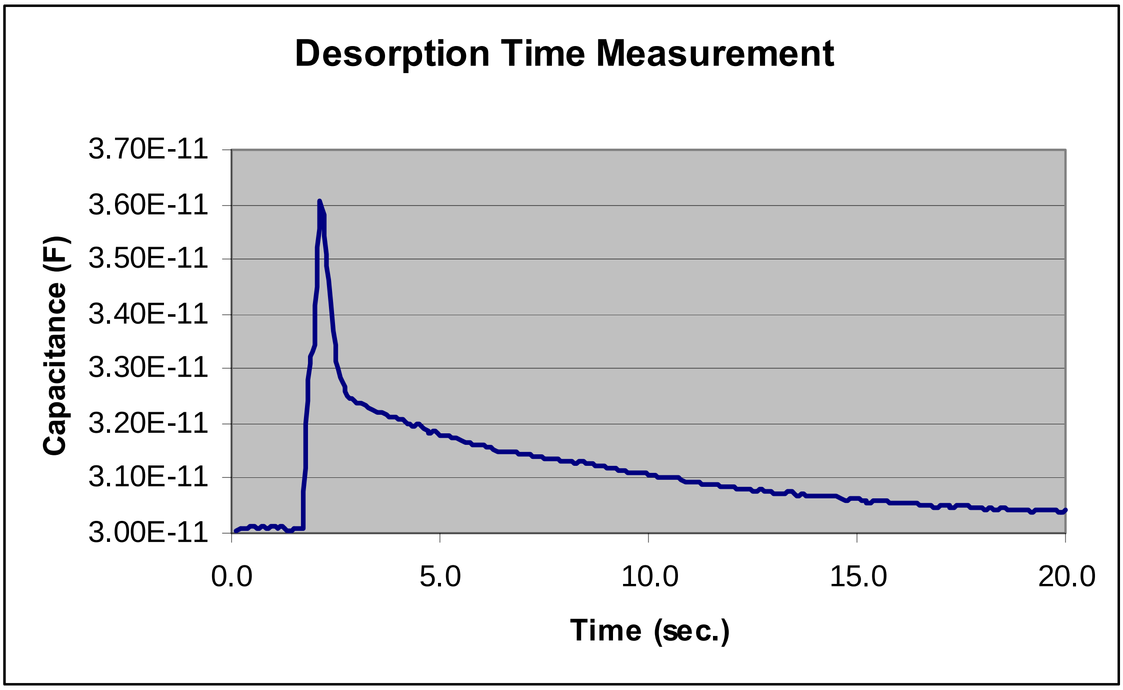

(b)

Figure 4.10: (a) The capacitance change monitored by the impedance analyzer during the desorption time measurement; (b) impedance analyzer data converted to excel graph. Desorption time is 12.1 seconds.

Table 4.1: Summary of the characterization results of the two capacitive humidity sensors types.

	Sensor 1	Sensor 2
Opening Width (μm)	25	50
Base Capacitance (pF@1kHz)	31.12	31.62
Humidity Sensitivity (fF/%RH)	145	149
Hysteresis	2.57% RH	2.59% RH
Absorption Time (second)	1.654	1.494
Desorption Time (second)	12.1	11.3

4.3 Integrated Heater Tests

The integrated heater was characterized by monitoring the resistance versus temperature characteristics. The sensor was heated inside the environmental chamber up to 100ºC, and resistance of the heater was measured by a multi-meter. Figure 4.11 shows the temperature response of the resistance of the heater electrode.

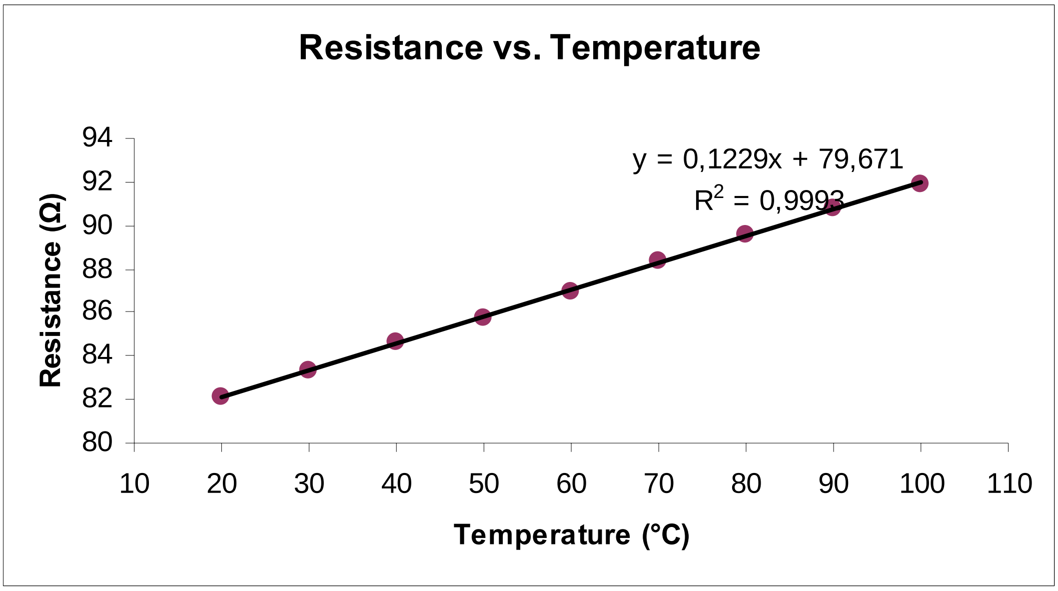

Figure 4.11: Temperature versus resistance curve of the heater electrode.

As observed from Figure 4.11, the resistance of the resistor increases with the increasing temperature. This is due to the positive temperature coefficient of resistance property of the aluminum. This property was used to figure out the heating characteristics of the resistor with the applied heating power. A dc voltage from 1 to 3 volts was applied on the heater resistor and current passing from the resistor was measured. According to this data, the resistance versus power curve was derived. Figure 4.12 shows the resistance versus power characteristics of the heater electrode. It can be derived from the two measurements that approximately 180mW of power is necessary to increase the temperature to 100ºC.

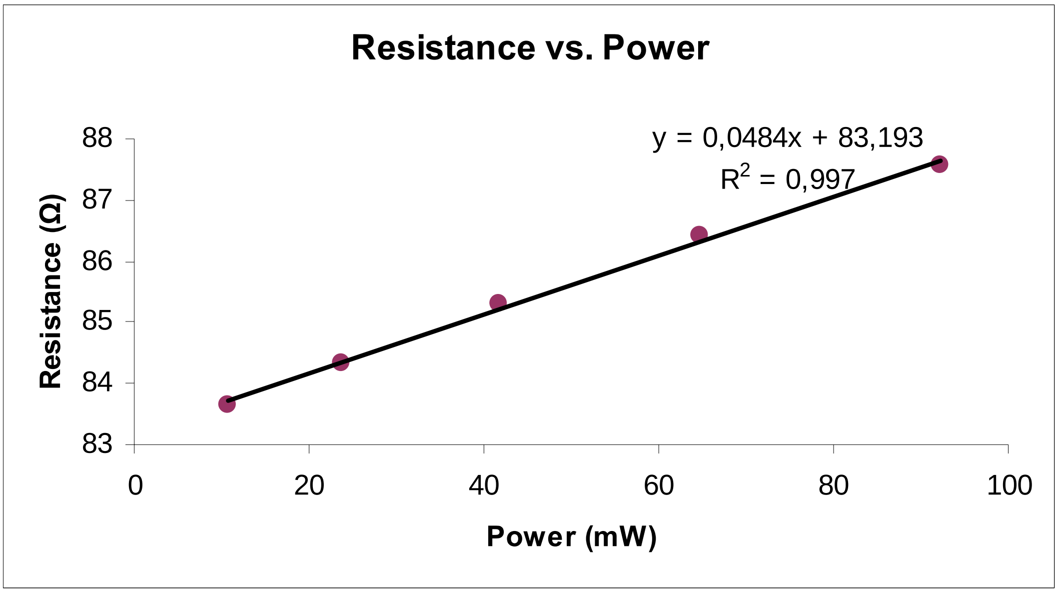

Figure 4.12: Resistance versus power characteristics of the heater electrode.

In order to test the operation of the heater, a voltage pulse was applied on the terminals of the resistor and the change in the sensor capacitance was observed. Figure 4.13 shows the capacitance versus time plot of the capacitive humidity sensor. A 2V pulse with duration of three seconds was applied five seconds after starting the measurement. Applying 2 volts generates approximately 50mW of power dissipation on the resistor. The capacitance of the sensor decreased from 31.7pF to 31pF, which shows that the moisture absorbed by the polyimide film was reduced.

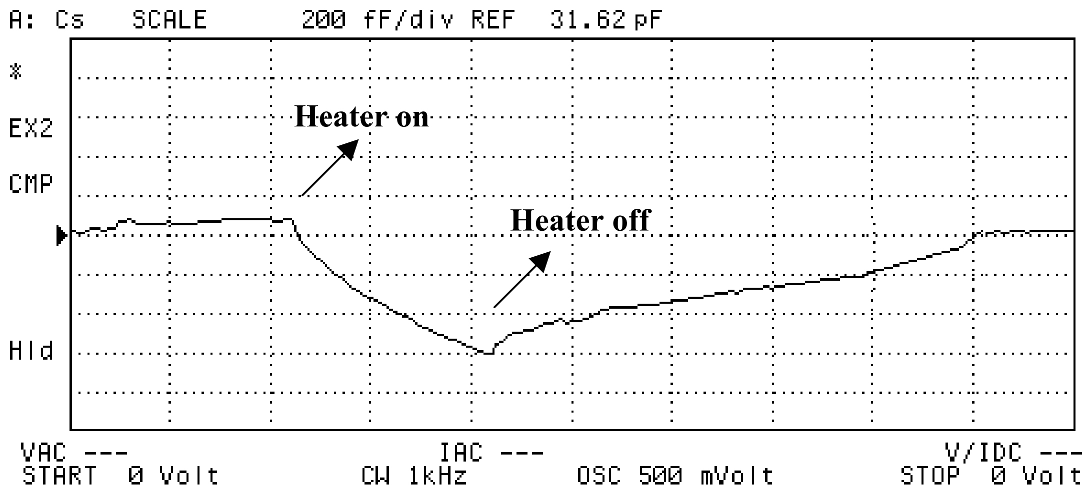

Figure 4.13: Capacitance versus time graph monitored during the heating power applied on the heater resistor.

Since the sensor response is dependent on the ambient temperature, the output of the sensor during the heating does not give any idea about the actual relative humidity level. To be able to use the heater at high relative humidity levels, characterization of the sensor is required at a constant heating level. A 50mW heating power was applied on the heater resistor, and the humidity response was measured within the 20% to 90% relative humidity range at 20ºC ambient temperature. Figure 4.14 shows the characterization results.

Characterization results show that the humidity response of the sensor becomes more linear at high relative humidity levels when the sensor is heated by applying constant power. In addition, capacitance values are smaller than the ones obtained without heating, which are given in Figure 4.6. This is due to the fact that the relative humidity that the polyimide sees is smaller than the actual relative humidity of the environment. As a result, the integrated heater can be used to measure high relative humidity levels where there is the risk of water condensation.

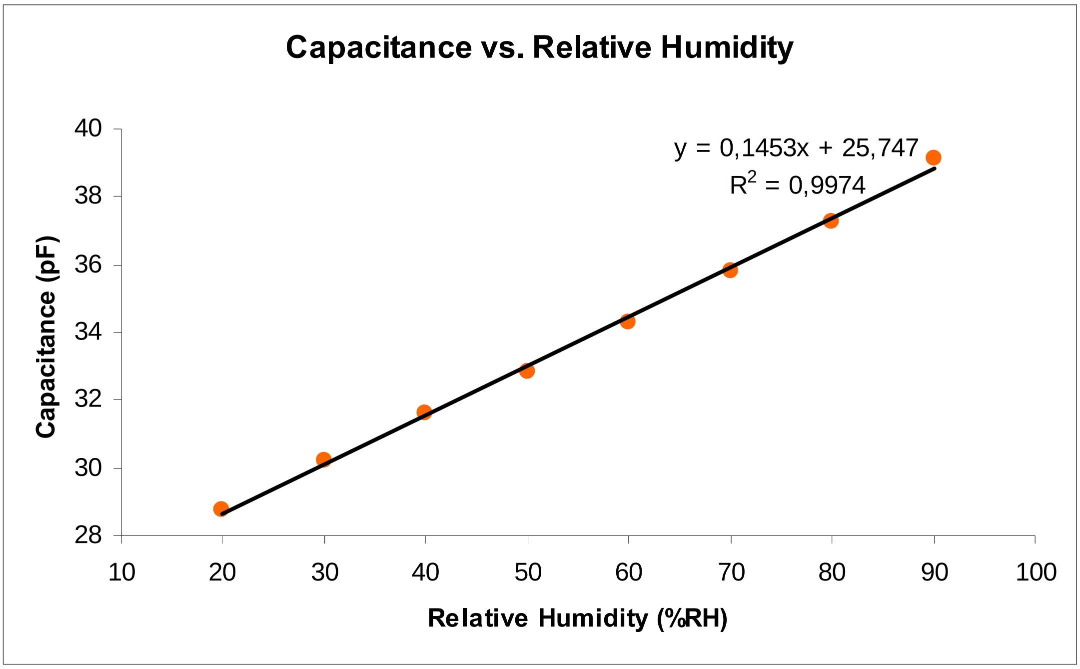

Figure 4.14: Capacitance versus relative humidity plot when the sensor is heated by applying 50mW power on the heater resistor at 20ºC ambient temperature. It is seen that the linearity of the capacitance change increases between 70%RH and 90% RH range.

4.4 The Hybrid Humidity Sensor Module

Capacitive humidity sensors were integrated with the readout circuit using hybrid integration. The capacitive readout circuit, a capacitive humidity sensor, and a reference capacitor were connected to each other on an alumina substrate by wire bonding. The alumina substrate was attached to a 12 pin TO package, and the input and output pads of the hybrid system were connected to the pins of the package. The reference capacitor is another capacitive humidity sensor, which is passivated against humidity. Passivation was achieved by covering the sensor with white epoxy. Figure 4.15 shows a picture of the hybrid humidity sensor system attached to the TO package.

Figure 4.15: The hybrid humidity sensor module integrated on the TO package.

For proper operation of the hybrid humidity sensor module, several input signals are required. Besides the 5V main power supply, the 2.5V analog ground and the bias signal of the operational transconductance amplifier should externally be applied. In addition, the clock input of the digital section should be provided by a function generator. It is a square wave with a peak to peak voltage of 5V and 2.5V dc offset. Figure 4.16 shows the oscilloscope screen showing the input signals of the integrator generated by the digital section and the output waveform.

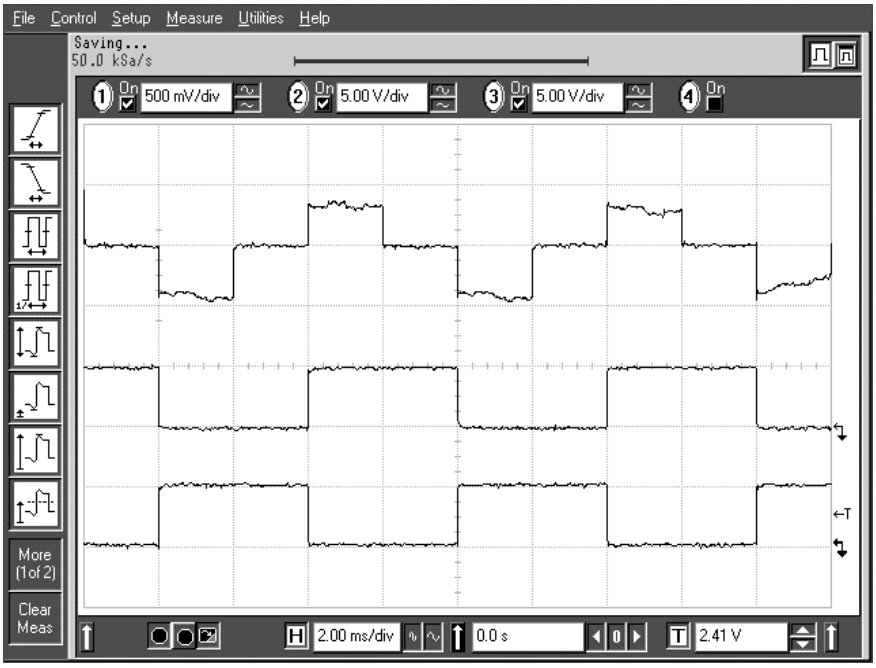

Figure 4.16: Input signals and the output waveform of the integrator.

The humidity sensor module was characterized inside the humidity chamber using the same method explained in the previous section. The humidity level inside the chamber was changed between 20% and 90% relative humidity, and the output voltage was monitored on the oscilloscope. Measurements were repeated for four different ambient temperature levels.

Figure 4.17 shows the characterization results of the hybrid humidity sensor module. Characterization results show that the output voltage tracks the change in the humidity with a sensitivity of 19.4mV/%RH with a nonlinearity of 0.17%. The sensor response has almost the same characteristic for different ambient temperature conditions. There is a shift in the output voltage with increasing temperature because of the increase in the capacitance level, as explained in Section 4.2.1. In order to demonstrate the temperature dependency of the sensor output, the output data was plotted with respect to the temperature at constant relative humidity values. Figure 4.18 shows the humidity sensor output versus temperature curves at different ambient relative humidity values.

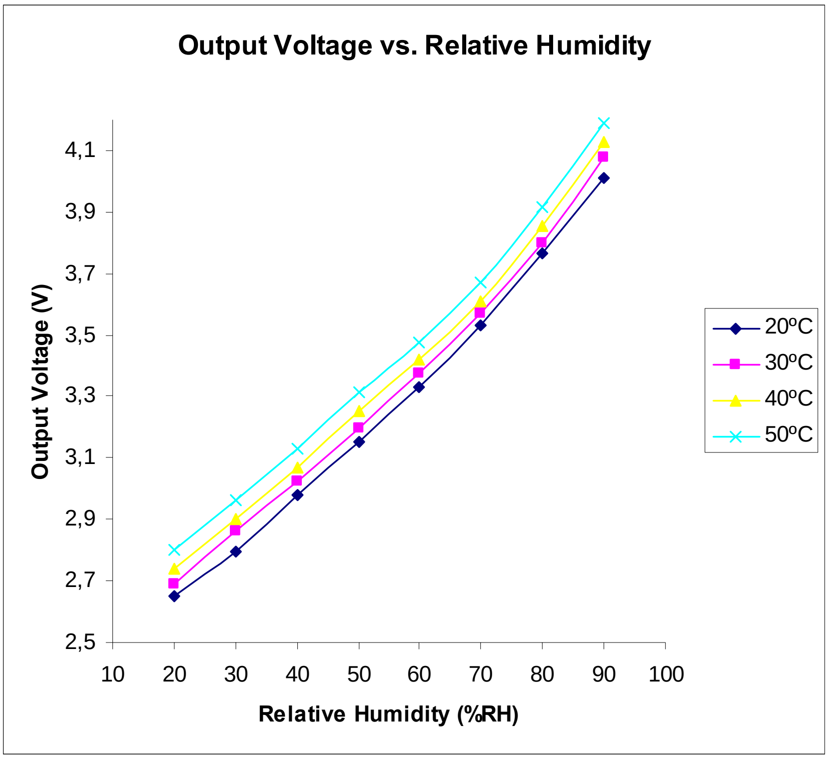

Figure 4.17: The output voltage response of the hybrid humidity sensor module. Sensitivity is 19.4mV/%RH with a nonlinearity of 0.17%.

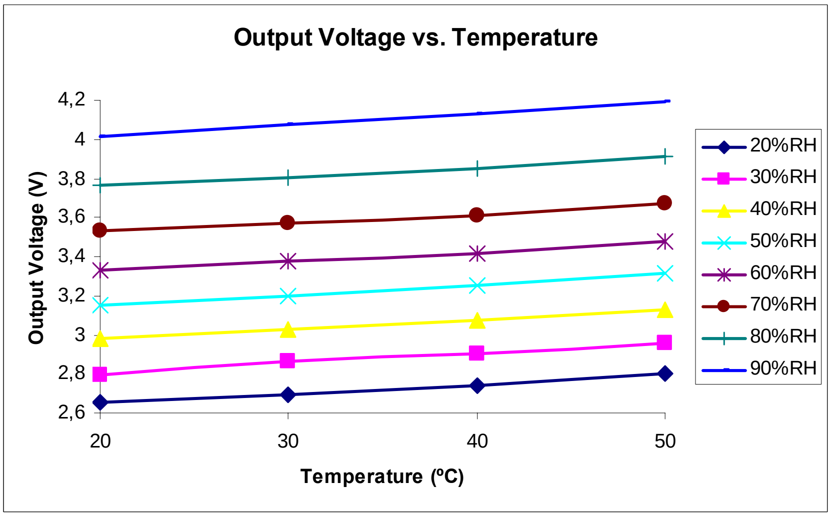

Figure 4.18: Humidity sensor output versus temperature curves at different ambient relative humidity values.

The hysteresis test was also repeated for the hybrid humidity sensor module. Relative humidity inside the chamber is increased from 20% to 90% then decreased back to 20%. Measurements were performed at 20ºC ambient temperature after waiting for 30 minutes at every measurement point. The output voltage is observed on the oscilloscope. Figure 4.19 shows the output voltage versus relative humidity curve for increasing and decreasing relative humidity conditions. The calculated hysteresis of the hybrid module is 2.54% relative humidity, which is a similar result to the hysteresis calculated for the capacitive sensor alone. These results show that the CMOS readout circuit properly converts the capacitance change into a voltage change.

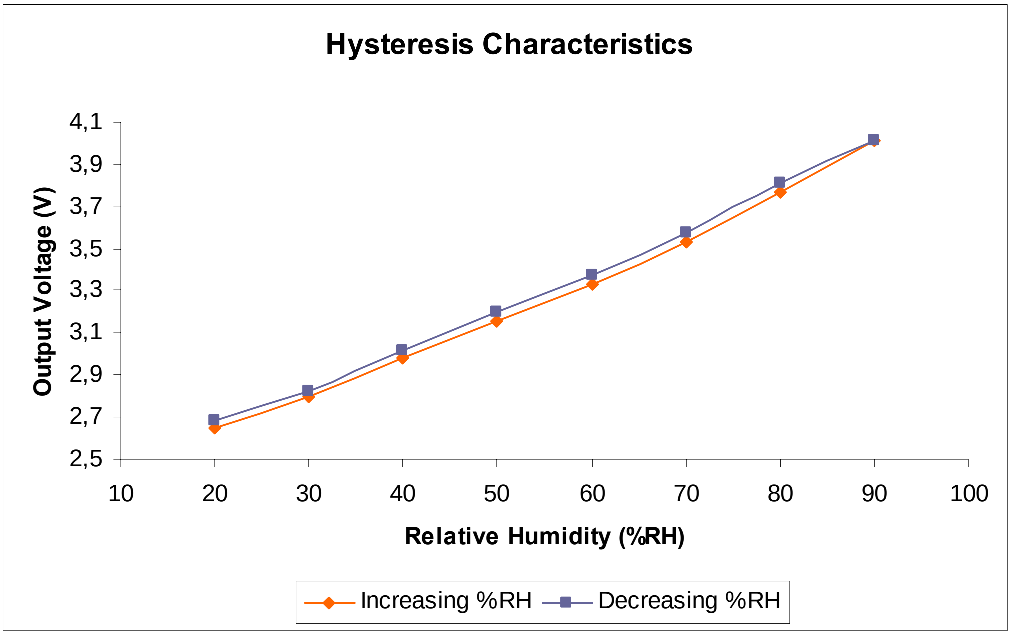

Figure 4.19: Hysteresis characteristics of the hybrid humidity sensor module. Calculated hysteresis is 2.54% RH.

Characterization results of the capacitive humidity sensor module were compared with the performance specifications of a commercial capacitive humidity sensor of Honeywell. Table 4.2 shows the comparison table for the performance specifications of the two humidity sensors.

Table 4.2: Comparison table for the performance parameters of the two humidity sensors.

	Hybrid Module	Commercial Sensor [58]
Sensitivity	19.4mV/%RH	30.68mV/%RH
Hysteresis	2.54% RH	1.2% RH
Response Time	1.6 seconds	15 seconds
Nonlinearity	0.17%	0.5%

4.5 Conclusion

In this chapter, test results of the capacitive humidity sensor, the integrated heater and the hybrid humidity sensor module were presented. The sensor was characterized inside the humidity chamber within the relative humidity range from 20% to 90% relative humidity at different ambient temperatures. The humidity response of the sensor is linear within the 20% to 70% relative humidity range. However, the nonlinearity increases above 70%, which is an expected result due to the nonlinear humidity response of the dielectric constant of the polyimide film. The sensitivity of the sensor was found as 145fF/%RH.

The hysteresis of the sensor was found as 2.57% RH at 20ºC ambient temperature by monitoring the sensor response both in increasing and decreasing relative humidity conditions. Response time measurements showed that the absorption time of the polyimide film is around 1.6 seconds while desorption time is around 12 seconds. It was also verified that the response time is dependent on the opening width for moisture diffusion.

The integrated heater was characterized by monitoring the resistance versus temperature and resistance versus heating power characteristics. It was verified that the heater is capable of reducing the amount of moisture absorbed by the polyimide film. The humidity response of the sensor at the presence of constant heating power was also measured. In addition, it was found out that approximately 180mW of power is necessary to increase the temperature to 100ºC.

Characterization tests were repeated on the hybrid humidity sensor module. The hybrid module showed a humidity sensitivity of 19.4mV/%RH with a nonlinearity of 0.17%. The hysteresis of the hybrid module is almost the same as the hysteresis of the capacitive sensor. In addition, the sensor is capable of measuring less than 3% change in the relative humidity.

CHAPTER 5

A THERMAL CONDUCTIVITY BASED HUMIDITY SENSOR IN A STANDART CMOS PROCESS

This chapter presents the design and implementation of a thermal conductivity based humidity sensor integrated with the readout circuit using standard CMOS fabrication. Section 5.1 explains the theory of humidity sensing using thermal conductivity of the air and the water vapor. Section 5.2 describes the sensor design and discusses the importance of some structural parameters in the performance of the sensor. This section also gives information about the thermal properties and the temperature sensitivity of the diodes, which are used as sensing elements in the sensor. Section 5.3 explains the readout circuit of the sensor and demonstrates the chip layout. Sections 5.4 and 5.5 discuss the post processing of the chip and the test results respectively.

5.1 Humidity Sensing Principle

The humidity sensor designed in this study uses a similar approach to the thermal conductivity based humidity sensors described in Section 1.3.5. In this humidity sensing method, the difference between the thermal conductivities of air and water vapor is used. Thermal conductivities of air and water vapor are both increasing functions of temperature, but the thermal conductivity of water vapor exceeds the thermal conductivity of air at high temperatures. Figure 5.1 shows the thermal conductivity versus temperature plots for air and water vapor [59].

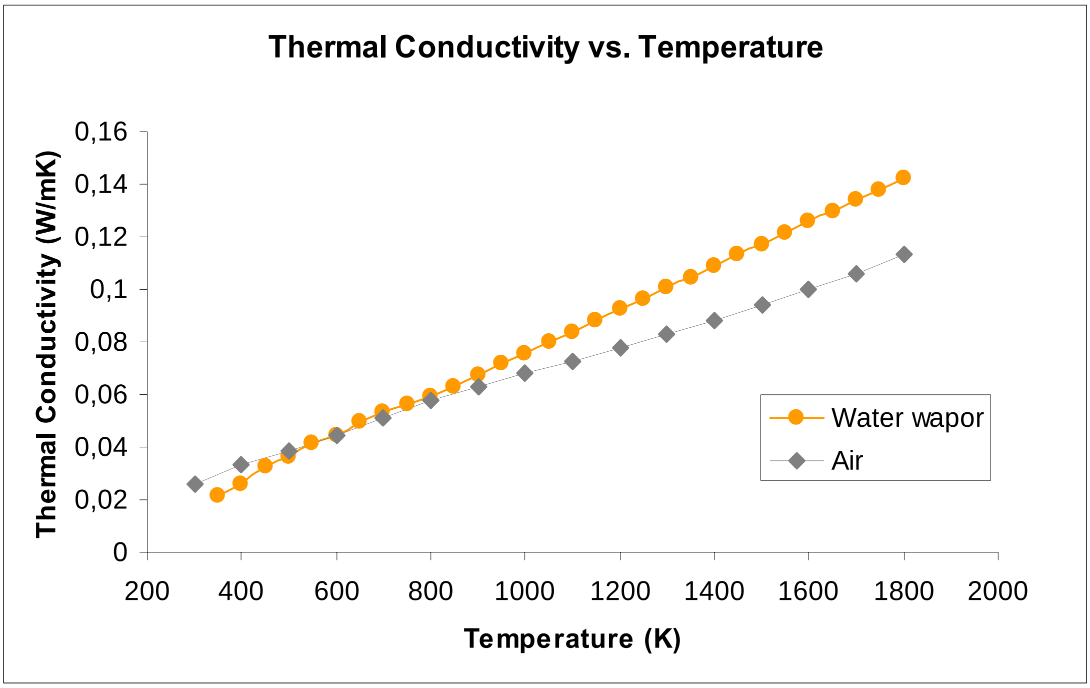

Figure 5.1: Thermal conductivity versus temperature plots for water vapor and air [59].

The humidity sensing idea is to expose a temperature sensitive element to humidity and compare the output of this element with a reference element, which is isolated from the humid environment. The output difference arises from the difference between the thermal conductivity of air and that of the water vapor. In the sensor system, the most important fact is to thermally isolate the sensor and the reference in order to achieve high sensitivity. This is achieved by isolating the sensor and the reference from the silicon substrate, which is a good thermal conductor. For thermal isolation, the substrate underneath the sensor and the reference element is etched and structures are suspended.

The most important fact that affects the sensitivity of the humidity sensor is the temperature sensitivity of the sensor element. In this work, p-n junction diodes are used as the humidity sensitive structures. The most important advantage of diodes is that they have high and almost constant temperature sensitivity in all temperature regions. In addition, they are compatible with the standard CMOS fabrication. Using standard CMOS fabrication, the sensor is monolithically integrated with the readout circuit. This idea has been used in other detector applications such as uncooled infrared microbolometer arrays [48-50].

5.2 Sensor Design

As stated above, the humidity sensor is composed of two diodes. Both of the diodes are isolated from the substrate by post processing after fabrication. Furthermore, the chip is packaged in such a way that the reference diode does not have any interaction with the humid environment. Figure 5.2 shows the cross sectional view of the proposed humidity sensor structure. It can be observed from Figure 5.1 that the thermal conductivity difference becomes significant at temperatures around 550°K. Due to this property, sensor and the reference elements should be heated up to temperatures around 550°K to be able to sense the humidity.

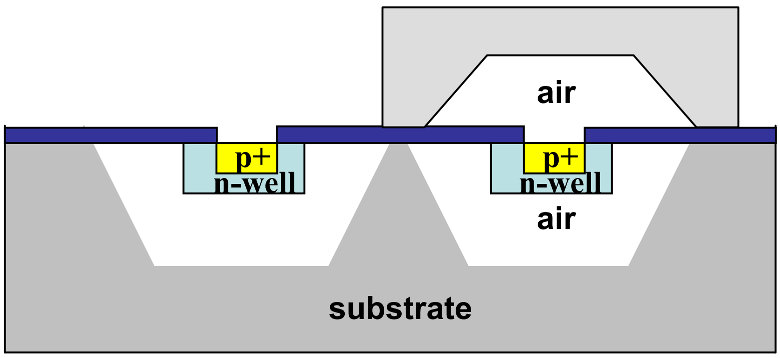

Figure 5.2: A symbolic cross sectional view of the proposed sensor structure.

In order to heat up the diodes around 550°K, they are biased with constant currents. Biasing with constant currents results in a self heating affect, increasing the temperature of the diodes expressed by:

$$\Delta T = \frac{P}{G_{th}} \tag{5.1}$$

where P stands for the electrical power applied on the diode and the G_{th} is the thermal conductance of the structure. The thermal conductance of the structure is dependent on two main parameters [39]. One of them is the thermal conductance of the interconnections of the diode to the constant current source and the readout circuit. The other one is the thermal conductance of the air between the diode and the substrate. Figure 5.3 shows the lumped element thermal circuit representing the self heating of a diode biased with constant current.

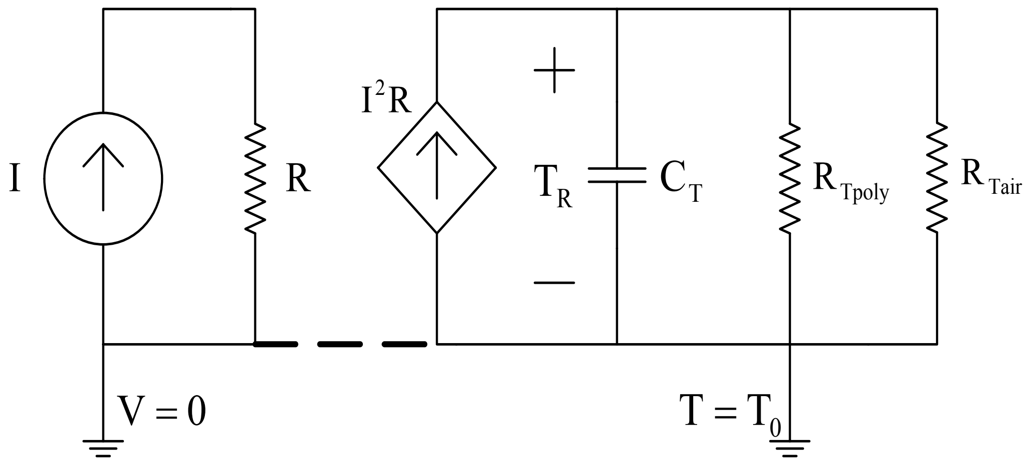

Figure 5.3: The lumped element thermal circuit representing the self heating of a diode biased with constant current.

In Figure 5.3, R_{Tpoly} and R_{Tair} stand for the thermal resistances of the polysilicon interconnections and air between the diode and the substrate. R is the electrical resistance of the structure, where C_T is the thermal capacitance. According to the humidity sensing principle, the temperature of the diode should change when exposed to humidity. This change comes from the change in the thermal conductivity of the air surrounding the diode due to the presence of water vapor. Consequently, it can be stated that to be able to sense the humidity, the thermal conductance of air should be larger than the thermal conductance of the interconnections of the diode. In other words, the thermal conductance of the interconnection should be as small as possible in order to increase the humidity sensitivity. Furthermore, it can be concluded from Equation 5.1 that, if the thermal conductance is low, it is possible to heat up the diodes to high temperatures with less power.

5.2.1 Temperature Sensitivity of Diodes

Temperature sensitivity of the semiconductor diodes can be derived considering the ideal diode equation as follows [51]. In the ideal diode equation, the diode current is given by:

$$I = I_s(e^{V/V_T} - 1) \tag{5.2}$$

where I_s is the saturation current of the diode, V is the diode voltage, and V_T is the thermal voltage. The ideal diode equation is affected by the temperature in two ways. First of all, the saturation current is dependent on the intrinsic carrier concentration, which is a function of temperature. Secondly, the thermal voltage is linearly dependent on the temperature. The effect of temperature on I_s is a result of the temperature dependence of the square of the intrinsic carrier concentration:

$$n_i^2(T) = KT^3 e^{-V_{go}/V_T} \tag{5.3}$$

where V_{go} is the bang-gap voltage. The fractional change in I_s per unit change in temperature is approximately equal to the fractional change in n_i^2 per unit change in temperature.

$$\frac{1}{I_s}\frac{dI_s}{dT} = \frac{1}{n_i^2}\frac{dn_i^2}{dT} \tag{5.4}$$

$$\frac{1}{I_s}\frac{dI_s}{dT} = \frac{3}{T} + \frac{1}{T}\frac{V_{go}}{V_T} \tag{5.5}$$

Near the room temperature, the first term is approximately 1%/K, and the second term is 14%/K. Finally, the temperature dependence of the diode voltage at a fixed current is expressed as:

$$\left.\frac{dV}{dT}\right|_{dI=0} = \frac{d[V_T \ln(I/I_s)]}{dT} \tag{5.6}$$

$$\left.\frac{dV}{dT}\right|_{dI=0} = \frac{V}{T} - V_T\left(\frac{1}{I_s}\frac{dI_s}{dT}\right) \tag{5.7}$$

At a constant forward current, the temperature coefficient of a silicon p-n junction diode is approximately -2mV/ºC. Furthermore, temperature sensitivity of the diode is almost constant in a wide temperature range.

5.2.2 Humidity Sensitive Diode Design

In the diode design, the most important design goal is to decrease the thermal conductance of the diode interconnections in order to increase the sensitivity of the sensor. As given in Section 2.3, the thermal conductance of a rectangular shaped resistor is given by:

$$G_{th} = \sigma \frac{A}{l} \tag{5.8}$$

where σ is the thermal conductivity, A is the cross sectional area, and l is the length of the resistor.

The humidity sensitive diode design was performed in a 0.6μm CMOS process. In this process, two metal and two poly-silicon layers are available for interconnection. Metal layers, having high thermal conductivity values, are not suitable for usage as interconnect layers. Polysilicon has a relatively low thermal conductivity, which can provide a low thermal conductance if it is used as the interconnect layer. However, it has a high resistivity, which is an important disadvantage for the temperature sensing applications. This disadvantage arises from the fact that the resistance is a function of temperature. The effect of temperature on the resistance is expressed as:

$$R = R_o(1+\alpha\Delta T) \tag{5.9}$$

where α is called the temperature coefficient of resistance (TCR), R_o is the initial resistance and ΔT is the temperature variation. The TCR of polysilicon is a positive value, which results in a positive temperature sensitivity of the resistor. As expressed in the previous subsection, the temperature sensitivity of the diode is negative. Consequently, positive temperature sensitivity of a resistor reduces the overall sensitivity of the structure. This phenomenon can be shown mathematically as follows. Since the diode is biased with a constant current, the output voltage is expressed as:

$$V = V_d + iR_{poly} \tag{5.10}$$

Temperature sensitivity of the output voltage is found by inserting equation 5.9 into equation 5.10 and taking the derivative of both sides with respect to temperature:

$$\frac{dV}{dT} = \frac{dV_d}{dT} + \alpha iR \tag{5.11}$$

It should be mentioned that the dV_d/dT term has a negative value, while the αiR term has a positive value; therefore, it reduces the sensitivity provided by the diode. The

αiR term is directly proportional to the bias current, the resistance and the TCR of the interconnect layer. In order to increase the sensitivity of the sensor, either the bias current or the resistance should be decreased. The resistance can be decreased by either decreasing the length or increasing the cross sectional area of the resistor. It should be noted that this operation increases the thermal conductance of the structure, which is an unwanted result. On the other hand, decreasing the current reduces the power dissipated on the resistor, so the final temperature of the device. However, the sensor should be heated up to a proper temperature level to be able to sense the humidity. In conclusion, there is a compromise between the bias current, the resistance, and the thermal conductance of the diode structure in terms of their effect on the performance of the sensor. In order to find an optimum bias level and a resistor dimension, MATLAB simulations were performed. The total pixel area was also fixed to a value which guarantees the etching of the silicon substrate during the post-CMOS process. The temperature sensitivity of the diode and the final temperature were plotted with respect to the polysilicon length to width ratio and the bias current.

Figure 5.4 shows the simulation results. As stated above, the diodes should be heated up to approximately 250ºC to be able to sense the humidity. Simulation results show that the final temperature increases and sensitivity of the sensor decreases with the increasing bias current and the length over width ratio. Consequently, the optimum design can be achieved by taking the values around the 250ºC final temperature level. The length over width ratio was selected as 140, which is the most suitable value for the post processing of the diode. The sensitivity, sensitivity over power dissipation, and the operating temperature curves were plotted with respect to the bias current. Figure 5.5 shows the simulation results.

As observed from Figure 5.5, the bias current of the diode should be larger than 100µA to be able to heat up the diodes to the desired temperature levels. Since the sensitivity is decreasing with the increasing bias current, minimum possible bias current is selected, which is 100µA.

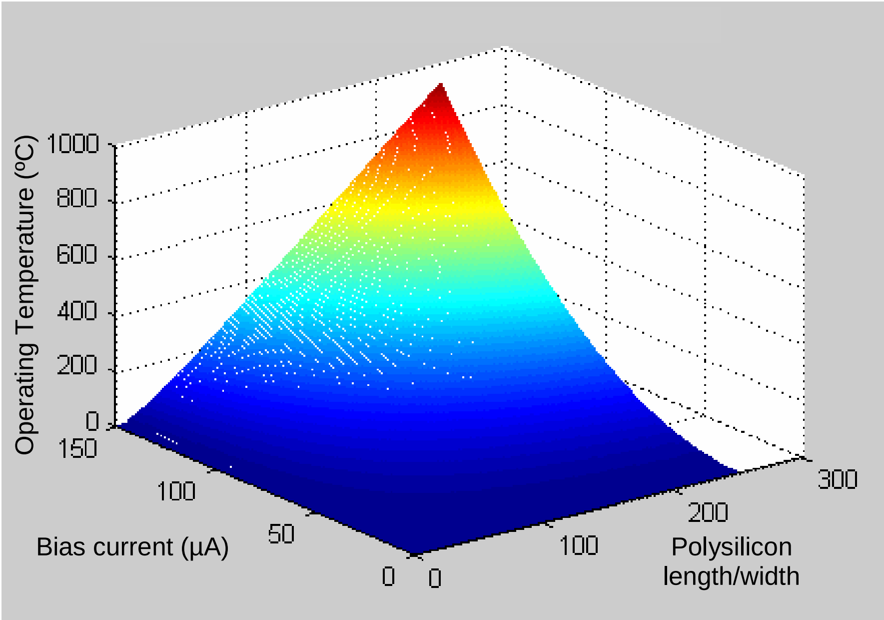

(a)

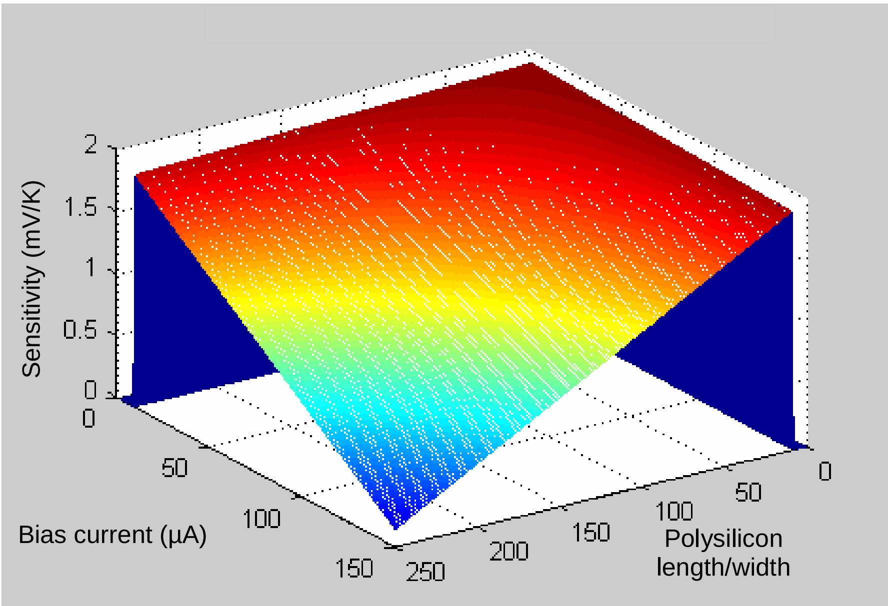

(b)

Figure 5.4: Graphics showing the diode parameters with respect to the bias current and the polysilicon length over width ratio: (a) operating temperature, (b) sensitivity.

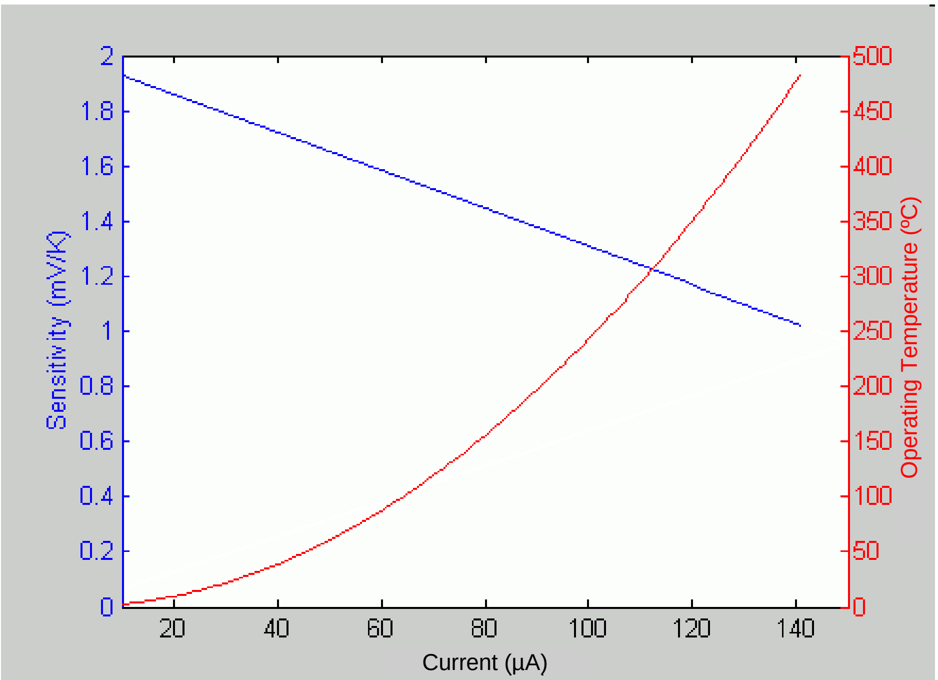

(a)

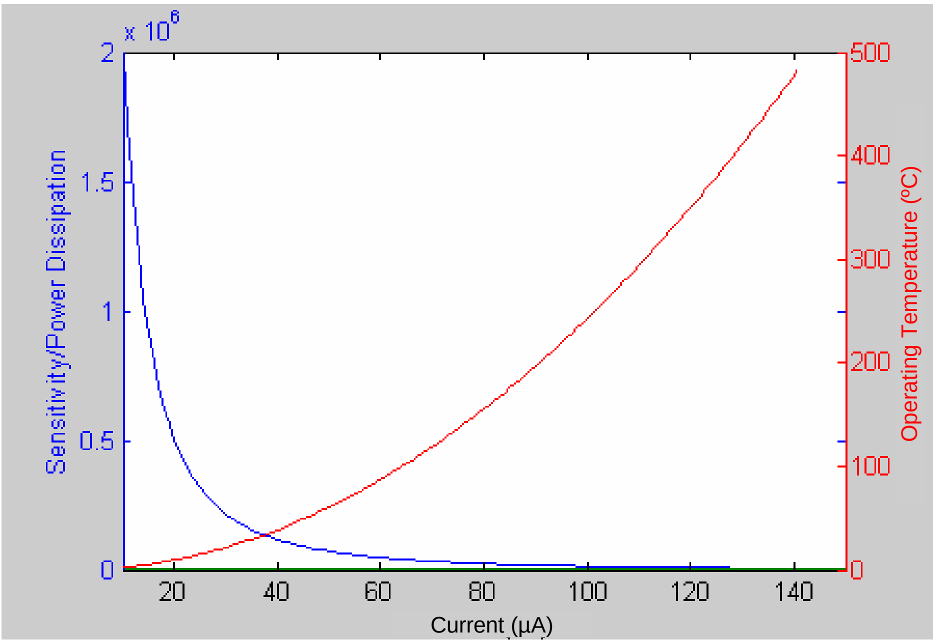

(b)

Figure 5.5: Graphics showing the diode parameters with respect to the bias current at fixed polysilicon dimensions: (a) sensitivity and operating temperature, (b) sensitivity over power dissipation and operating temperature.

Table 5.1 gives the values of important design parameters of the humidity sensitive diode. The thermal conductance of the air between the diode and the substrate was calculated by the help of Equation 5.8. In the equation, thermal conductivity was taken as the thermal conductivity of air, where the area was taken as the diode area and the length was taken as the average length between the diode and the substrate [52].

Table 5.1: Important design parameters of the humidity sensitive diode.

Thermal Conductance of Air	3.64×10^{-7} W/K
Thermal Conductance of Interconnections	1.575×10^{-8} W/K
Overall Thermal Conductance	3.798×10^{-7} W/K
Interconnect Resistance	9.4kΩ
Diode Temperature (@100µA bias level)	248ºC
Temperature Sensitivity	-1.3mV/K

5.2.3 The Diode Layout

Figure 5.6 shows the layout of the humidity sensitive diode. The diode layout was designed in the AMS 0.6µm CUP process. The most important problem with the diode layout design is the length of the polysilicon interconnections. Since the total pixel area is also a critical value in terms of the thermal conductance of the structure, long polysilicon interconnections should be inserted into a limited area. This is achieved by drawing the polysilicon lines around the diode.

Another important point on the layout design is the opening area around the diode. During the CMOS fabrication, this area should be opened up to the silicon substrate to be able to suspend the diodes by post processing. In the diode layout, all of the contact, via, and diffusion layers were drawn on top of each other so that the field oxides of the standard CMOS process were removed during the fabrication [57].

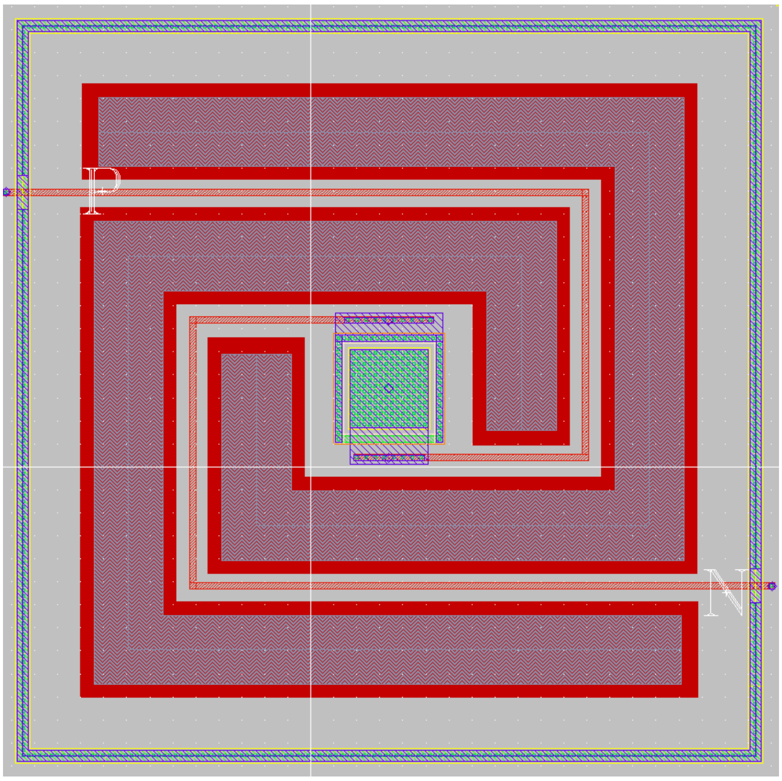

Figure 5.6: The layout of the humidity sensitive diode designed in AMS 0.6µm CUP process. Diode dimensions are 25µm x 25µm, where total layout dimensions are 160µm x 160µm.

5.3 The Readout Circuit

The humidity sensitive diode proposed in this study is biased with a constant current, and the output voltage change is observed. This is a well known method that has been used in the development of uncooled infrared microbolometer arrays [48-50]. High performance readout circuits for this type of detectors have also been presented such as the differential buffered injection capacitance transimpedance amplifier (DBI-CTIA) circuit [53]. A similar approach was used in the readout circuit designed in this study. The readout circuit consists of a transconductance amplifier and a switched capacitor integrator. Figure 5.7 demonstrates the block diagram of the readout circuit.

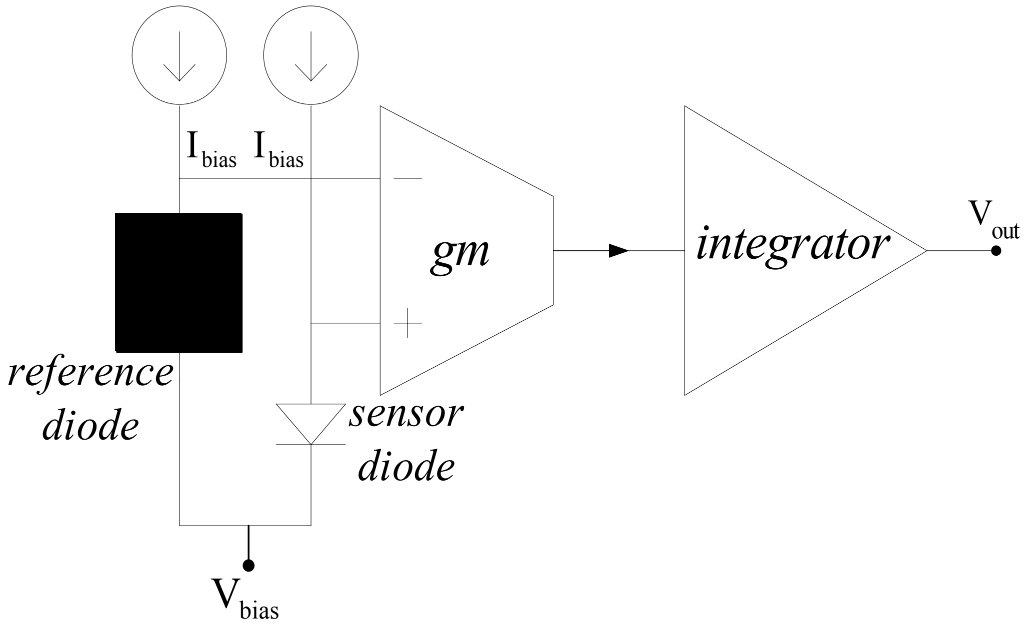

Figure 5.7: The block diagram of the readout circuit designed for the thermal conductivity based humidity sensor chip.

The transconductance amplifier converts the voltage difference between the sensor and the reference diode into current change. This current change is integrated through a switched capacitor integrator. The integration operation converts the output current of the transconductance amplifier into voltage, providing a proper gain to the system.

The transconductance amplifier designed in this study is a CMOS differential amplifier with n-channel input transistors. Figure 5.8 shows the circuit schematic of the differential amplifier. The differential pair is loaded by a p_channel current mirror. The amplifier is biased with a constant current generated by an n-channel transistor connected to the common source terminal of the input pair transistors.

Gain of the differential pair is derived as follows. The input transistor M1 generates a small signal current of $i_{d1} = gm_{1,2}(v_1 - v_0)$, where v_1 is the input voltage of M1 transistor, *gm* is the transconductance, and v_0 is the voltage at the source terminals of the input stage transistors. The small signal current of M1 is mirrored by the current mirror. This current is subtracted from the small signal current generated by the M2 transistor resulting which is equal to $i_{d2} = gm_{1,2}(v_2 - v_0)$, resulting in an output current expressed as:

$$i_{out} = gm_{1,2}(v_1 - v_2) \tag{5.12}$$

As a result, the difference of the input voltages is converted into current with a transconductance, which is equal to the transconductance of the input stage transistors.

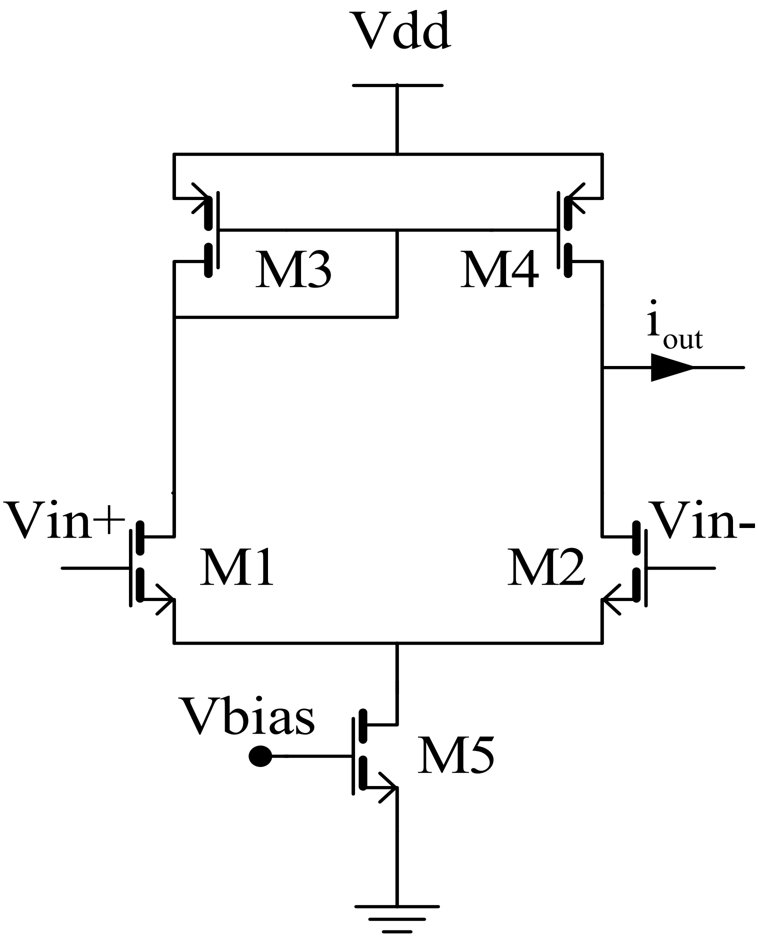

Figure 5.8: The circuit schematic of the transconductance amplifier.

The output current of the transconductance amplifier is integrated through the switched capacitor integrator. The switched capacitor integrator has an inverting amplifier structure, whose circuit schematic is demonstrated in Figure 5.9. Switching configuration is designed for cancellation of the input offset voltage of the operational amplifier.

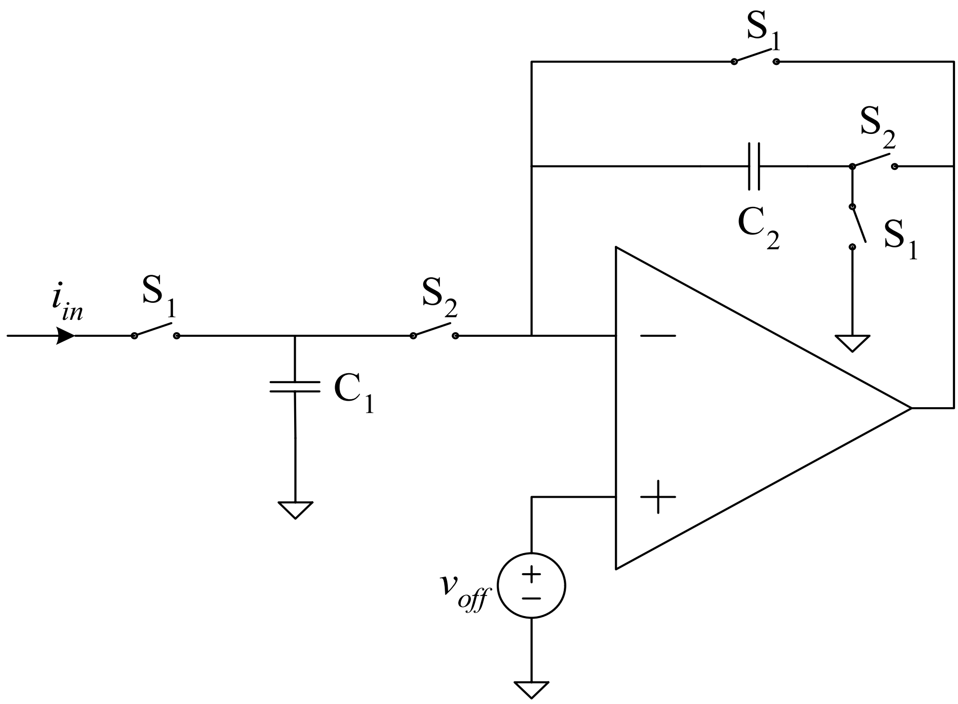

Figure 5.9: The circuit schematic of the switched capacitor integrator with switching configuration designed for offset cancellation.

The operation of the integrator is as follows. When the S_1 switch is on, C_1 capacitor is charged by the input current. During this period, the feedback capacitor C_2 stores the input offset voltage of the operational amplifier and the output is reset to the virtual ground level. At the instant that the S_1 switch turns off, the voltage on the C_1 capacitor is expressed by the following equation:

$$V_{c1} = \frac{i_{in} T_{\text{int}}}{C_1} \tag{5.13}$$

where T_{int} is the charging time of the capacitor and i_{in} is the current that charges the C_1 capacitor. When the S_2 switch turns on, the charge stored by the C_1 capacitor is injected to the C_2 capacitor. The output voltage of the integrator at this state is given by:

$$V_{out} = -V_{C1}\frac{C_1}{C_2} \tag{5.14}$$

At this state, the offset voltage stored on the C_2 capacitor is also subtracted from the output voltage. It should be noted that the i_{in} parameter of Equation 5.13 is the output current of the transconductance amplifier given by Equation 5.12. In order to find the gain of the overall system, Equations 5.12 and 5.13 are inserted into Equation 5.14. Gain is expressed by the ratio of the output voltage to the differential input voltage, which is equal to:

$$\frac{V_{out}}{V_{in}} = \frac{gm_{1,2}T_{\mathrm{int}}}{C_2} \tag{5.15}$$

It should be noted that the integration operation is performed on the C_1 capacitor, so value of the C_1 capacitor is also important although it is not present at the output expression. In fact, the gain of the system is determined by the C_1 capacitor according to Equation 5.13, and then it is scaled by the C_2 capacitor.

Figure 5.10 shows the layout of the humidity sensitive diode chip. The layout of the chip was designed in the AMS 0.6µm CUP process. In the layout design, the post processing and the packaging of the chip was also considered. The reference diode was placed in the middle of the die, and it was surrounded by a 250µm wide metal3 ring. This ring was placed to indicate the area that will be isolated from the environment. Figure 5.11 shows a schematic view of the complete sensor system.

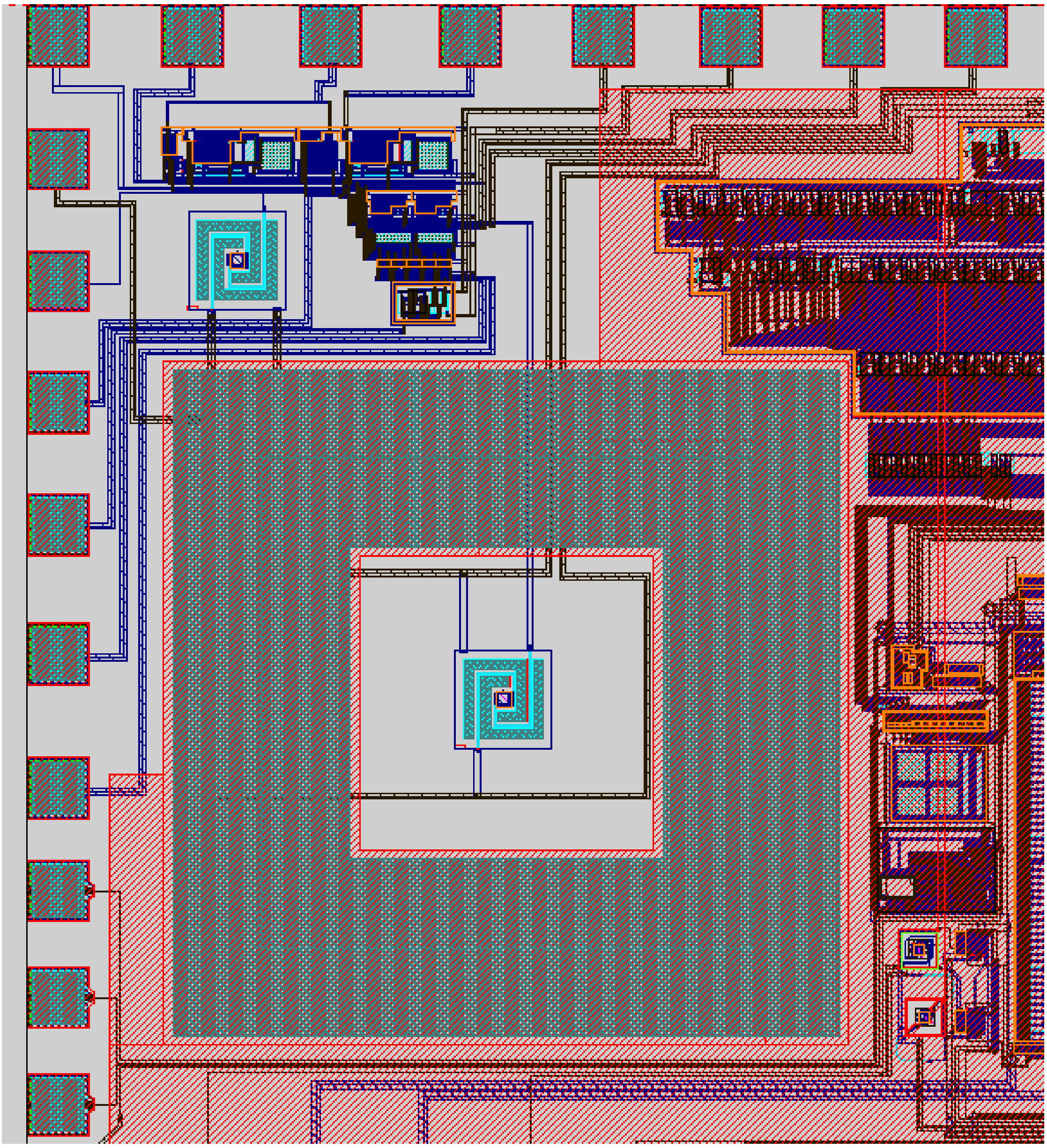

Figure 5.10: The layout of the humidity sensitive diode chip designed in the AMS 0.6µm CMOS process. Total layout dimensions are 1650µm x 1900µm.

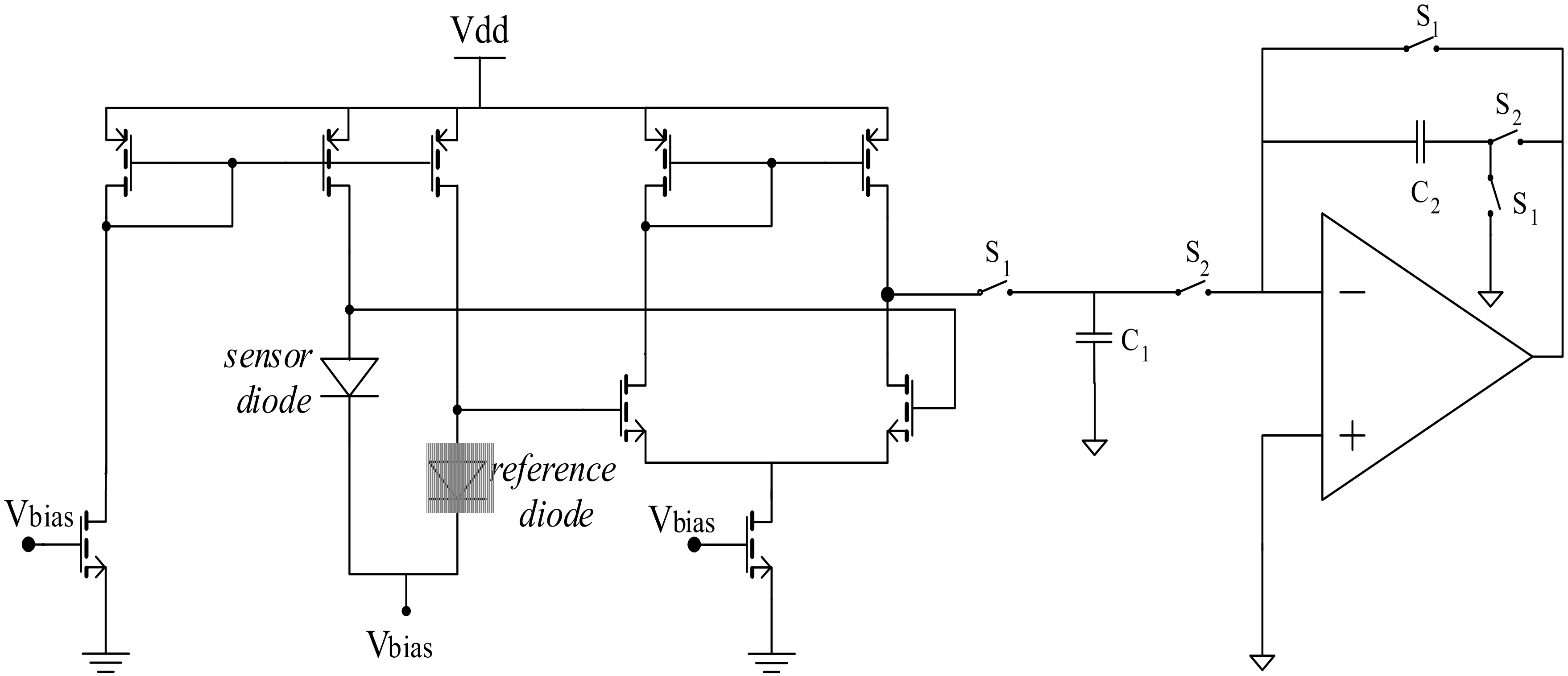

Figure 5.11: A schematic view of the thermal conductivity based humidity sensor system.

5.4 Post Processing

After the fabrication of the chip in the standard CMOS process, post processing is required to provide thermal isolation of the diodes from the substrate*. Thermal isolation was achieved by anisotropic bulk silicon etching. Before the bulk silicon etching, the humidity sensor sample was placed on an alumina substrate and necessary wire connections were made. N-well and substrate pads and the corresponding bonding wires were covered with white epoxy for protection against the etchant. Figure 5.12 shows the humidity sensitive diode sample placed on an alumina substrate.

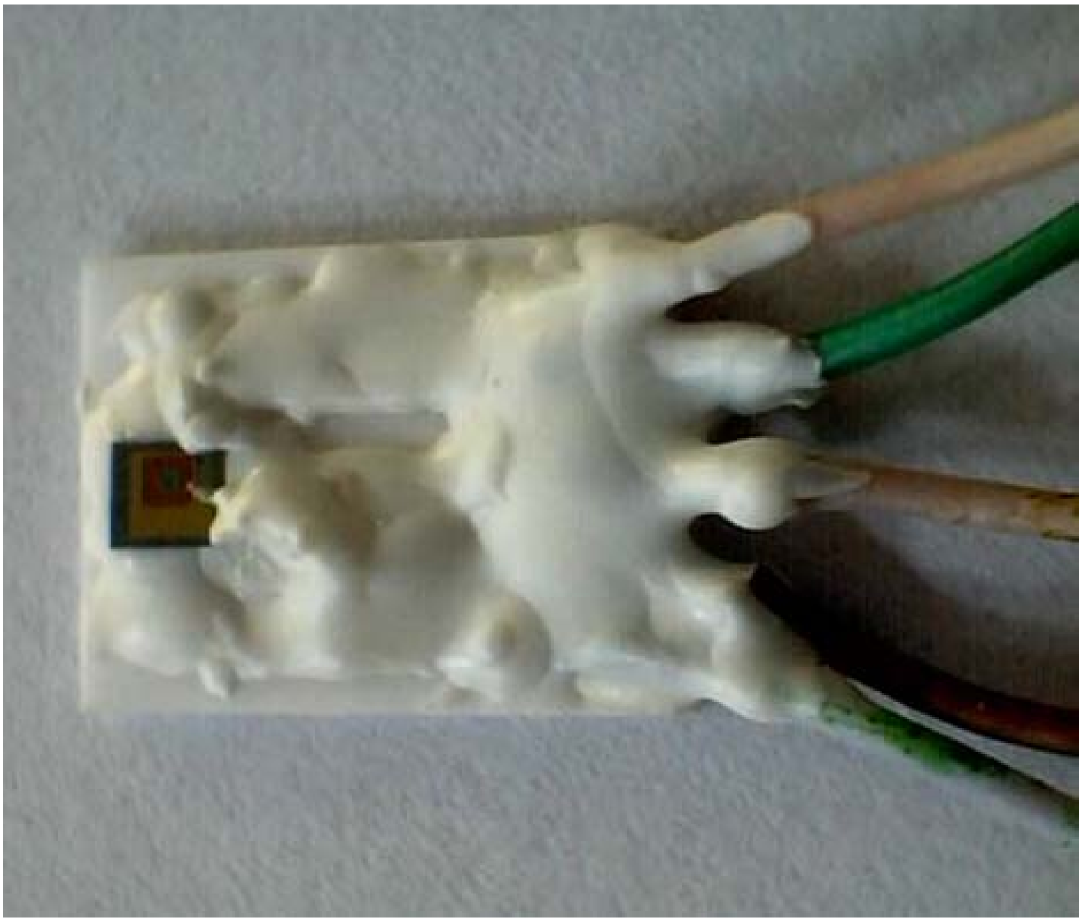

Figure 5.12: The humidity sensitive diode chip placed on an alumina substrate.

* The post-CMOS etching is performed by Mr. Yusuf Tanrıkulu.

There are three main materials that can be used for anisotropic bulk silicon etching. These are potassium hydroxide (KOH), ethylene diamine pyrocathecol (EDP), and tetramethly ammonium hydroxide (TMAH) [54]. In this work, TMAH was used as the bulk silicon etchant due to some advantages with respect to other etchants. The major advantage of TMAH is that it does not attack aluminum if certain amount of silicon is dissolved in the solution [55]. In addition, TMAH is safer and easier to handle, so it was decided to be used for the post processing of the humidity sensitive diode chips.

The most important part of the anisotropic bulk silicon etching process is the protection of the diodes against the etchant. In this process, electrochemical etch stop technique was used. In the electrochemical etch stop technique, the p-n junction, which is formed between the substrate and the n-well is reverse biased so that the electrons are pulled away from the n-type silicon. This operation results in SiO_2 formation on the silicon surface when the p-type silicon is completely etched away [56]. As a result, etching of the n-well layer is prevented. The voltage applied on the n-well is called the passivation voltage. Voltages higher than the passivation voltage can stop etching. The voltage applied to the substrate must be less than its passivation voltage, while the voltage applied to the n-well must be higher than the passivation voltage. This way, the substrate around the diode is etched and the diode is protected.

Electrochemical etch stop was performed using four electrode etch control configuration. Figure 5.13 demonstrates the schematic view of the four electrode configuration. In the four electrode configuration, p and n-type silicon are biased at the same time with respect to the etching solution. The potential of the solution is measured with a reference electrode and fed back to a potentiostat, which continuously controls the bias voltages.

Before starting the process, 16gr/lt of silicon powder was dissolved in 5% TMAH solution to prevent the etching of aluminum. At the beginning of the etching, 0.4gr/100 ml of ammonium peroxidisulfate ($(NH_4)_2S_2O_8$) was also added to the etching solution. This material prevents the formation of hillocks on the surface, but it slows down the etching process [55]. At the beginning of the etching process there is no need to bias the n-well layer, since the n-well is not directly exposed to the solution. Furthermore, when the passivation voltage is applied, the etch rate decreases. Therefore, in order not to decrease the etch rate at the beginning of the process, n-well was not biased. The time it takes for the solution to reach the n-well was determined experimentally, and the etch stop potential was applied accordingly. Table 5.2 gives the important parameters of the etching process.

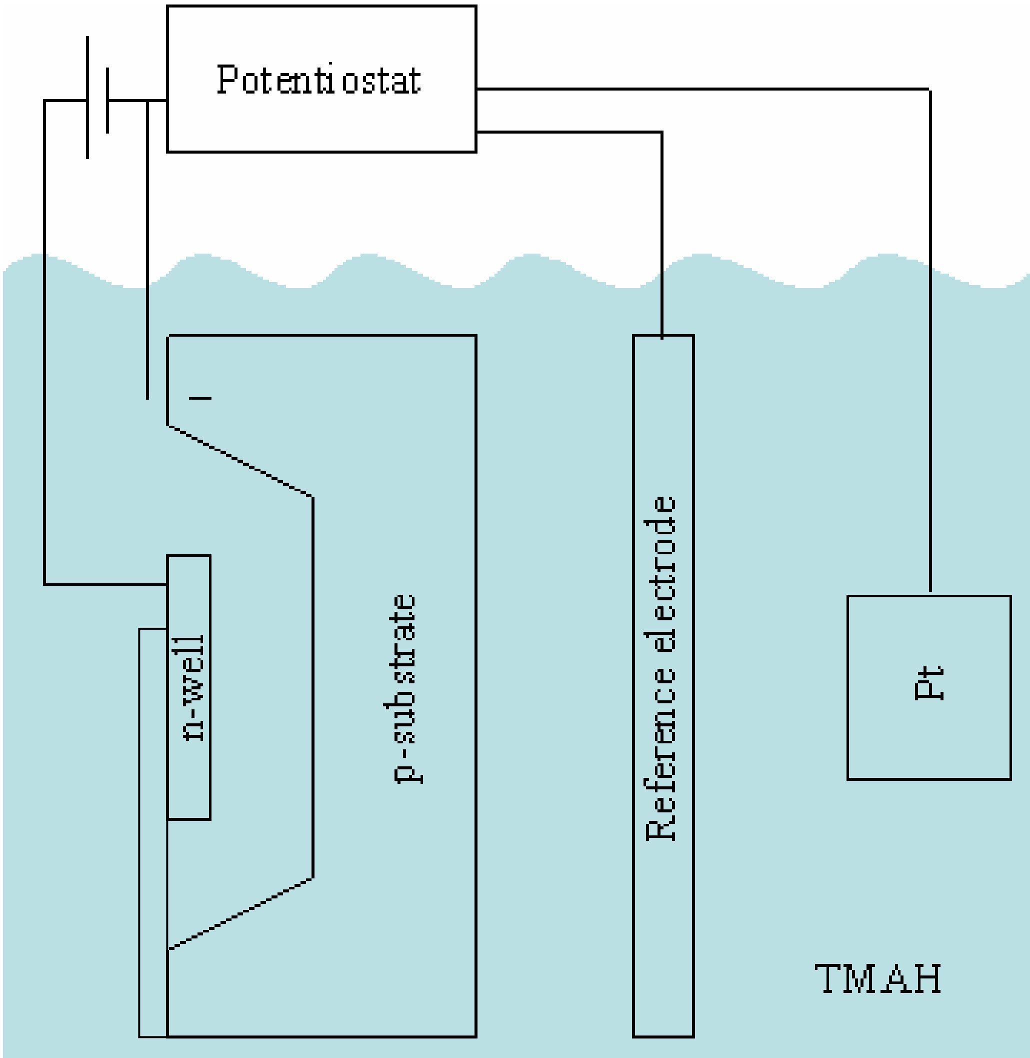

Figure 5.13: Four-electrode electrochemical etch stop configuration.

Table 5.2: Important parameters of the TMAH etching and electrochemical etch stop processes.

Etchant	$(NH_4)_2S_2O_8$ amount	Pre-etch duration	Substrate bias	N-well bias	Etch duration
5% Si doped TMAH	0.4gr/100ml	5 minutes	-1.45 V	0 V	3 hours

5.5 Fabrication and Test Results

Humidity sensitive diode chips were fabricated in the AMS 0.6µm CMOS process. After the standard CMOS fabrication, thermally isolated diodes were obtained using bulk silicon etching and electrochemical etch stop techniques*. Figure 5.14 shows an SEM picture of the fabricated chip. Figure 5.15 shows the SEM pictures of the thermally isolated diodes.

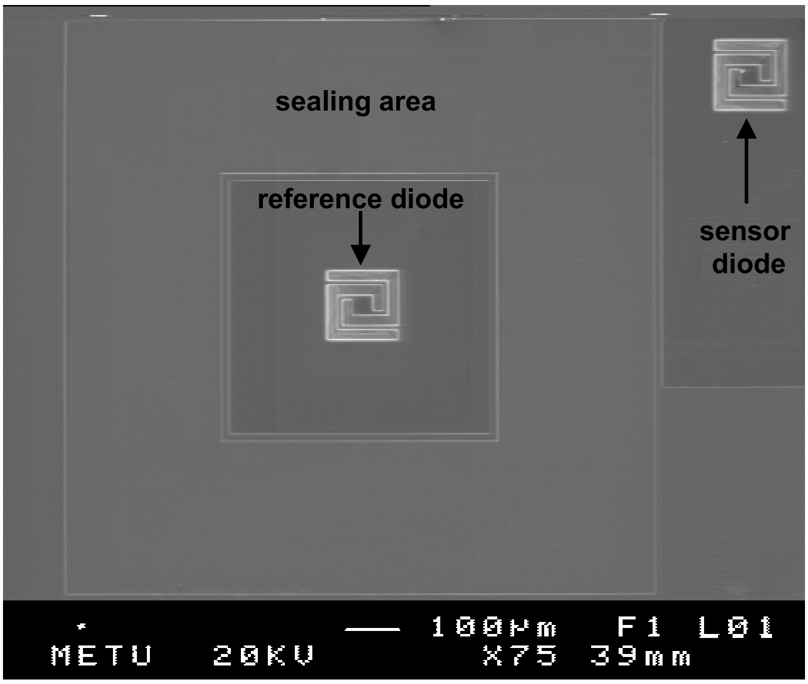

Figure 5.14: An SEM picture of the fabricated chip.

* The post-CMOS etching is performed by Mr. Yusuf Tanrıkulu.

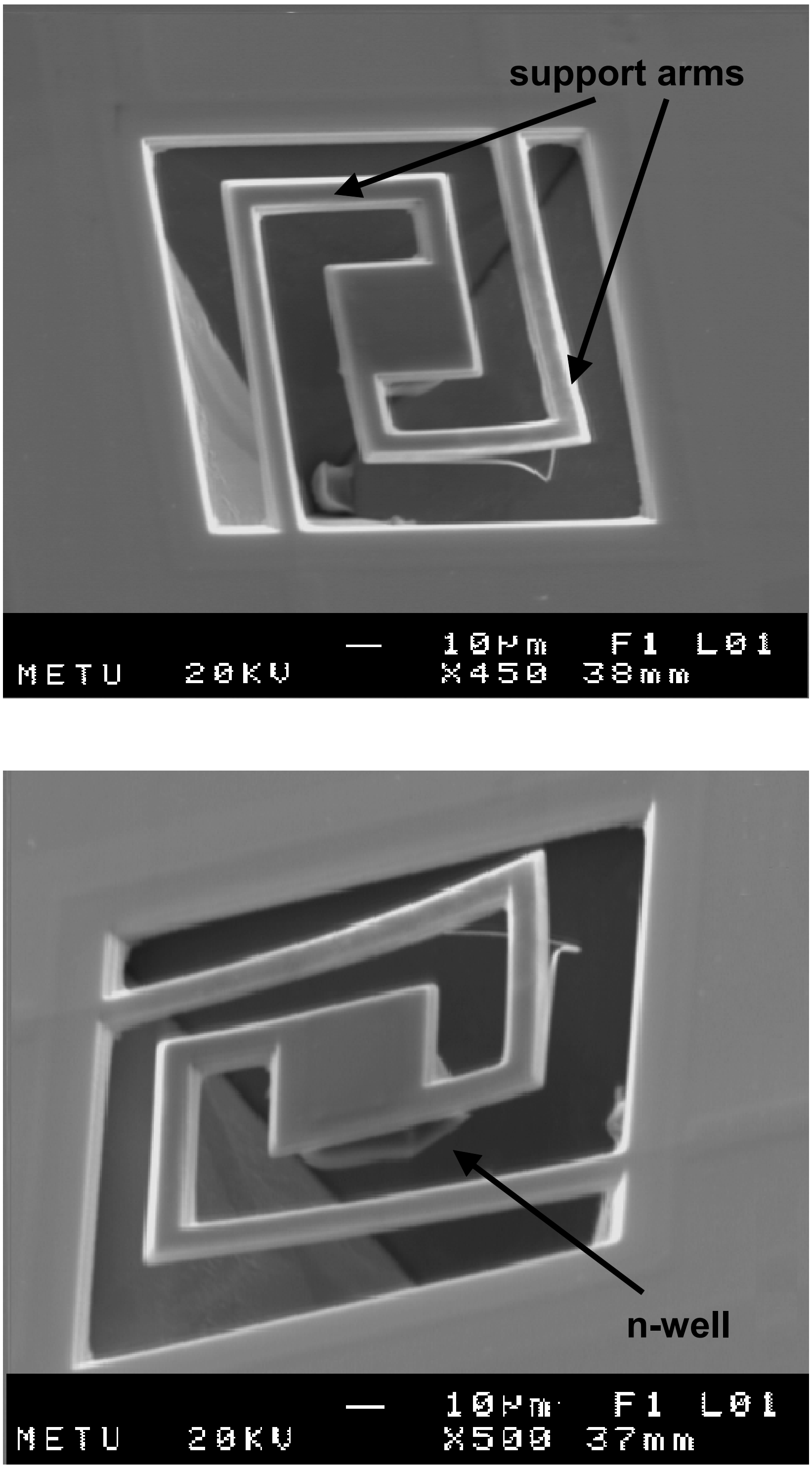

Figure 5.15: SEM pictures of the thermally isolated diode by post-CMOS anisotropic bulk silicon etching.

The reference diode in the chip needs to be isolated from the humid environment for proper operation. This isolation can be achieved by attaching a silicon cap on top of the reference diode. However, this requires the development of die level packaging technique, which is a difficult subject. Since the die level packaging of the chip could not be performed within the time frame of this study, diodes of different chips were used for the characterization measurements. Diodes were connected to the readout circuit on a printed circuit board and the reference diode was sealed by putting a metal cap on it. The metal cap was stuck on the PCB using white epoxy to ensure that it does not allow humidity inside. Figure 5.16 shows the PCB used for the measurements. The PCB also includes biasing circuitries for the readout chip. This PCB is used to determine the humidity response of the sensor and to perform hysteresis measurements as explained in the following sections.

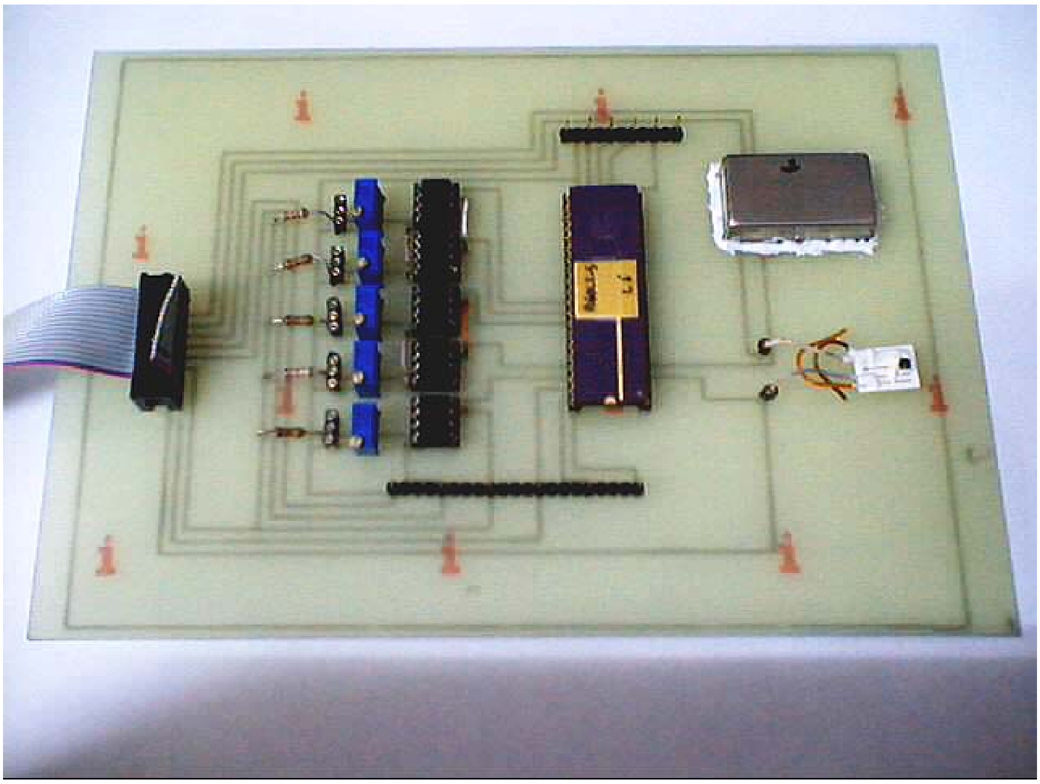

Figure 5.16: The PCB used for the characterization of the thermal conductivity based humidity sensor.

5.5.1 Temperature Sensitivity Test

The first test performed on the sensors is the temperature sensitivity of the diodes. Temperature sensitivity was measured within the temperature range from 150ºC to 250ºC. The humidity sensitive diode chip was stuck on an alumina substrate and heated on a hot plate. For this measurement, unsuspended diodes were used to ensure that the diodes were heated up to the temperature levels set on the hot plate. Diode voltages were measured at 100µA bias level. Figure 5.17 shows the output voltage versus temperature plots for the diodes. Temperature sensitivity of the diodes were found as -1.3mV/K, which is close to the theoretical calculations presented in Section 5.2.2. The mismatch between the output voltage of the sensor and the reference diodes is determined to be very small.

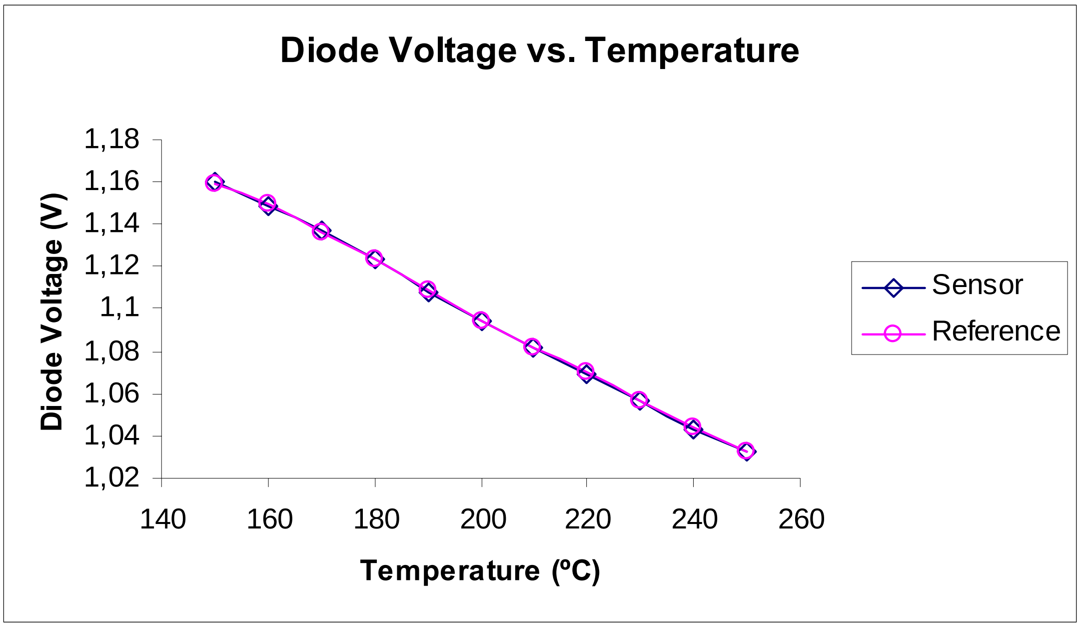

Figure 5.17: Output voltage versus temperature curves for the sensor and the reference diodes at 100µA bias level.

5.5.2 The Humidity Response

Characterization of the sensor was performed inside the environmental chamber. The sensor was exposed to relative humidity ranging from 20% RH to 90% RH at 20ºC ambient temperature conditions, and the output voltage of the circuit was monitored. Figure 5.18 shows the humidity response of the sensor. The humidity sensitivity of the sensor was found as 14.3mV/%RH with a nonlinearity of 0.13%.

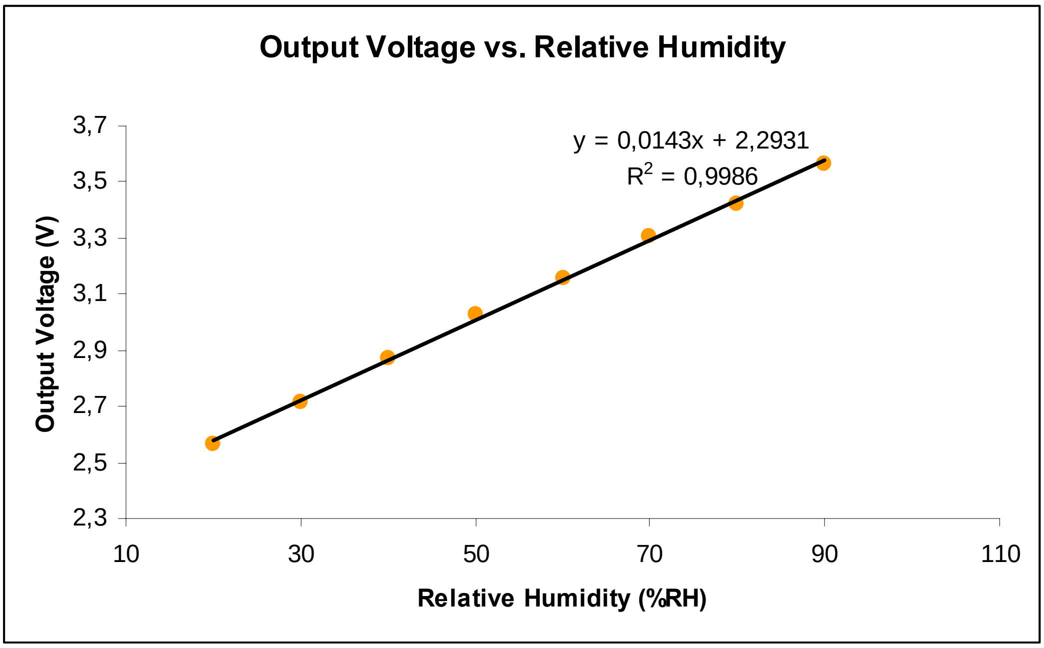

Figure 5.18: Output voltage versus relative humidity curve for the thermal conductivity based humidity sensor. Humidity sensitivity is 14.3mV/%RH at 20ºC.

In order to investigate the effect of the ambient temperature on the sensor output, the same characterization was performed at different temperatures, whose results are shown in Figure 5.19. It was realized that the sensor response is highly dependent on the ambient temperature. This is an expected result since the thermal conductance of the air is directly proportional to the amount of water vapor in the air. In other words, the sensor output is proportional to the amount of absolute moisture in the air. The amount of absolute moisture increases with increasing temperature at the same relative humidity conditions, so the characterization curve of the humidity sensor changes at different ambient temperature conditions. The sensitivity of the sensor was found as 14.3mV/%RH, 26mV/%RH, and 46.9mV/%RH for 20ºC, 30ºC, and 40ºC respectively. At 40ºC, the output of the sensor saturates to the positive supply voltage above 60% relative humidity.

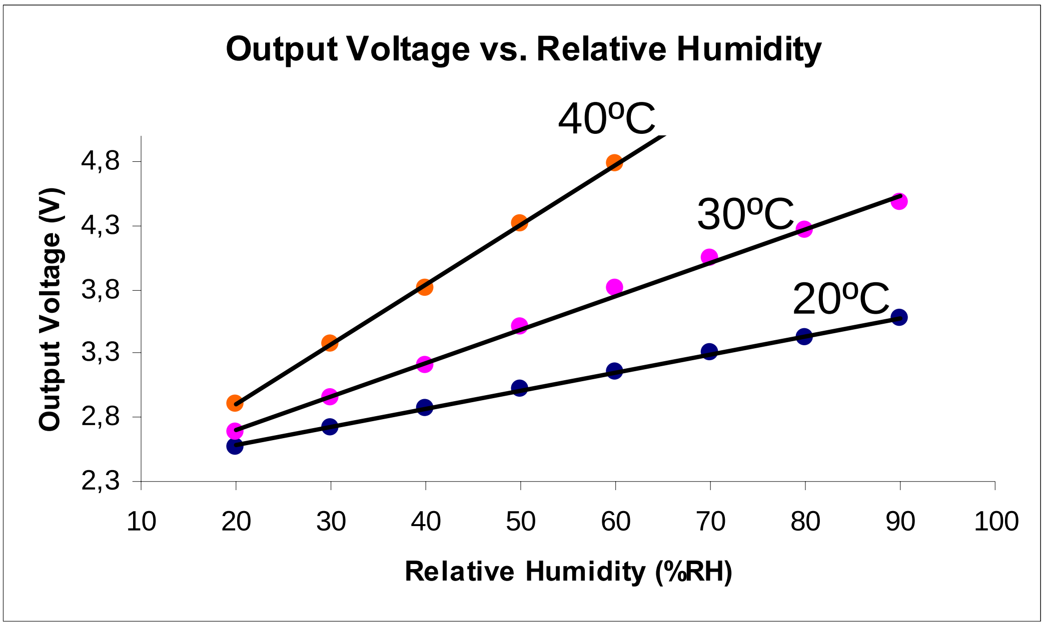

Figure 5.19: Output voltage versus relative humidity curves for different ambient temperature conditions.

5.5.3 Hysteresis Characteristics

Hysteresis of the sensor was measured inside the environmental chamber by increasing the relative humidity from 20% to 90% and then decreasing back to 20%. Measurement was performed after waiting for 30 minutes at every measurement point. Figure 5.20 shows the hysteresis test results of the humidity sensor, which is less than 1% relative humidity.

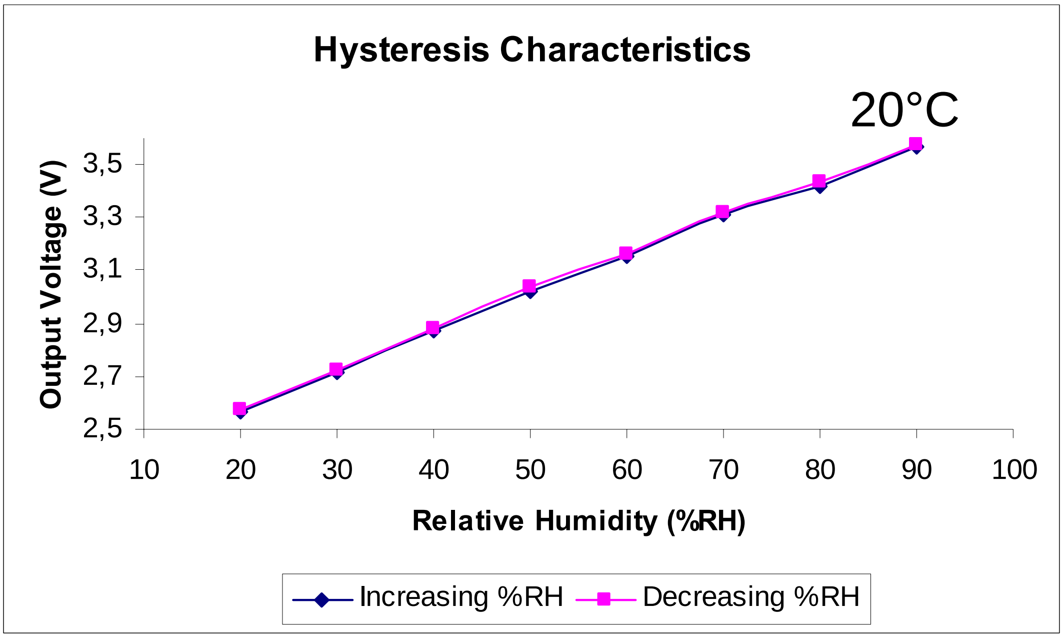

(a)

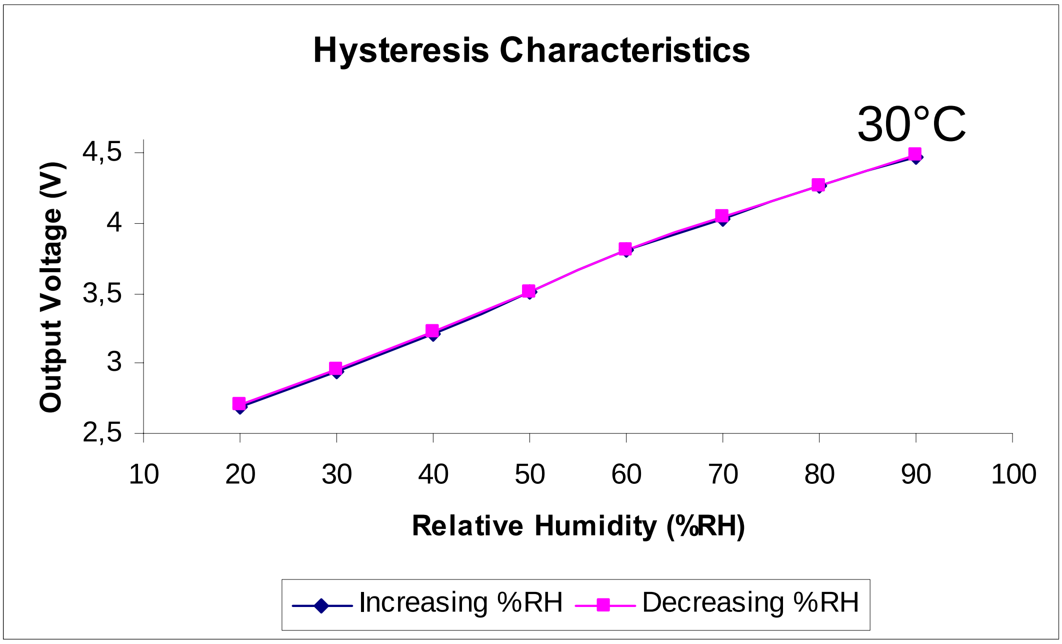

(b)

Figure 5.20: Hysteresis test results of the humidity sensor at (a) 20ºC and (b) 30ºC ambient temperatures.

The hysteresis of the sensor is less than 1% RH at 20ºC and 30ºC ambient temperature. This is an expected result since the moisture is not absorbed by the sensor. Table 5.3 shows a summary of the characterization results of the thermal conductivity based humidity sensor.

Table 5.3: Characterization summary of the thermal conductivity based humidity sensor.

Humidity Sensitivity	20ºC	14.3 (mV/%RH)
	30ºC	26 (mV/%RH)
	40ºC	46.9 (mV/%RH)
Hysteresis	20ºC	< 1%RH
	30ºC	< 1%RH
Power Dissipation	1.38mW	

5.6 Conclusion

This chapter presented the development and implementation results of a new thermal conductivity based humidity sensor. The sensor was fabricated using standard CMOS and post-CMOS anisotropic bulk silicon etching processes. Using standard CMOS fabrication, the sensor was integrated with the readout circuit monolithically. Test results showed that the humidity sensitivity of the sensor is 14.3mV/%RH, 26mV/%RH, and 46.9mV/%RH for 20ºC, 30ºC, and 40ºC, respectively. The hysteresis of the sensor is less than 1% RH at 20ºC and 30ºC ambient temperature. Total power dissipation of the circuit including the readout circuit is only 1.38mW, which is the major advantage of this sensor compared to the thermal conductivity based humidity sensors present in the literature.

CHAPTER 6

CONCLUSIONS AND FUTURE WORK

This thesis presents the design and implementation of humidity sensors using MEMS and standard CMOS technologies. Two different humidity sensors were implemented using capacitive and thermal conductivity based humidity measurement techniques. The capacitive humidity sensor was hybrid connected to a CMOS switched capacitor readout circuit, which is also developed in this study; while the thermal conductivity based humidity sensor was monolithically integrated with the readout circuit using standard CMOS fabrication and post-CMOS processing. Achievements of this research can be summarized as follows:

1. A capacitive humidity sensor with an integrated heater was designed and fabricated by three mask surface micromachining process using the clean room facilities of METU. The sensor was characterized by monitoring the humidity response, hysteresis characteristics, and measuring the response time in an environmental chamber. The operation of the integrated heater was verified by measuring the resistance versus temperature and resistance versus heating power characteristics.

2. A switched capacitor readout circuit was designed and fabricated in the AMS 0.8μm CMOS process. The readout circuit was connected to the sensor by wire bonding on an alumina substrate, which is attached to a commercial package. The hybrid module was characterized inside the environmental

chamber. Sensitivity of the sensor was found as 19.4mV/%RH, with a nonlinearity of 0.17%. Hysteresis of the sensor was found as 2.54% RH.

3. A thermal conductivity based humidity sensor, which is monolithically integrated with the readout circuit was designed and implemented in the AMS 0.6μm CMOS process. The fabrication was completed by post-CMOS anisotropic bulk silicon etching process and electrochemical etch-stop techniques.

4. The thermal conductivity based humidity sensor was characterized by measuring the humidity response and the hysteresis characteristics. A proper test setup was prepared on a printed circuit board for the characterization measurements. The sensor provides a sensitivity of 14.3mV/%RH, 26mV/%RH, and 46.9mV/%RH for 20ºC, 30ºC, and 40ºC ambient temperatures respectively. The sensing diodes are heated up to 250ºC, so the sensor does not allow water condensation. Total power dissipation of the sensor is only 1.38mW.

Although the major goals of this research were achieved, following tasks can be suggested as future work:

1. Different polyimide types, which allow the formation of thinner dielectric layers, can be used as the humidity sensitive layer in order to obtain higher sensitive capacitive humidity sensors. Another alternative is to use glass substrate instead of a silicon substrate.

2. The capacitive humidity sensor can be implemented on a diaphragm to provide thermal isolation from the substrate in order to operate the integrated heater with less power.

3. The integrated heater of the capacitive humidity sensor can be fabricated from a metal, which has less thermal conductivity than aluminum in order to increase the power efficiency of the heater.

4. Die level packaging of the thermal conductivity based humidity sensor needs to be completed in order to complete the fabrication of the sensor as a prototype for mass production.

This study is the first national study to implement humidity sensors using MEMS and silicon micromachining technologies, and it is hoped that the results of this study can be used to implement humidity sensors to be used in industry.

REFERENCES

[1] H. L. Penman, *Humidity*, The Institute of Physics, London, 1955.

[2] F. W. Gole, *Introduction to Meteorology*, John Wiley & Sons Inc., New York, 1970.

[3] G. J. Visscher, “Standard Psychrometers: a matter of preferences,” Meas. Sci. Technology, Vol. 6, pp. 1451-1461, 1995.

[4] Z. M. Rittersma, “Recent Achievements in Miniaturized Humidity Sensors-a Review of Transduction Techniques,” Sensors and Actuators A, Vol. 96, pp. 196-210, 2002.

[5] L. J. Golonka, B. W. Licznerski, K. Nitsch, H. Terycz, “Thick Film Humidity Sensors,” Measurement Science and Technology, Vol. 8, pp. 92-98, 1997.

[6] E. Traversa, “Ceramic Sensors for Humidity Detection: the State of the Art and Future Developments,” Sensors and Actuators B, Vol. 23, pp. 1335-1356, 1995.

[7] N. Serin, T. Serin, B. Unal, “The Effect of Humidity on Electronic Conductivity of an Au/CuO/Cu_2O/Cu Sandwich Structure,” Semiconductor Science and Technology, Vol. 15, pp.112-116, 2000.

[8] S. Chakraborty, “The Humidity Dependent Conductance of $Al_2(SO_4)_3.16H_2O$,” Smart Materials and Structures, Vol. 4, pp. 368-369, 1995.

[9] W. Qu, J. U. Meyer, “Thick Film Humidity Sensors Based on Porous $MnWO_4$ Material,” Measurement Science and Technology, Vol. 8, pp. 593-600, 1997.

[10] W. Qu, R. Green, M. Austin, “Development of Multi-Functional Sensors in Thick-Film and Thin-Film Technology,” Measurement Science and Technology, Vol. 11, pp. 1111-1118, 2000.

[11] H. Wang, C. D. Feng, S. L. Sun, C. U. Segre, J. R. Stetter, “Comparison of Conductometric Humidity Sensing Polymers,” Sensors and Actuators B, Vol. 40, pp. 211-216 ,1997.

[12] C. D. Feng, S. L. Sun, H. Wang, C. U. Segre, J. R. Stetter, “Humidity Sensitive Properties of Nafion and Sol-gel Derived SiO_2/Nafion Composite Thin Films,” Sensors and Actuators B, Vol. 40, pp. 217-222, 1997.

[13] Y. Sakai, M. Matsuguchi, H. Makihata, “A New Type LiCl Dew Point Hygrometer Probe Fabricated with a Composite of Porous Polymer and the

Salt," *The 10th International Conference on Solid-State Sensors and Actuators (TRANSDUCERS'99),* pp. 1664-1667, Sendai, Japan, June 1999.

[14] K. Sager, A. Schroth, A. Nakladal and G. Gerlach, "Humidity-Dependent Mechanical Properties of Polyimide Films and Their Use for IC-Compatible Humidity Sensors," Sensors and Actuators A Vol. 53, pp. 330-334, 1996.

[15] R. Buchhold, A. Nakladal, G. Gerlach, P. Neumann, "Design Studies on Piezoresisitive Humidity Sensors," Sensors and Actuators B, Vol. 53, pp. 1-7, 1998.

[16] N. T. T. Ha, D. K. An, P. V. Phong, P. T. N. Hoa, L. H. Mai, "Study and Performance of Humidity Sensor Based on the Mechanical-Optoelectronic Principle for the Measurement and Control of Humidity in Storehouses," Sensors and Actuators B, Vol. 66, pp. 200-202, 2000.

[17] E. Radeva, V. Georgiev, L. Spassov, N. Koprinarov, St. Kanev, "Humidity Absorptive Properties of Thin Fullerene Layers Studied by Means of Quartz Microbalance," Sensors and Actuators B, Vol. 42, pp. 11-13, 1997.

[18] F. Pascal-Delannoy, B. Sorli, A. Boyer, "Quartz Crystal Microbalance (QCM) Used as Humidity Sensor," Sensors and Actuators A, Vol. 84, pp. 285-291, 2000.

[19] J. Reibel, U. Stahl, T. Wessa, M. Rap, "Gas Analysis with SAW Sensor Systems," Sensors and Actuators B, Vol. 65, pp. 173-175, 2000.

[20] E. T. Zellers, M. Morishita, Q. C. Cai, "Evaluating Porous Layer Open-Tubular Capillaries as Vapor Preconcentrators in a Microanalytical System," Sensors and Actuators B, Vol. 67, pp. 244-253, 2000.

[21] C. Bariain, R. Matias, F. J. Arregui, M. Amo, "Optical Fiber Humidity Sensor Based on a Tapered Fiber Coated with Agarose Gel," Sensors and Actuators B, Vol. 69, pp. 127-131, 2000.

[22] F. Arregui, Y. Liu, R. Matias, R. Claus, "Optical Fiber Humidity Sensor Using a Nano Fabry-Perrot Cavity Formed by the Ionic Self-Assemblt Method," Sensors and Actuators B, Vol. 59, pp. 54-59, 1999.

[23] B.C. Gupta, Ratnanjali, "A Novel Probe for a Fiber Optic Humidity Sensor," Sensors and Actuatros B, Vol. 80, pp. 132-135, 2001.

[24] M. Kimura, "A New Method to Measure the Absolute Humidity Independently of the Ambient Temperature," *The 8th International Conference on Solid-State Sensors and Actuators (TRANSDUCERS'95),* pp. 843-846, Stockholm, Sweden, 1995.

[25] D. Lee, H. Hong, C. Park, G. Kim, Y. Jeon, J. Bu, "A Micromachined Robust Humidity Sensor for Harsh Environment Applications," *The 14th IEEE International Conference on Micro Electro Mechanical Systems (MEMS 2001),* pp. 558-561, January 2001.

[26] W. Qu, W. Wlodarski, "A Thin-film Sensing Element for Ozone, Humidity and Temperature," Sensors and Actuators B, Vol. 64, pp. 42-48, 2000.

[27] W. Qu, J. Meyer, "A Novel Thick Film Humidity Sensor," Sensors and Actuators B, Vol. 40, pp. 175-182, 1997.

[28] C.M.A. Ashruf, P.J. French, P.M.M.C. Bressers, J.J. Kelly, "Galvanic Porous Silicon Formation without External Contacts," Sensors and Actuators A, Vol. 74, pp. 118-122, 1999.

[29] Z.M. Rittersma, A. Splinter, A. Bödecker, W. Benecke, "A Novel Surface Micromachined Capacitive Porous Silicon Humidity Sensor," Sensors and Actuators B, Vol. 68, pp. 210-217, 2000.

[30] A. Foucaran, B. Sorli, M. Garcia, F. Pascal-Delannoy, A. Giani, A. Boyer, "Porous Silicon Layer Coupled with Thermoelectric Cooler: a Humidity Sensor," Sensors and Actuators A, Vol. 79, pp. 189-193, 2000.

[31] M. Matsuguch, T. Kuroiwa, T. Miyagishi, S. Suzuki, T. Ogura, Y. Sakai, "Stability and Reliability of Polyimide Humidity Sensors Using Crosslinked Polyimide Films," Sensors and Actuators B, Vol. 52, pp. 53-57, 1998.

[32] A. R. K. Ralston, C. F. Klein, P. E. Thoma and D. D. Denton, "A model for the relative environmental stability of a series of polyimide capacitance humidity sensors," Sensors and Actuators B, Vol. 34, pp. 343-348, 1996.

[33] R. Jachowicz, J. Weremczuk, "Sub-cooled Water Detection in Silicon Dew Point Hygrometer," Sensors and Actuators A, Vol. 85, pp. 75-83, 2000.

[34] U. Kang, K. D. Wise, "A High Speed Capacitive Humidity Sensor with On-Chip Thermal Reset," IEEE Transactions on Electron Devices, Vol. 47, pp. 702-710, 2000.

[35] C. Laville, C. Pellet, "Interdigitated Humidity Sensors for a Portable Clinical Microsystem," IEEE Transactions on Biomedical Engineering, Vol. 49, pp.1162-1167, 2002.

[36] Y. Y. Qui, C. Azeredo-Leme, L. R. Alcacer, J. E. Franca, "A CMOS Humidity Sensor with On-Chip Calibration," Sensors and Actuators A, Vol. 92, pp. 80-87, 2001.

[37] M. Dokmeci, K. Najafi, "A high-sensitivity polyimide capacitive relative humidity sensor for monitoring anodically bonded hermetic micropackages," IEEE Journal of Microelectromechanical Systems, Vol. 10, pp. 197-204.

[38] A. R. K. Ralston, M. C. Buncick, and D. D. Denton, "Effects of Aging on Polyimide: A Model for Dielectric Behavior", *The 6th International Conference on Solid-State Sensors and Actuators (TRANSDUCERS'91),* pp. 759-763.

[39] S. D. Senturia, *Microsystem Design*, Kluwer Academic Publishers, Massachusetts, 2001.

[40] B. Wang, T. Kajita, T. Sun, G. Temes, "New High Precision Circuits for on-chip Capacitor Ratio Testing and Sensor Readout," *The 8th International Conference on Solid-State Sensors and Actuators (TRANSDUCERS'95),* pp. 138-141, Stockholm, Sweden, 1995.

[41] X. Li, G. Meijer, "An Accurate Interface for Capacitive Sensors," IEEE Transactions on Instrumentation and Measurement, Vol. 51, pp. 935-939, 2002.

[42] X. Shi, H. Matsumoto, K. Murao, "A High Accuracy Digital Readout Technique for Humidity Sensor," IEEE Transactions on Instrumentation and Measurement, Vol. 50, pp. 1277-1280, 2001.

[43] M. Pedersen, W. Olthius, P. Bergveld, "An Integrated Silicon Capacitive Microphone with Frequency Modulated Digital Output," Sensors and Actuators A, Vol. 69, pp. 267-275, 1998.

[44] T. Bolthauser, C. Leme, H. Baltes, "High Sensitivity CMOS Humidity Sensors with on-chip Absolute Capacitance Measurement System," Sensors and Actuators B, Vol. 15, pp. 75-80, 1993.

[45] R. Gregorian, *Introduction to CMOS Op-Amps and Comparators*, John Wiley & Sons Inc., 1999.

[46] J. E. France, Y. Tsividis, *Design of Analog-Digital VLSI Circuits for Telecommunications and Signal Processing*, Prentice Hall 1994.

[47] C. Laville, C. Pellet, "Comparison of Three Humidity Sensors for a Pulmonary Function Diagnosis Microsystem," IEEE Sensors Journal, Vol. 2, pp. 96-101, 2002.

[48] T. Ishikava, M. Ueno, Y. Nakaki, K. Endo, Y. Ohta, J. Nakanishi, Y. Kosasayama, H. Yagi, T. Sone, M. Kimata, "Performance of 320x240 Uncooled IRFPA with SOI Diode Detectors," Proceedings of SPIE, Vol. 4130, pp. 1-8, 2000.

[49] S. Eminoglu, D. Tezcan, M. Tanrikulu, T. Akin, "A Low-Cost, Small Pixel Uncooled Infrared Detector for Large Focal Plane Arrays Using a Standard CMOS Process," Proceedings of SPIE, Vol. 4721, pp. 111-121, 2002.

[50] S. Eminoglu, D. Tezcan, M. Tanrikulu, T. Akin, "Low-Cost Uncooled Infrared Detectors in CMOS Process," *The 16th European Conference on Solid State Transducers (Eurosensors XVI)*, pp. 263-264, Prague, Czech Republic, September 2002.

[51] D. Hodges, H. Jackson, *Analysis and Design of Digital Integrated Circuits*, McGraw-Hill, 1988.

[52] P. W. Kruse, D. D. Skatrud, *Uncooled Infrafer Imaging Arrays and Systems,* Semiconductors and Semimetals 47, Academic Press 1997.

[53] S. Eminoglu, M. Y. Tanrikulu, T.Akin, "A Low-Cost 64x64 Uncooled Infrared Detector in Standard CMOS," *The 12th International Conference on Solid-State Sensors, Actuators, and Microsystems (TRANSDUCERS'03)*, pp. 316-319, Boston, USA, June 2003.

[54] N. Maluf, *An Introduction to Microelectromechanical Systems Engineering*, Artech House, 2000.

[55] G. Yan, P. Chan, M. Hsing, R. Sharma, J. Sin, Y. Wang, "An Improved TMAH Si-etching Solution Without Attacking Exposed Aluminum," Sensors and Actuators A, Vol. 89, pp. 135-141, 2001.

[56] S. M. Sze, *Semiconductor Sensors*, John Wiley and Sons, 1994.

[57] M. Parameswaran, H. Baltes, L. Ristic, D. Dhaded, and A. Robinson, "A New Approach for the Fabrication of Micromechanical Structures," Sensors and Actuators A, Vol. 19, pp. 289-307, 1989.

[58] HIH-3610 Series Humidity Sensor Product Sheet, Honeywell.

[59] http://www.wpi.edu.

APPENDIX

FABRICATION PROCESS FLOW OF THE CAPACITIVE HUMIDITY SENSOR

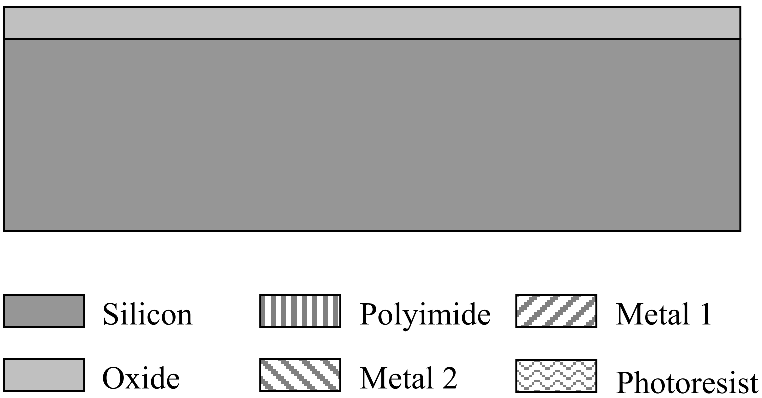

SiO_2 is deposited on top of a three inch silicon wafer.

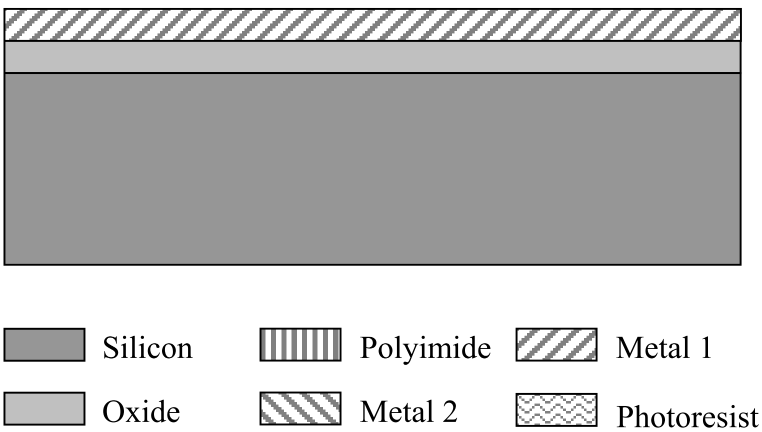

Aluminum is sputter deposited for the formation of the bottom electrode.

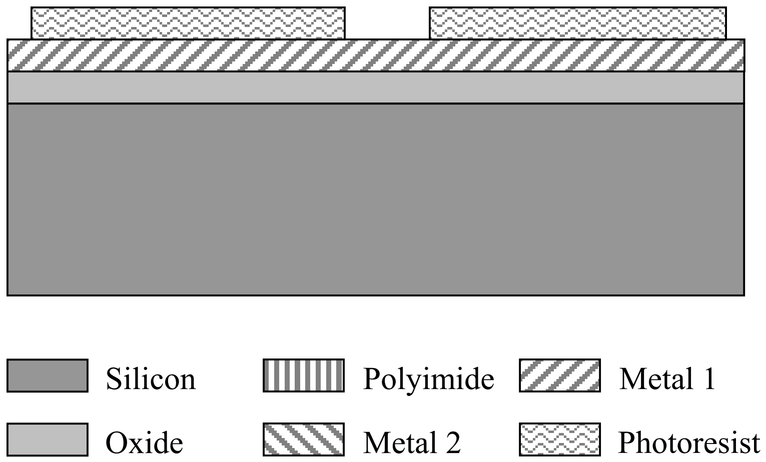

Photoresist is coated and patterned for aluminum etching.

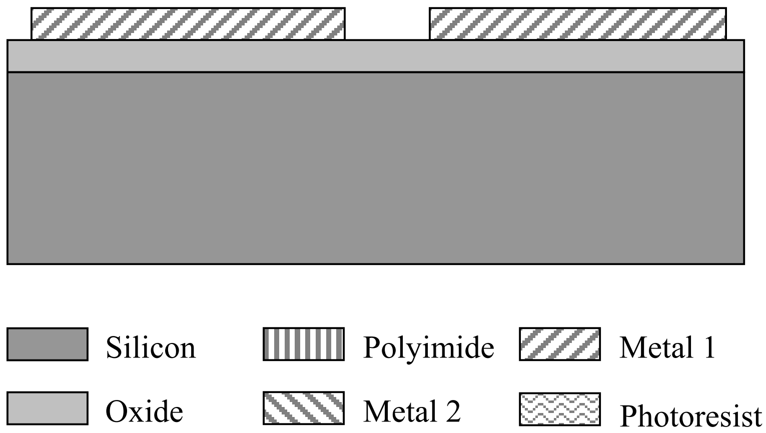

Aluminum is etched and photoresist is removed.

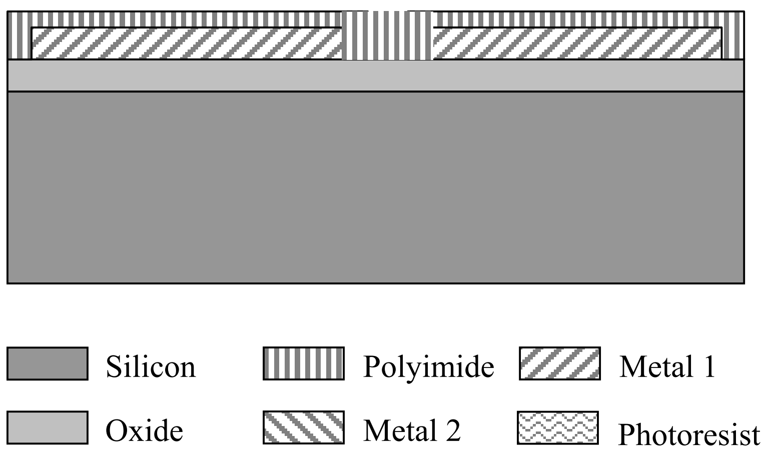

Polyimide is spin coated on the bottom electrode.

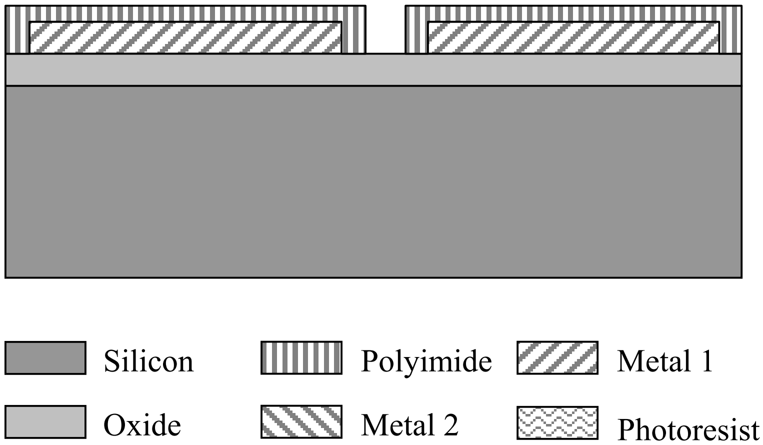

Polyimide is patterned by photolithography.

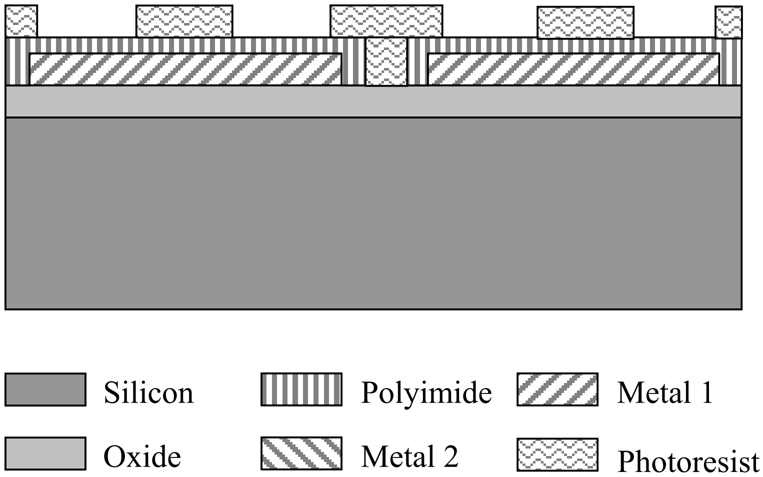

Photoresist is coated and patterned for lift off.

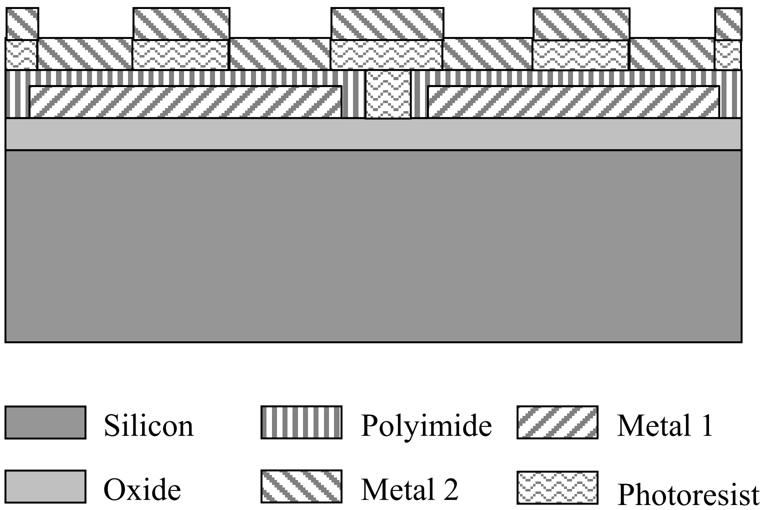

Cr/Au is deposited by thermal evaporation for the formation of the top electrode.

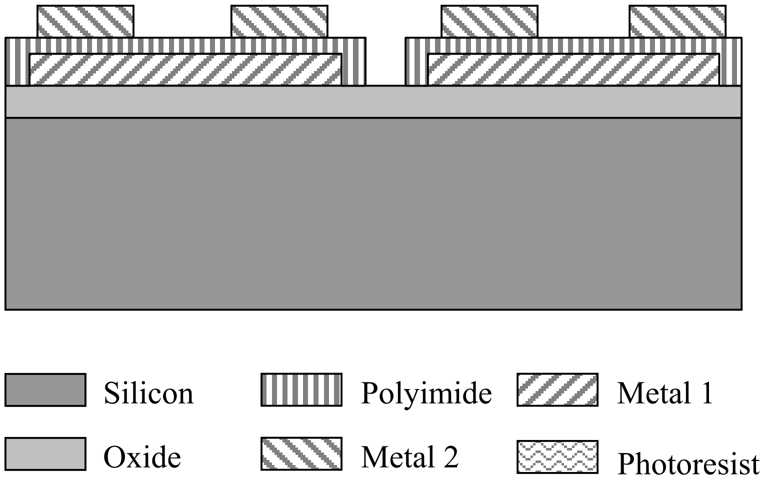

Top electrode is patterned by removing the photoresist.

CAPACITIVE HUMIDITY SENSOR FABRICATION PROCESS FLOW			
Step#	Process	Process Details	Comments and Explanations
1	Al deposition	Sputter deposition at 2kW power for 20 minutes.	Deposition of the bottom electrode metal. Aluminum thickness is 0.5μm.
2	Lithography	Deydration bake (115ºC 30 min.)	Patterning of the bottom electrode.
		Spin coating photoresist	
		Soft bake (115ºC 60 sec. hot plate)	
		UV Exposure (20 sec.)	
		Development (MF319)	
		Rinse (DI water)	
3	Al etch	H3PO4:HNO3:CH3COOH:H2O = 75:3:15:2 (40°C 7 min.)	Bottom electrode is patterned
		DI-H2O rinse 15 min.	
4	Polyimide deposition and patterning	Dehydration Bake (130ºC 30 min.)	Formation of the dielectric layer
		Spin coating (4500 rpm. 35 sec.)	
		Soft bake (4 min. 75ºC hot plate)	
		UV exposure (200mJ/cm^2)	
		Development (45 sec in DE6180)	
		Overlap (7 sec. Developer/Rinser)	
		Rinse (45 sec. in RI9180)	
5	Lithography	Deydration bake (115ºC 30 min.)	Top electrode pattern is formed before lift-off.
		Spin coating photoresist	
		Soft bake (115ºC 60 sec. hot plate)	
		UV Exposure (20 sec.)	
		Development (MF319)	
		Rinse (DI water)	

6	Cr/Au Deposition	Cr/Au evaporation	Deposition of the top electrode metal. Cr/Au thickness is 0.2µm.
7	Lift-off	Photoresist removal (5 min. in acetone).	Top electrode is formed by removing the photoresist.